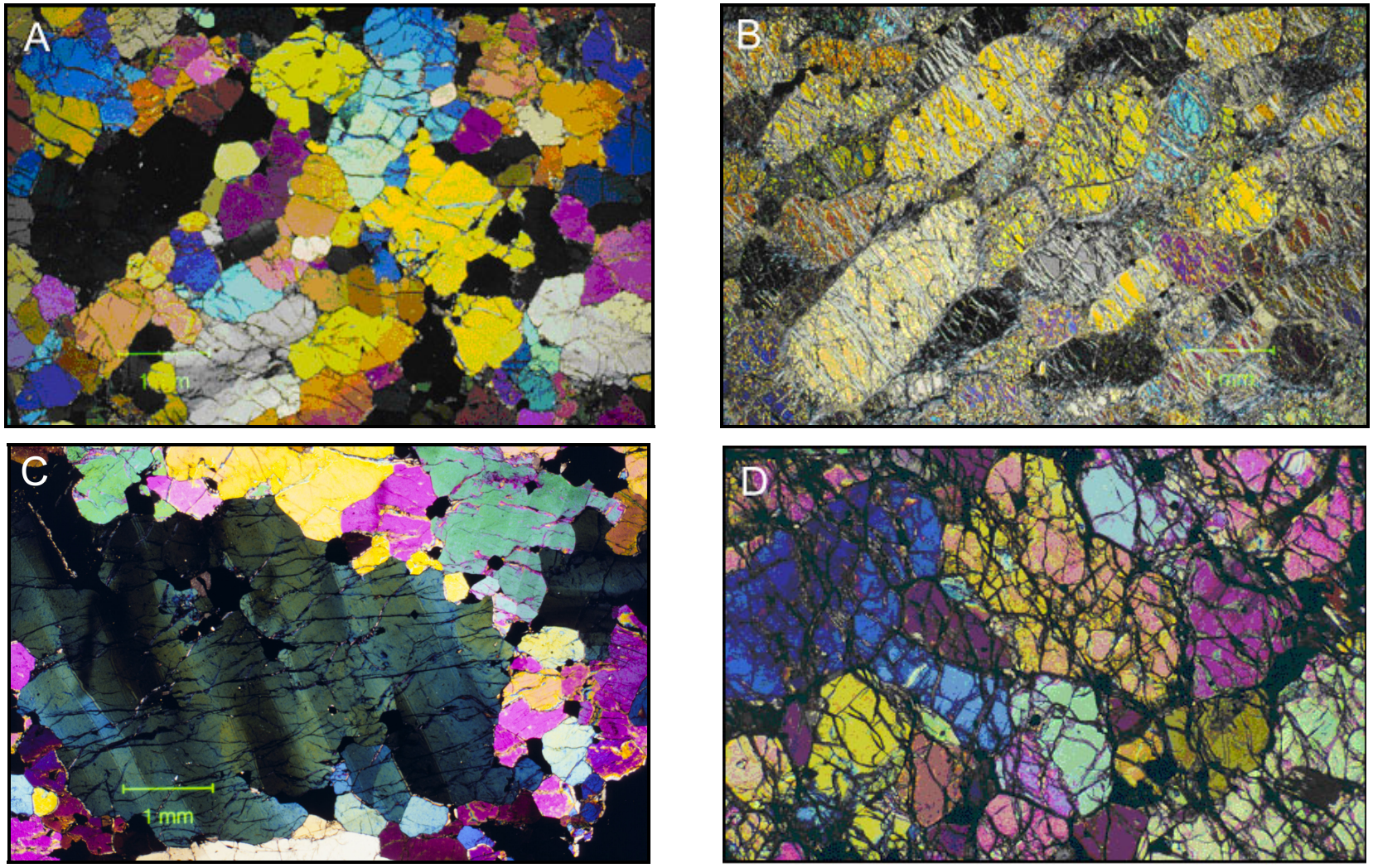

Figure 8.1 Photomicrographs of textures and mineralogy of olivine adcumulate rocks from the TNB, under cross-polarized light: a) neoblastic olivine cumulate, Mid Lake (86291-2060), b) partially serpentinized ovoid to idiomorphic cumulate olivines, Mystery Lake North (89234-2641.1B), c) strained olivine megacryst surrounded by neoblastic olivine, Mid Lake (89291-2211), and d) equigranular olivine, Hambone East (74289-929).

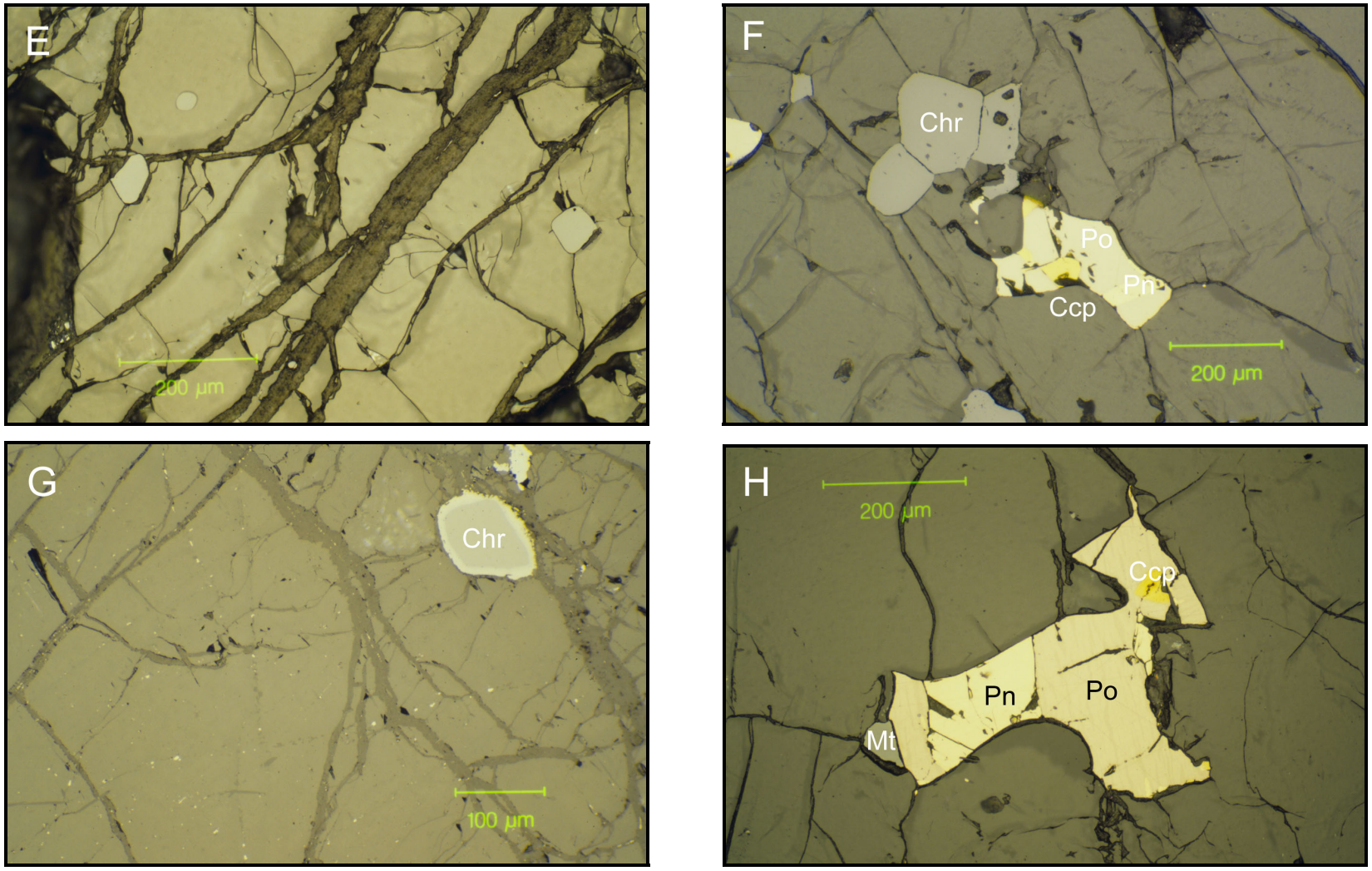

Figure 8.1 (Contd.) Photomicrographs of textures and mineralogy of olivine adcumulate rocks from the TNB under reflected light: e) subhedral to anhedral chromite inclusions within olivine grains, Hambone East (74289-929), and f) euhedral intercumulus chromite grains and sulfide bleb, Mid Lake (86291-2060), g) disseminated opaque micro-inclusions in olivine, Mystery Lake North (89234-2845.5), h) intergranular sulfide bleb, Mid Lake (86291-2060).

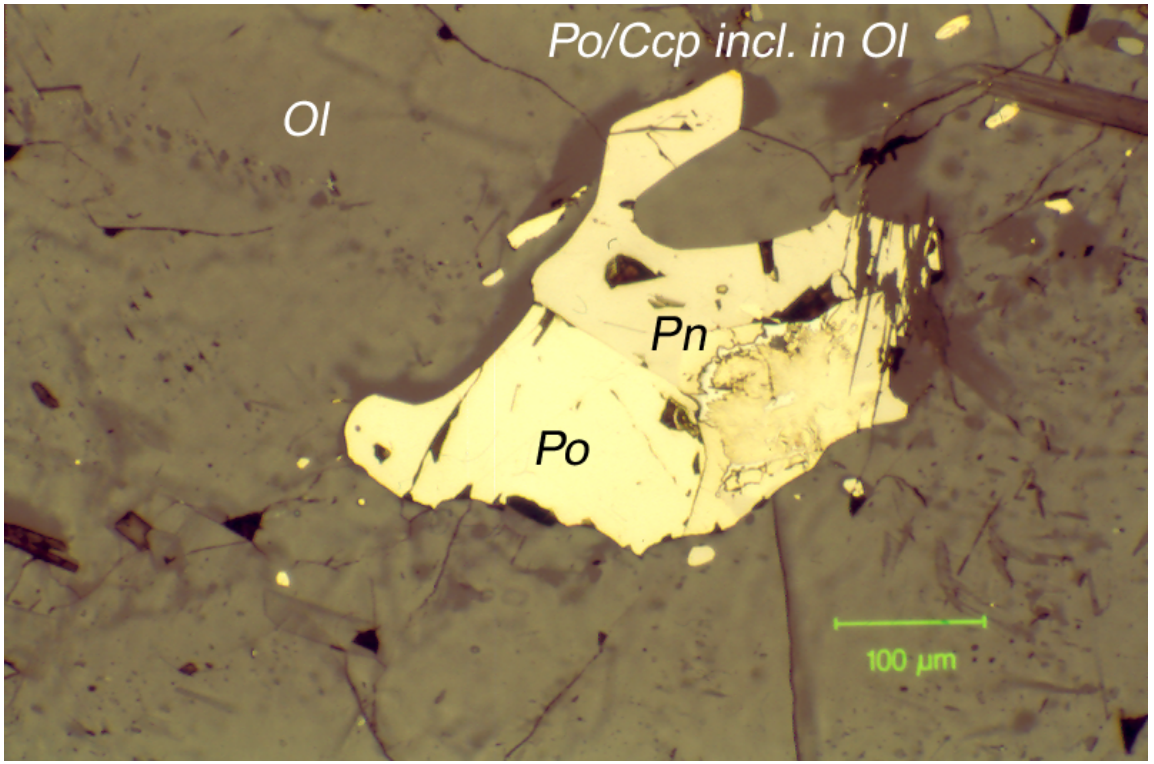

Figure 8.1 (Contd.) Photomicrographs of textures and mineralogy of olivine adcumulate rocks from the TNB under reflected light: i) intergranular sulfide bleb and sulfide inclusions in olivine, Pipe 1 (86242-2-3599).

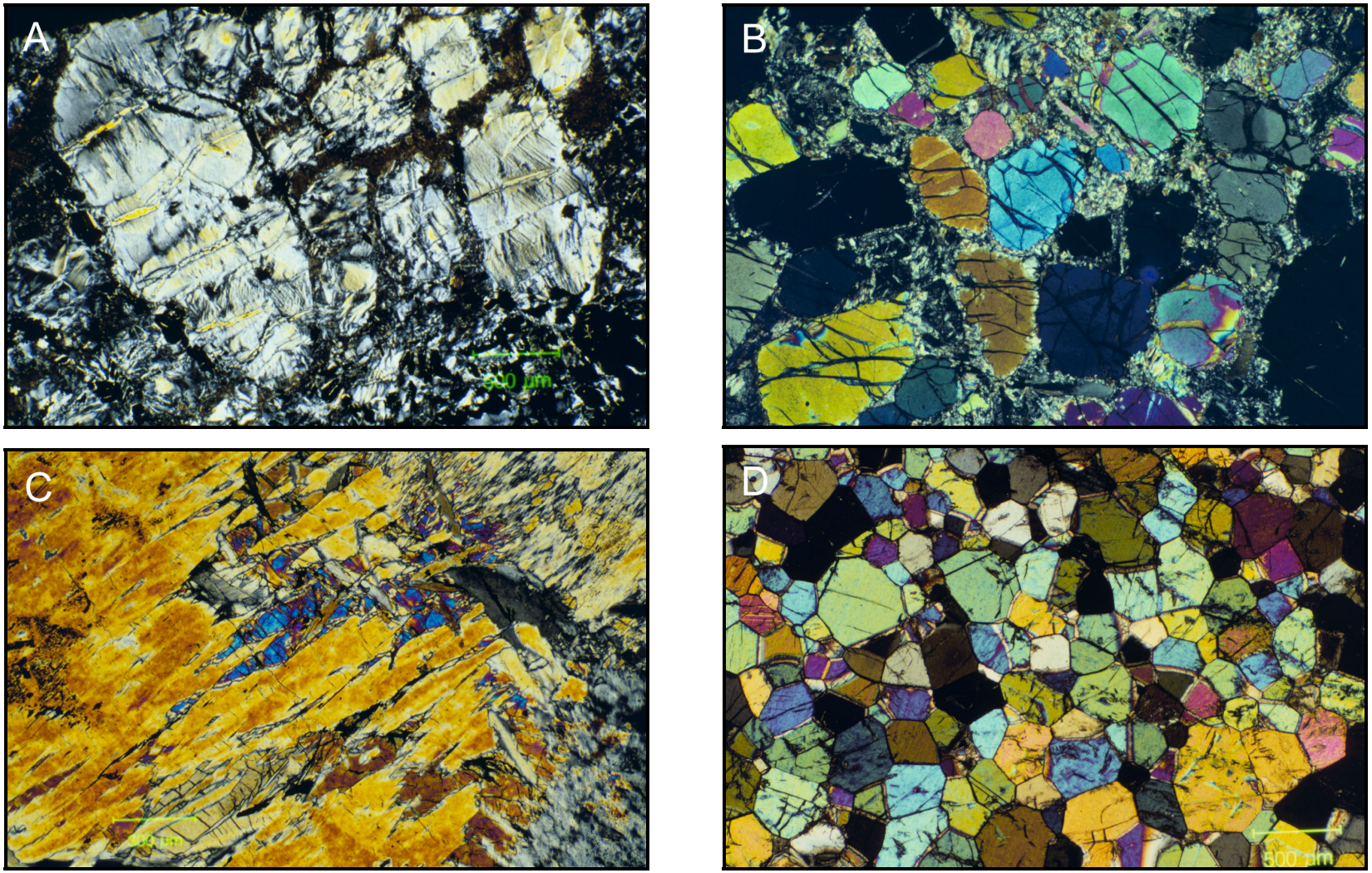

Figure 8.2 Photomicrographs of textures and mineralogy of olivine orthocumulate and pyroxenitic rocks from the TNB, under cross-polarized light: a) serpentinized metaperidotite, Spur South (86227-1068), b) partially serpentinized peridotite, North Manasan (89299-2356), c) relict fragments of olivine in olivine pyroxenite along the margins of the Spur South ultramafic body (89227-1097.2), and d) equigranular clinopyroxenite layer, South Central TNB (WB02047A, DDH WL95-106)

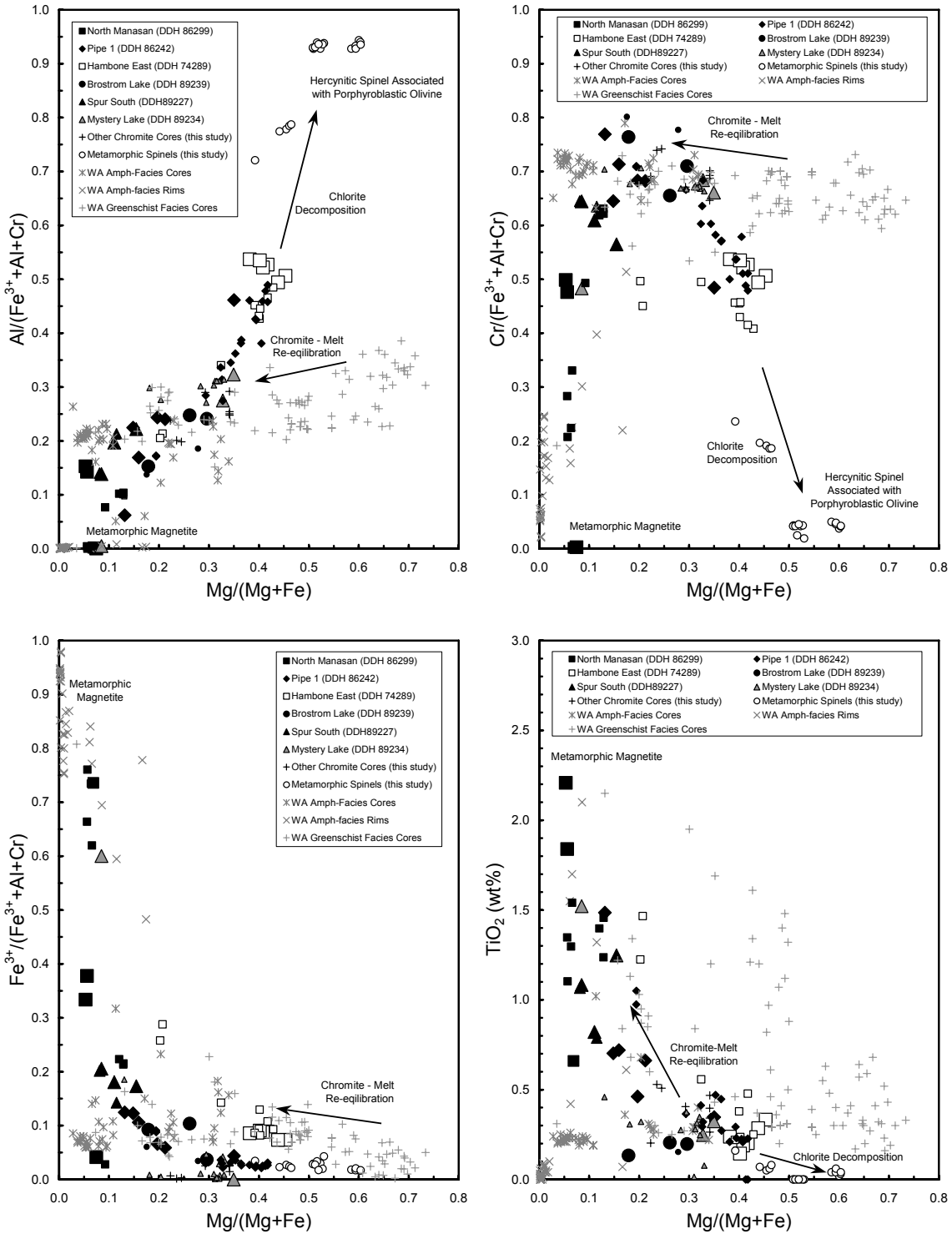

Figure 8.3 Compositions of chromites (small symbols) and opaque inclusions in olivines (large symbols) from the cores of ultramafic bodies from the TNB. Data for Western Australian komatiites from Barnes (1998, 2000). Compositions screened for low SiO_2 and Total Oxides > 95% in order to remove analyses that contained a contribution from the enclosing olivine.

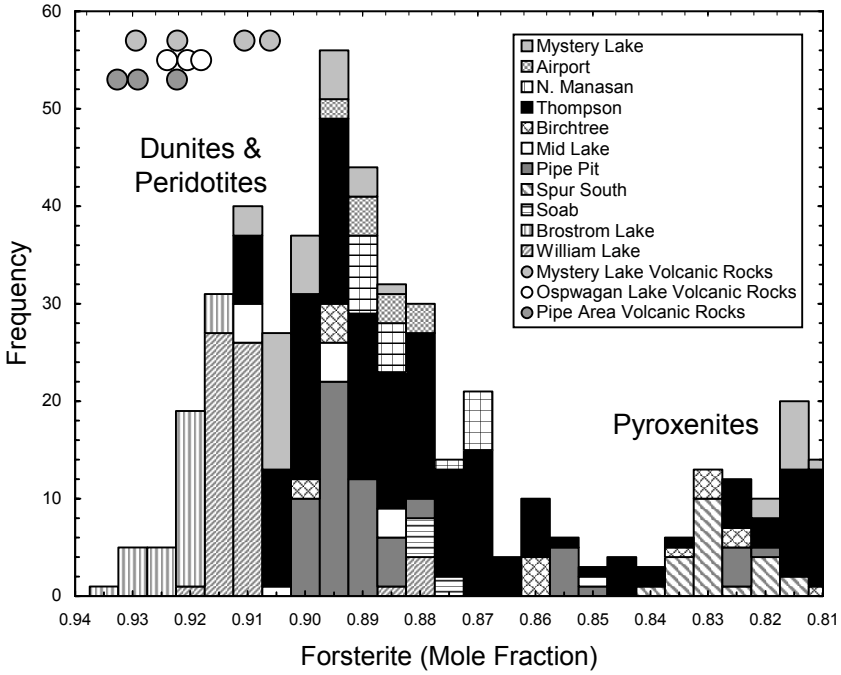

Figure 8.4 Histogram of relict magmatic olivine compositions from TNB ultramafic bodies and calculated compositions of olivines in equilibrium with volcanic rocks from the Mystery Lake, Ospwagan Lake and Pipe areas (circles). Olivine compositions calculated using the compositionally dependent exchange coefficients of Beattie et al. (1991). Additional data for Thompson, Birchtree, Soab, Mystery Lake, Thompson Airport and Pipe Pit from L. Hulbert (pers. comm., 2000).

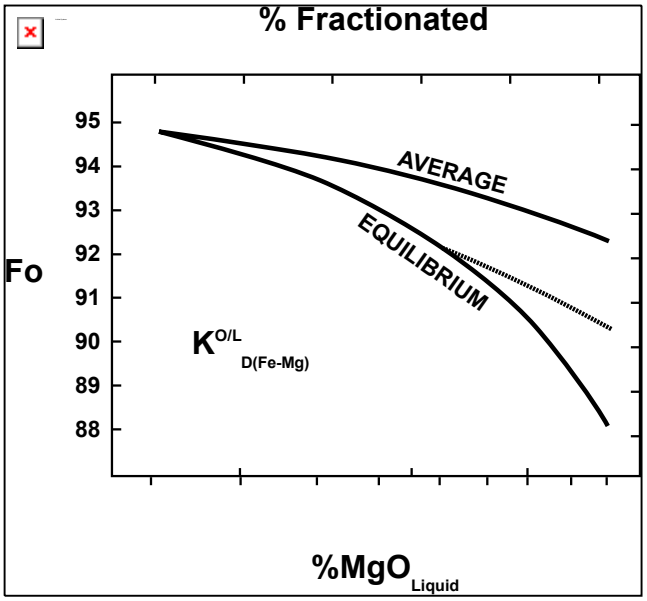

Figure 8.5 Equilibrium and average olivine compositional variations with fractional crystallization of a komatiitic magma. The equilibrium curve shows the compositions of olivine in equilibrium with silicate liquids (assuming constant $D_{Ni}^{sil/ol}$) and should correspond to the profile of a zoned olivine assuming perfect fractional crystallization and no diffusion during growth. The average curves show the compositions of olivines derived by fractionation of magmas containing 32 and 24 wt% MgO with complete homogenisation. Modified after Lesher (1983).

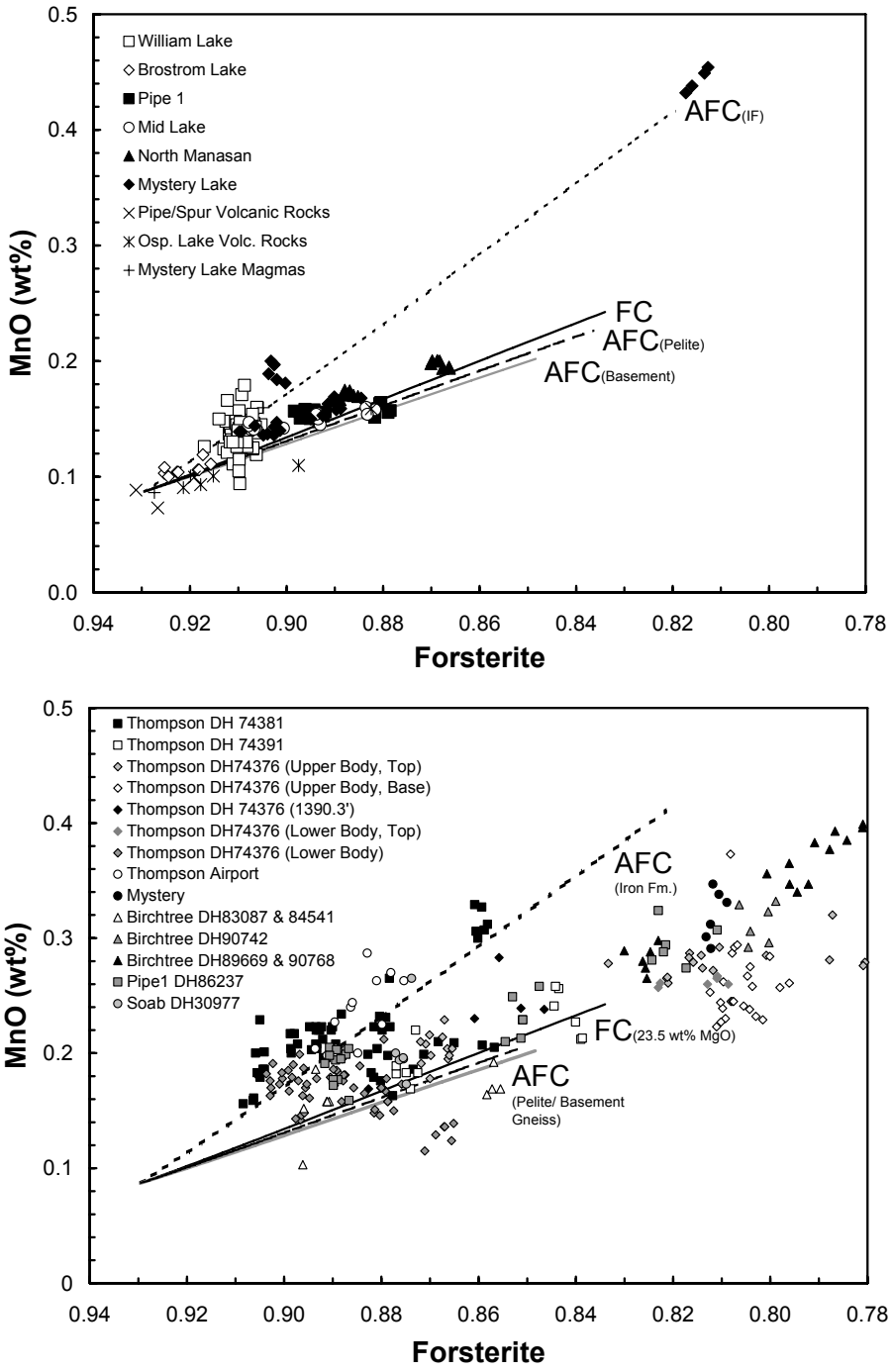

Figure 8.6 MnO contents of TNB olivines plotted as a function of forsterite content. Upper plot, this study. Lower plot, Olivine data obtained from L. Hulbert (pers. comm., 2000) Fractionation trends calculated for an initial magma composition similar to that of an aphyric komatiitic basalt collected from Mystery Lake (DDH89234-3932), using the exchange coefficients of Beattie et al. (1991), and $Fe^{3+}/Fe^{2+} = 0.1$ in the magma. Assimilation modelled using typical compositions determined for sulfide-free P_2 pelitic rocks, silicate facies iron formations of the P_3 unit and felsic basement rocks from Pipe Pit, and an assimilation: fractionation ratio of 3:5 (r = 0.6). Large crosses indicate the calculated compositions of olivines in equilibrium with ultramafic rocks from Ospwagan Lake, Mystery Lake, and Pipe Pit.

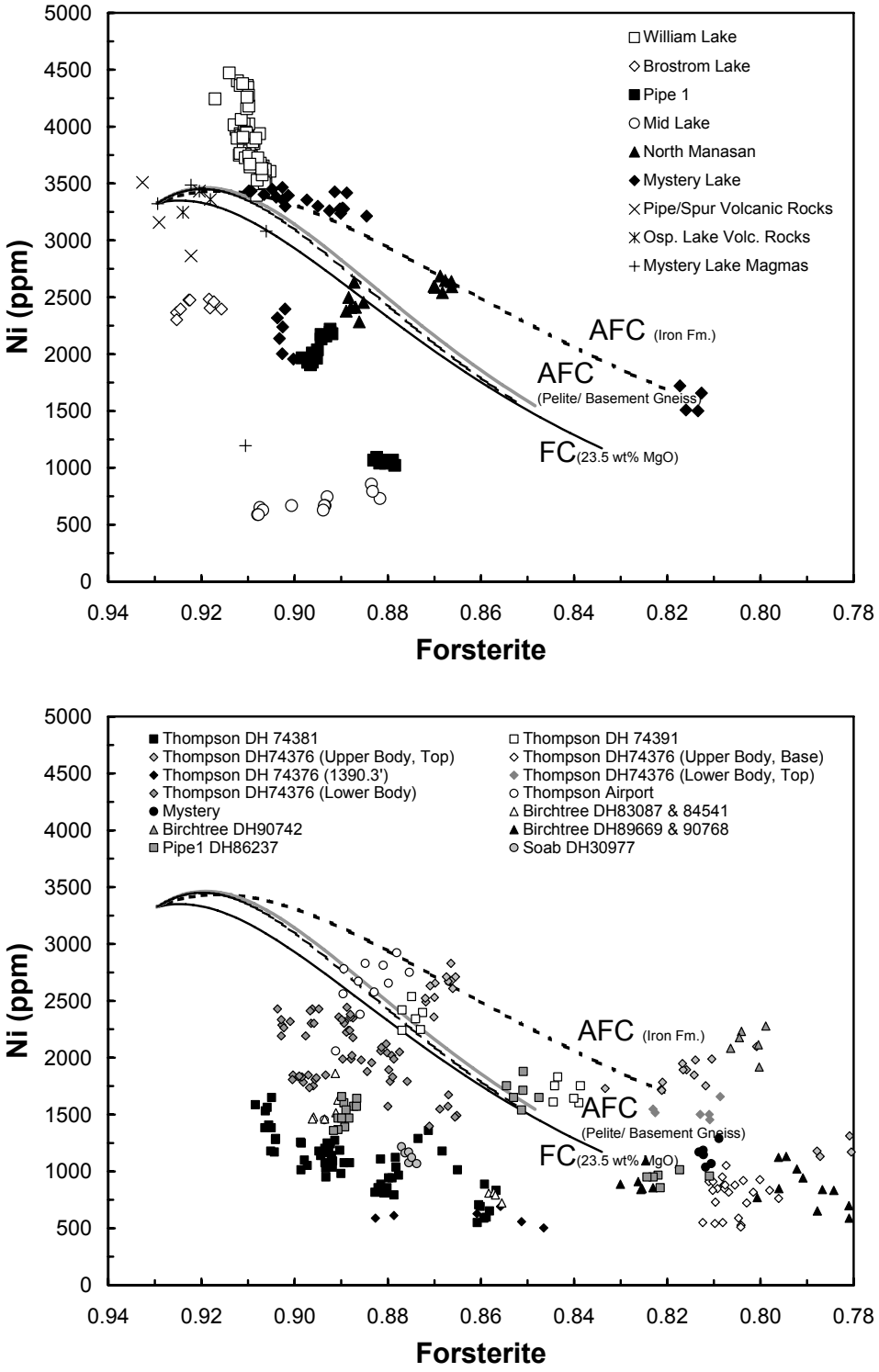

Figure 8.7 Ni contents of TNB olivines plotted as a function of forsterite content. Upper plot, this study. Lower plot, Olivine data obtained from L. Hulbert (pers. comm., 2000). Fractionation trends calculated as per **Figure 8.6**.

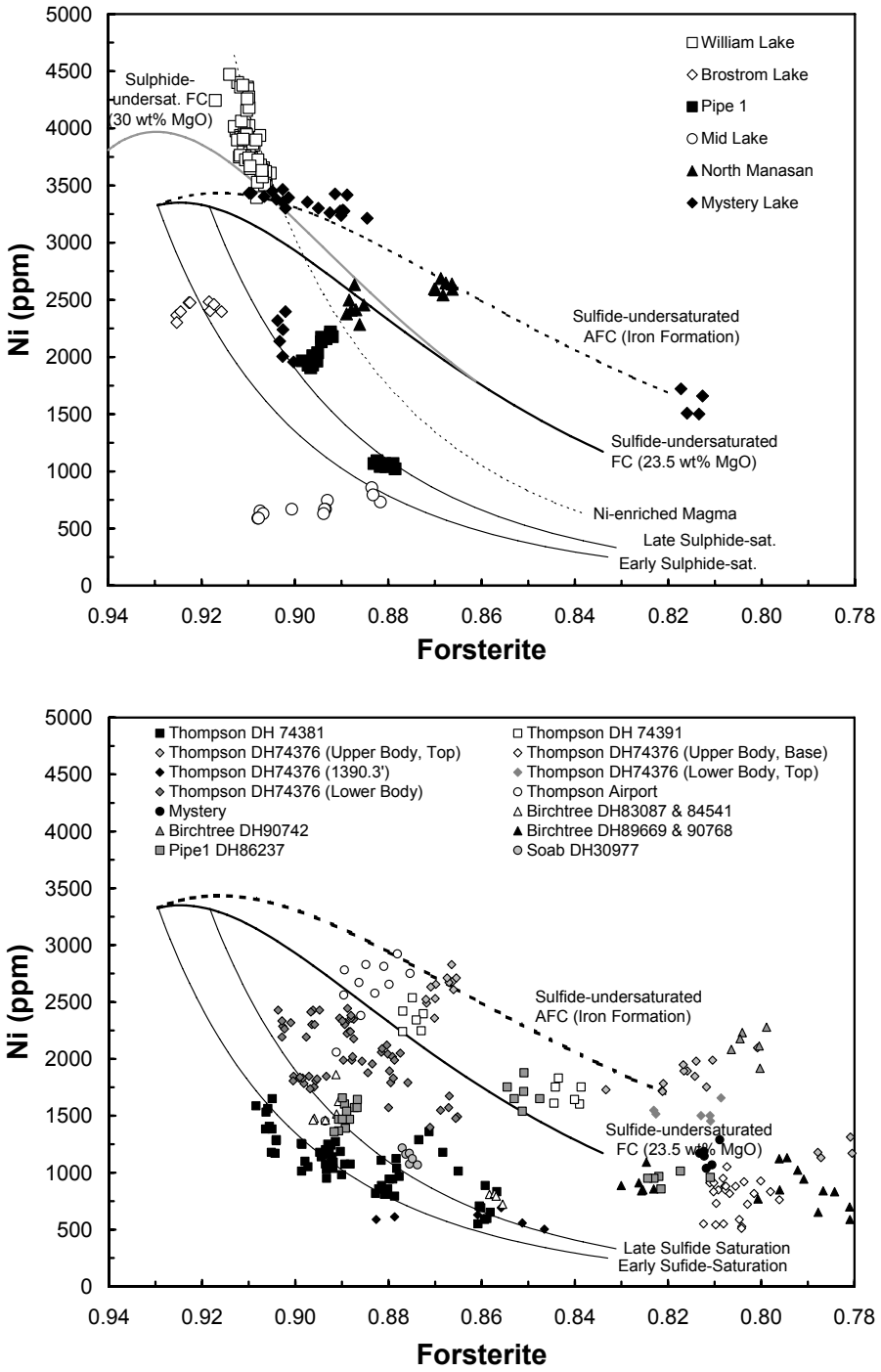

Figure 8.8 Comparison of measured olivine compositions with those expected for fractional crystallization of olivine and sulfide from a sulfide-saturated magma (olivine : sulfide = 50:1). Upper plot, this study. Lower plot, olivine data obtained from L. Hulbert (pers. comm., 2000). Initial magma composition and sulfide-undersaturated trends similar to those in **Figure 8.6**, except thick grey line in upper plot, which assumed an more magnesian initial magma composition (30 wt% MgO, 1780 ppm Ni). $D_{liquid/sul}$ = 150, $D_{liquid/ol}$ calculated using the exchange coefficients of Beattie et al. (1991).

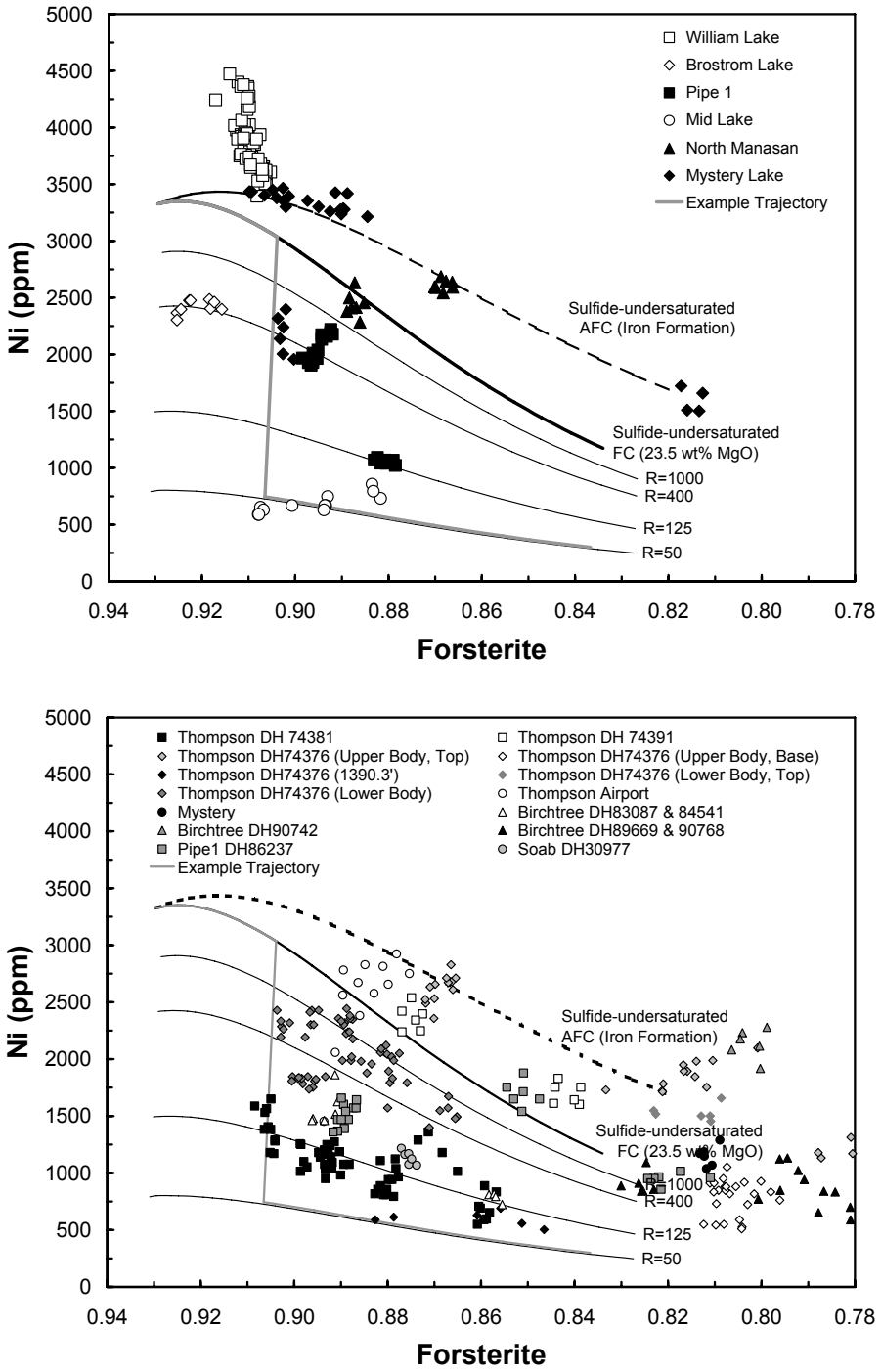

Figure 8.9 Comparison of measured olivine compositions with those expected for batch equilibration of a evolving magma with an externally derived sulfide liquid. Upper plot, this study. Lower plot, olivine data obtained from L. Hulbert (pers. comm., 2000). Initial magma composition and sulfide-undersaturated trends similar to those in **Figure 8.6**. Thick grey line in indicates a typical trajectory for an ultramafic magma that interacts with a sulfide liquid at a low silicate:sulfide ratio (R). $D_{liquid/sul}$ = 150, $D_{liquid/ol}$ calculated using the exchange coefficients of Beattie et al. (1991).

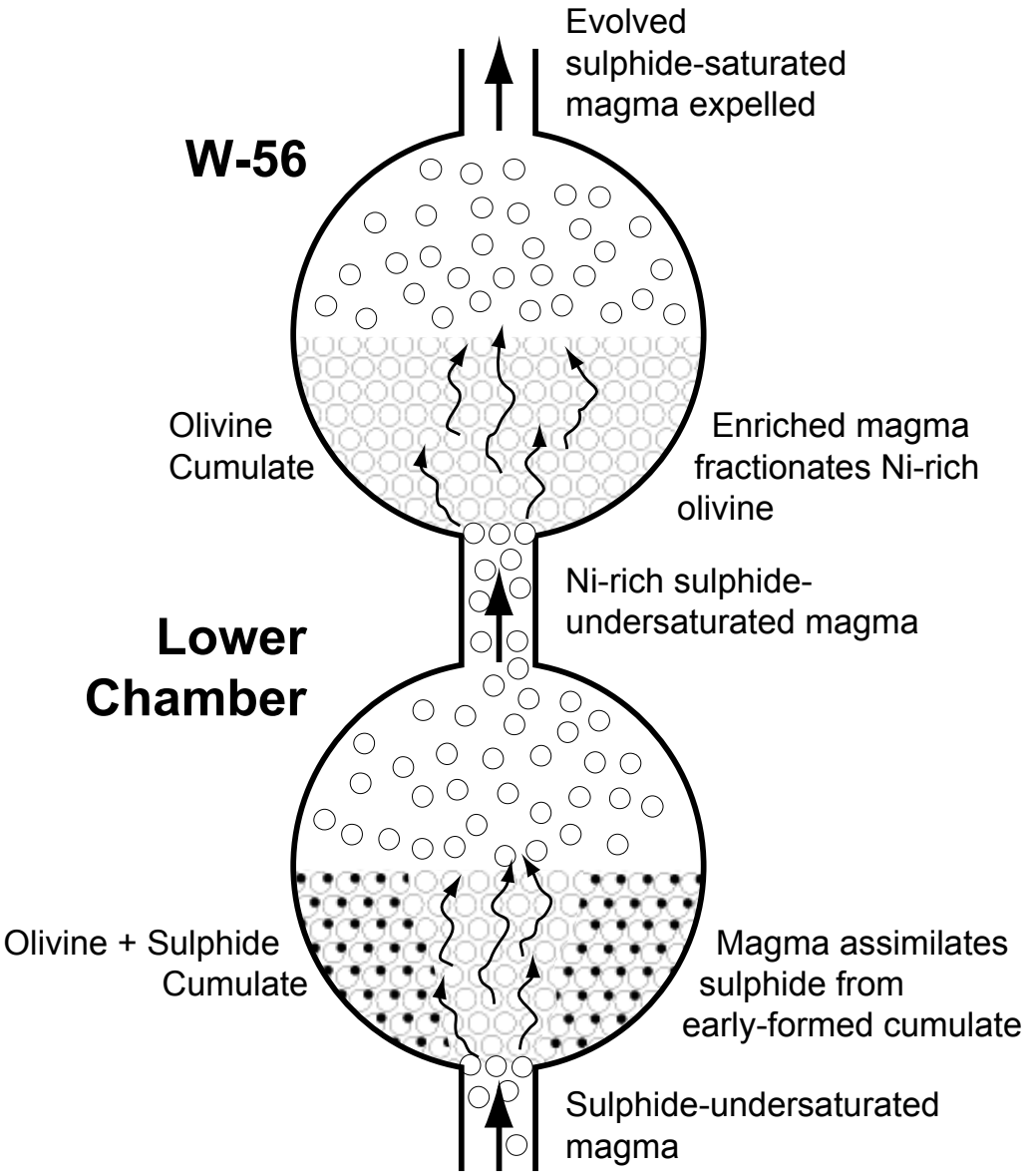

Figure 8.10 A model for the development of high Ni contents in the olivines of the W-56 ultramafic body. For details, see text.

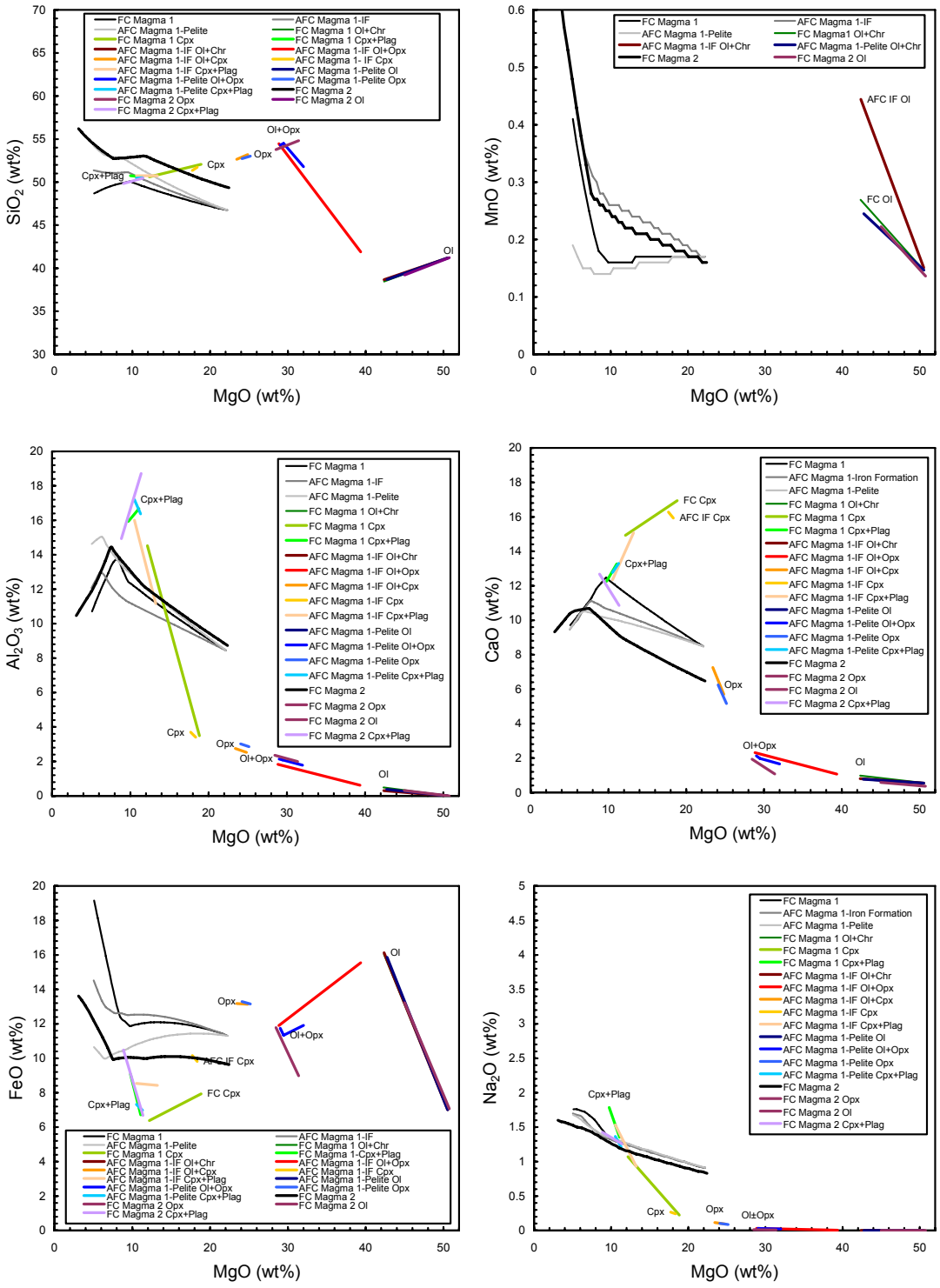

Figure 8.11 Plots of major element compositions of liquids (grey and black lines) and cumulate assemblages produced during pure fractional crystallization of an ultramafic magma (Magmas 1 & 2: green and purple lines) or fractionation with the assimilation of either a pelitic (blue lines), or an iron-rich (red lines) component by Magma 1. AFC calculations performed using the MELTS program of Ghiorso & Sack (1995).

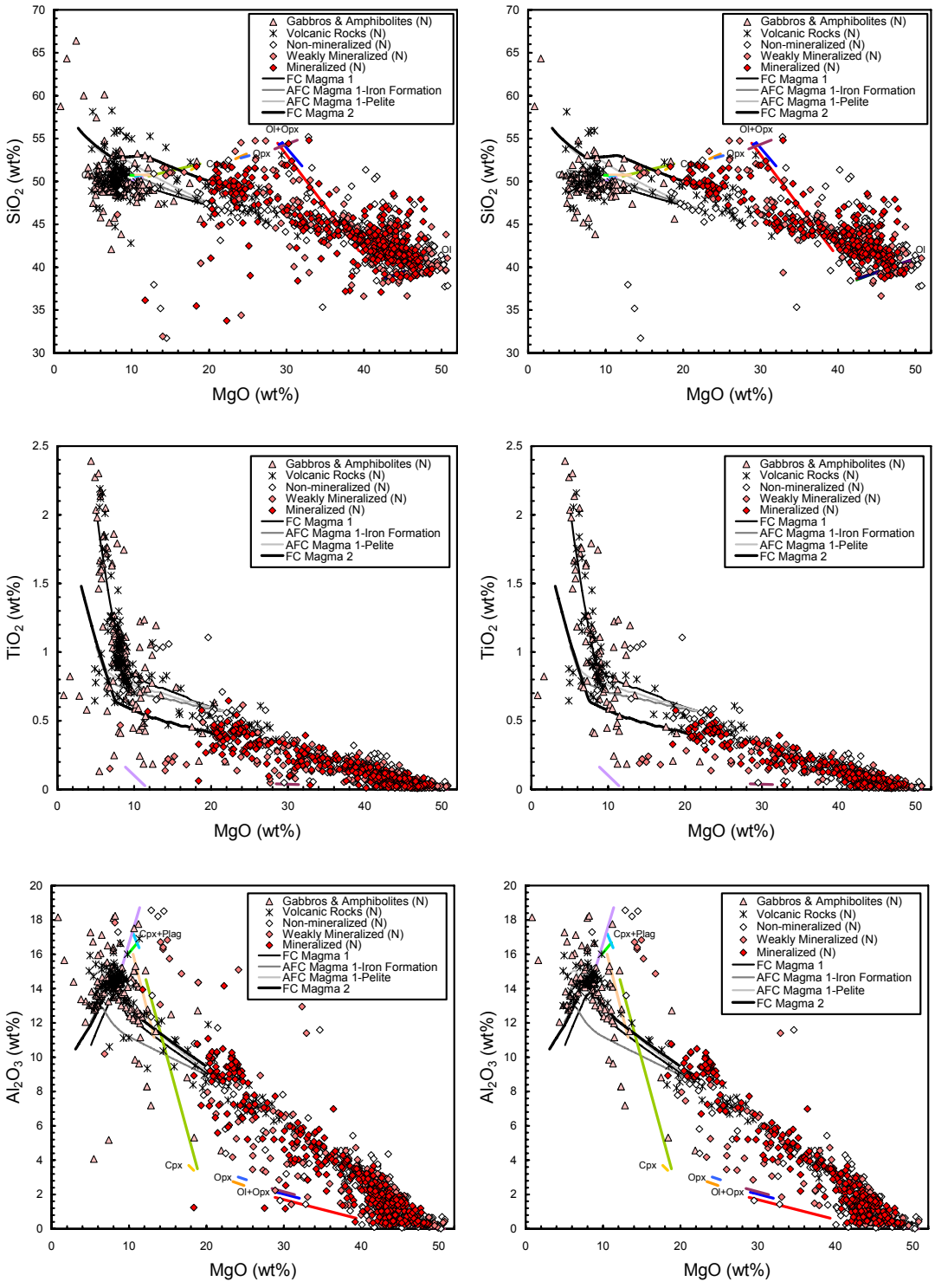

Figure 8.12 Plots of major element compositions as a function of MgO content for mafic and ultramafic rocks from the northern region of the TNB. Left, all data. Right, data for samples with < 1% sulfur (~ 2.5% sulfide). Data are broken down according to lithology and the mineralization status of ultramafic body (see **Appendix 2**). Fractionation trends and cumulate assemblages as shown in **Figure 8.11**.

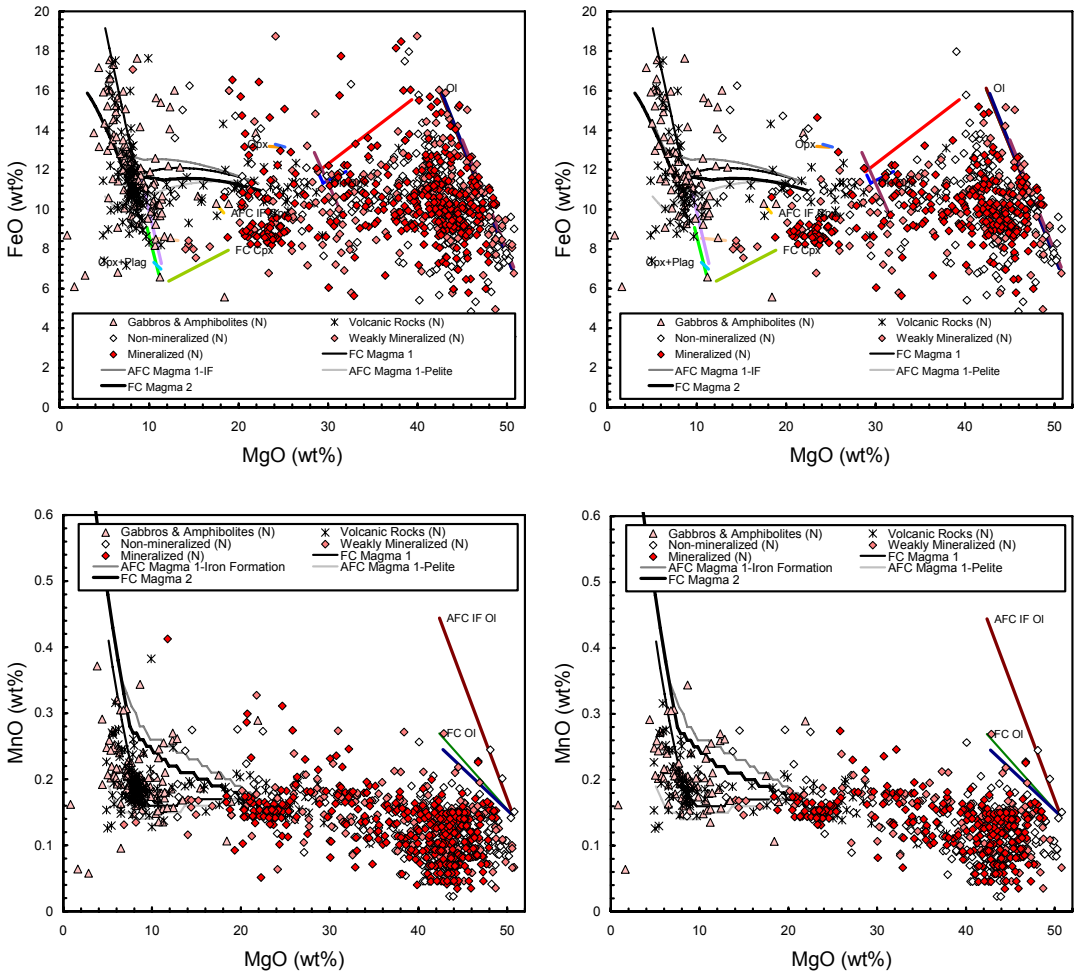

Figure 8.12 (cont.) Plots of major element compositions as a function of MgO content for mafic and ultramafic rocks from the northern region of the TNB. Left, all data. Right, data for samples with < 1% sulfur (~ 2.5% sulfide). Data are broken down according to lithology and the mineralization status of ultramafic body (see **Appendix 2**). Fractionation trends and cumulate assemblages as shown in **Figure 8.11**.

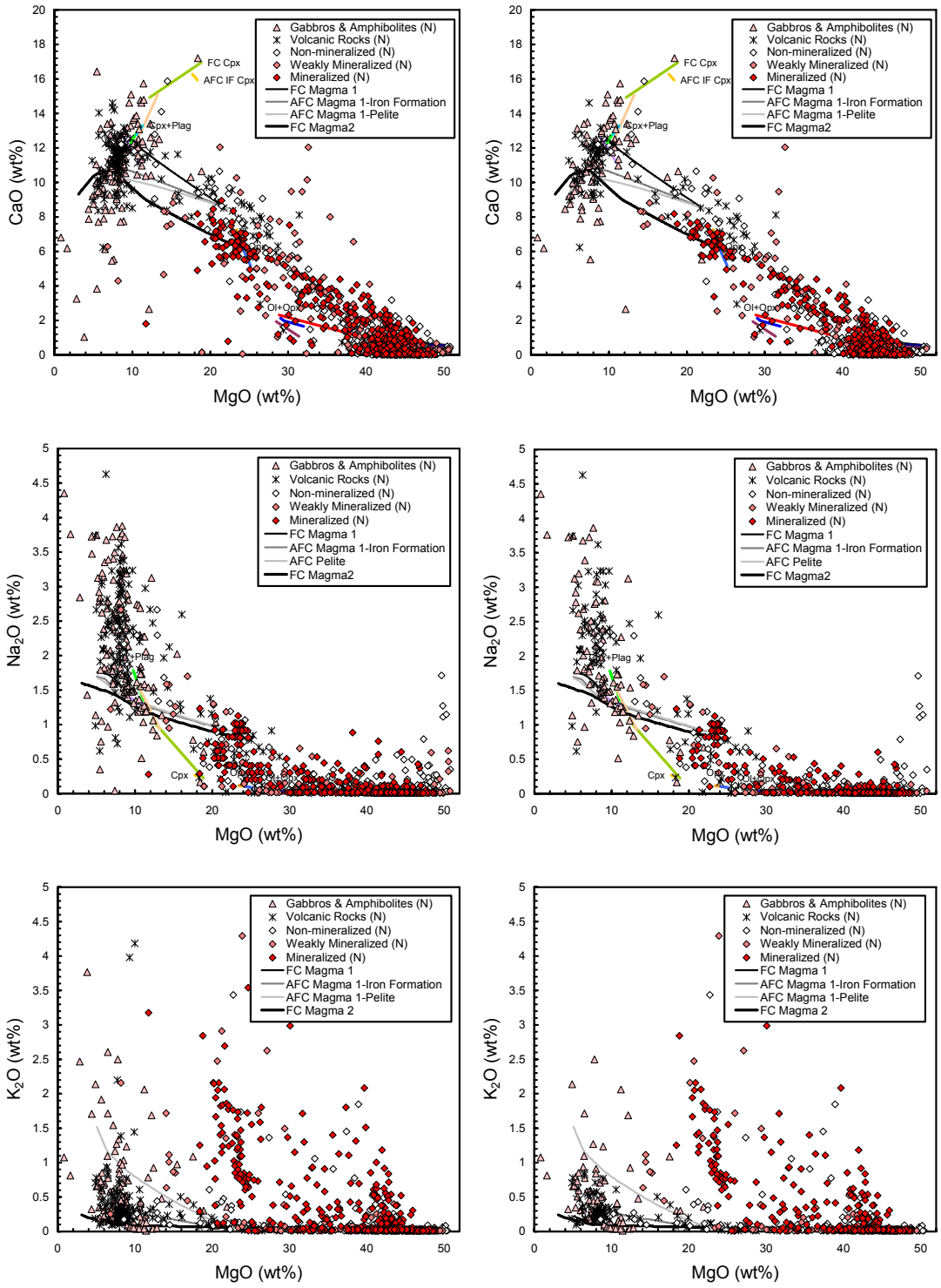

Figure 8.12 (cont.) Plots of major element compositions as a function of MgO content for mafic and ultramafic rocks from the northern region of the TNB. Left, all data. Right, data for samples with < 1% sulfur (~ 2.5% sulfide). Data are broken down according to lithology and the mineralization status of ultramafic body (see **Appendix 2**). Fractionation trends and cumulate assemblages as shown in **Figure 8.11**.

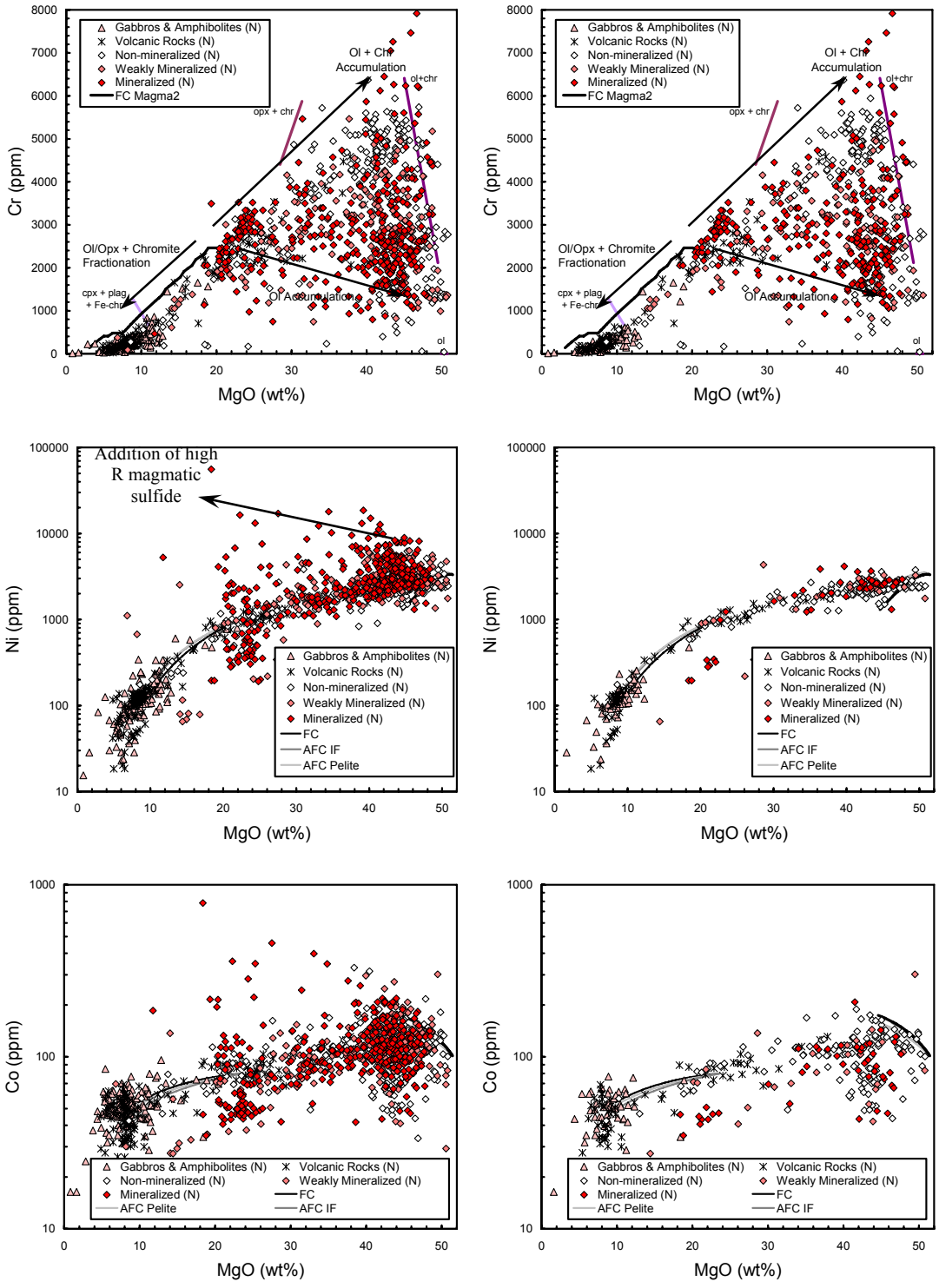

Figure 8.12 (cont.) Plots of compatible minor element contents versus MgO content for mafic and ultramafic rocks from the northern region of the TNB. Left, all data. Right, data for samples with < 0.1% sulfur (~ 0.25% sulfide). Data are broken down according to lithology and the mineralization status of ultramafic body (see **Appendix 2**). Fractionation trends calculated using the MELTS program of Ghiorso & Sack (1995) for MgO and iterative mass balance calculations using the bulk partition coefficients for Ni and Co after Beattie et al. (1991).

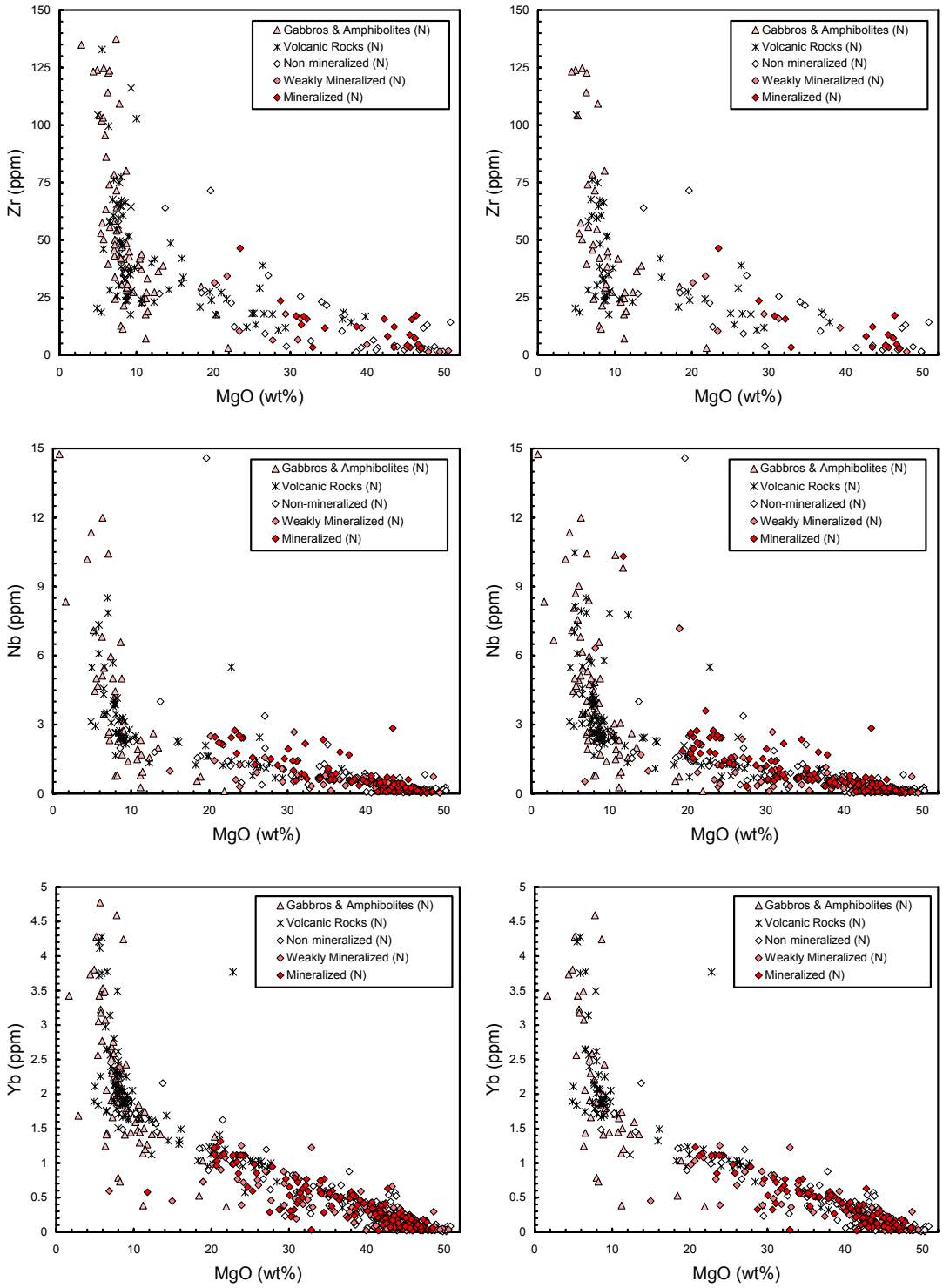

Figure 8.12 (cont.) Plots of incompatible, immobile trace element compositions as a function of MgO content for mafic and ultramafic rocks from the northern region of the TNB. Left, all data. Right, data for samples with < 1% sulfur (~ 2.5% sulfide). Data are broken down according to the mineralization status of ultramafic body (see **Appendix 2**).

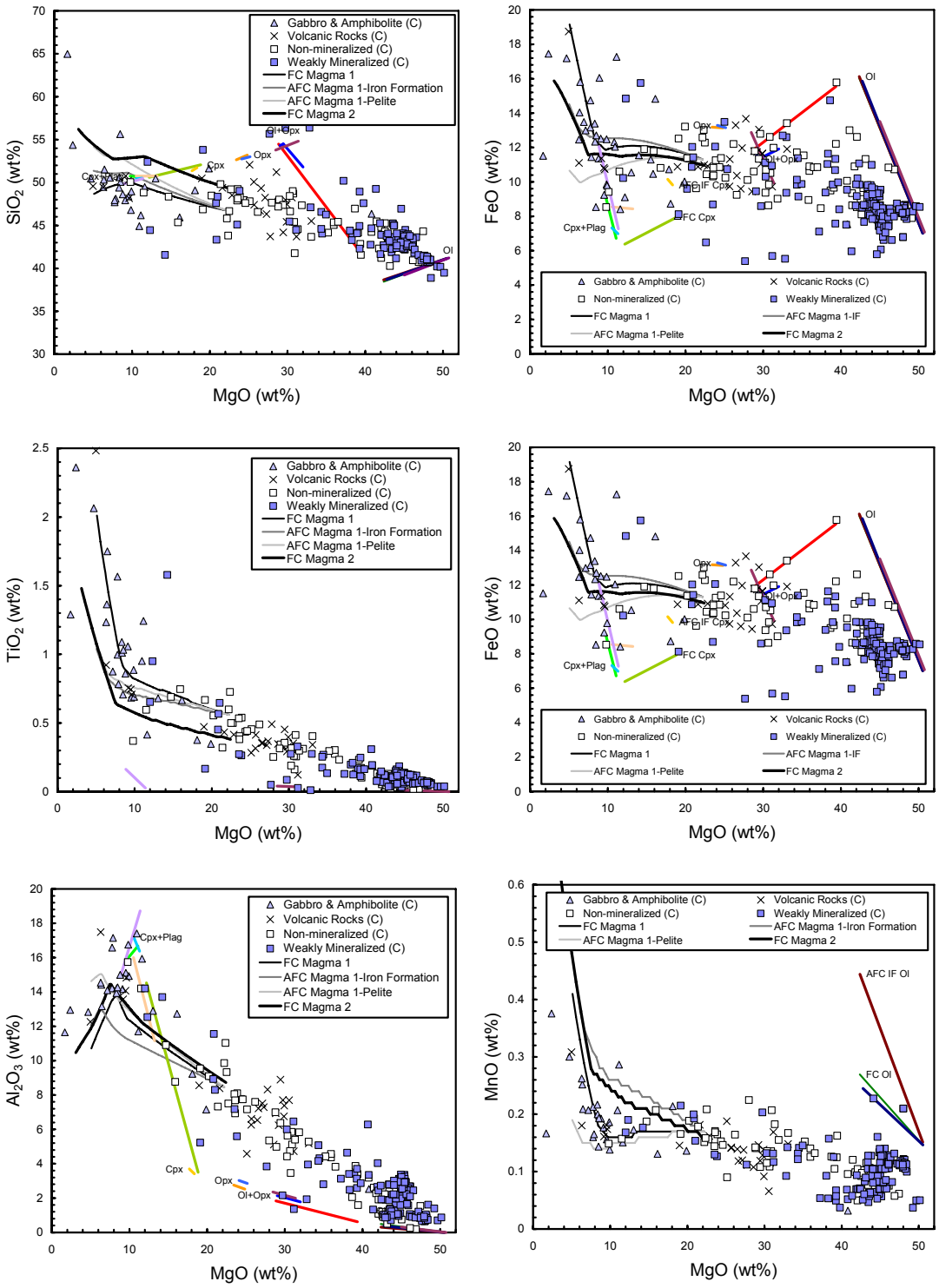

Figure 8.13 Plots of major element compositions as a function of MgO content for mafic and ultramafic rocks from the central region of the TNB. Data are broken down according to lithology and the mineralization status of ultramafic bodies (see **Appendix 2**). Fractionation trends and cumulate assemblages as shown in **Figure 8.11**.

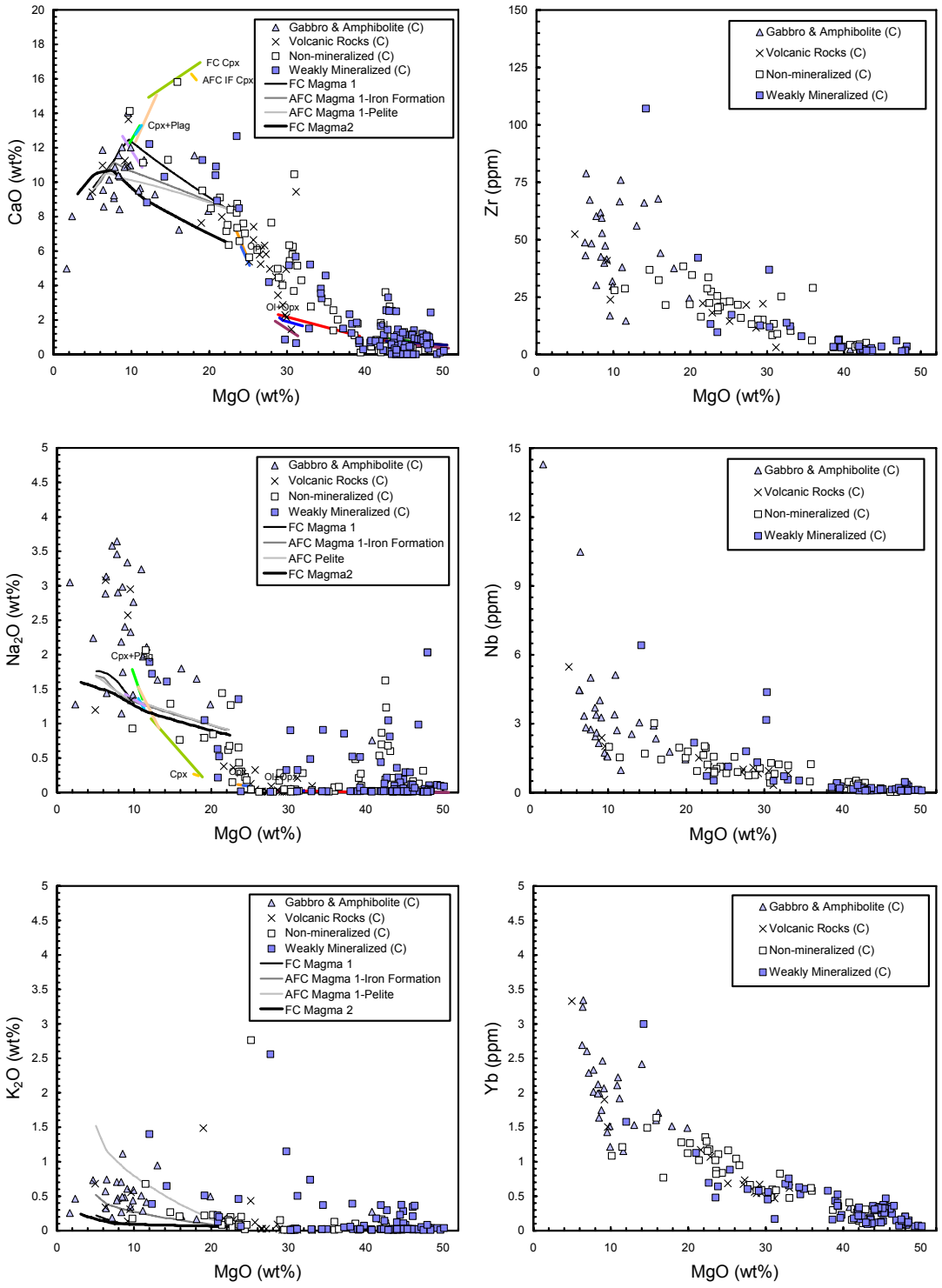

Figure 8.13 (cont.) Plots of incompatible major and trace element compositions as a function of MgO content for mafic and ultramafic rocks from the central region of the TNB. Left, all data. Right, data for samples with < 1% sulfur (~ 2.5% sulfide). Data are broken down according to the mineralization status of ultramafic body (see **Appendix 2**). Fractionation trends and cumulate assemblages as shown in **Figure 8.11**.

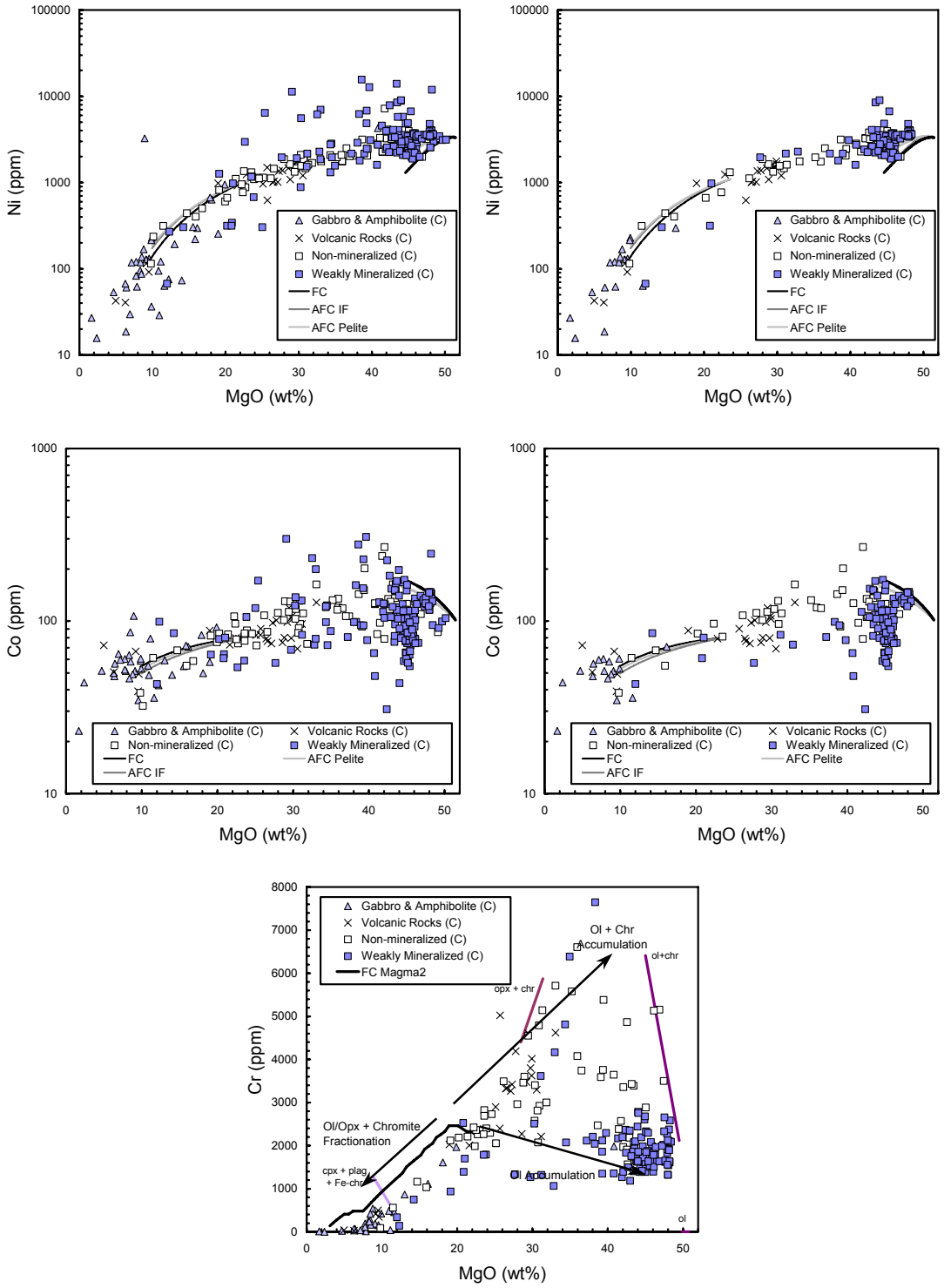

Figure 8.13 (cont.) Plots of compatible minor element contents versus MgO content for mafic and ultramafic rocks from the central region of the TNB. Left, all data. Right, data for samples with < 0.1% sulfur (~ 0.25% sulfide). Data are broken down according to lithology and the mineralization status of ultramafic body (see **Appendix 2**). Fractionation trends calculated using the MELTS program of Ghiorso & Sack (1995) for MgO and iterative mass balance calculations using the bulk partition coefficients for Ni and Co after Beattie et al. (1991).

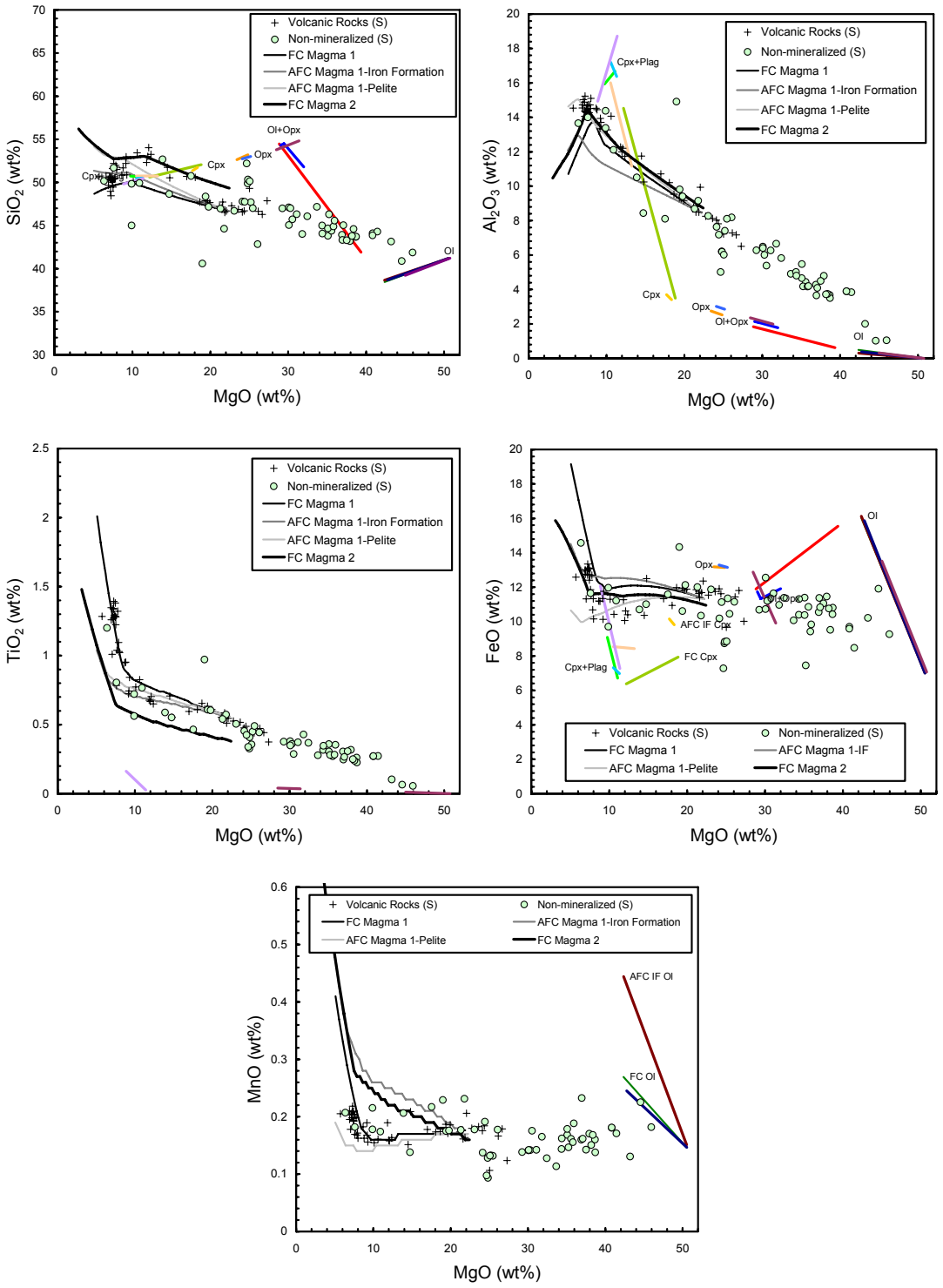

Figure 8.14 Plots of major element compositions as a function of MgO content for mafic and ultramafic rocks from the southern region of the TNB. Data are broken down according to lithology and the mineralization status of ultramafic bodies (see **Appendix 2**). Fractionation trends and cumulate assemblages as shown in **Figure 8.11**.

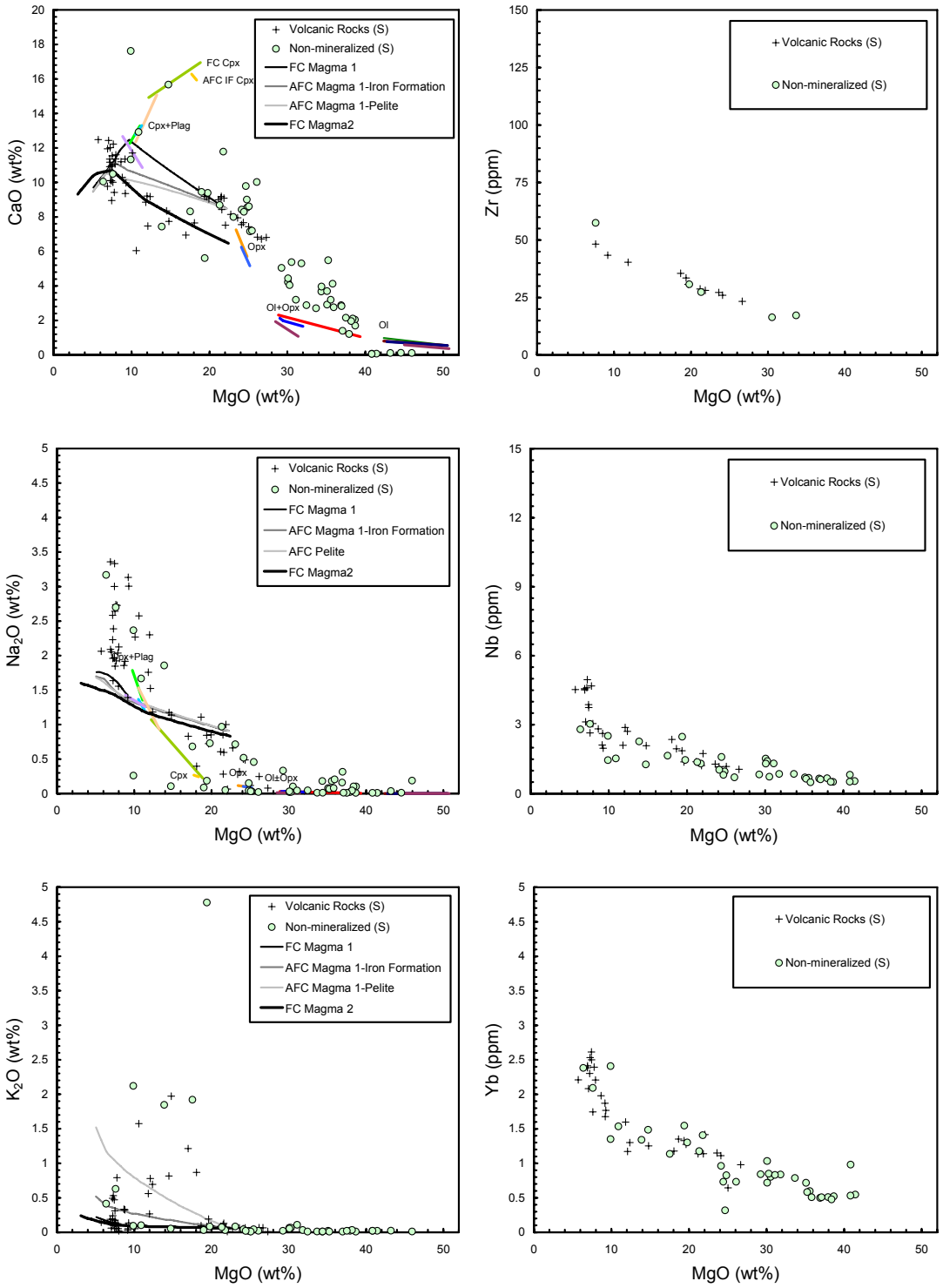

Figure 8.14 (cont.) Plots of incompatible major and trace element compositions as a function of MgO content for mafic and ultramafic rocks from the southern region of the TNB. Left, all data. Right, data for samples with < 1% sulfur (~ 2.5% sulfide). Data are broken down according to the mineralization status of ultramafic body (see **Appendix 2**). Fractionation trends and cumulate assemblages as shown in **Figure 8.11**.

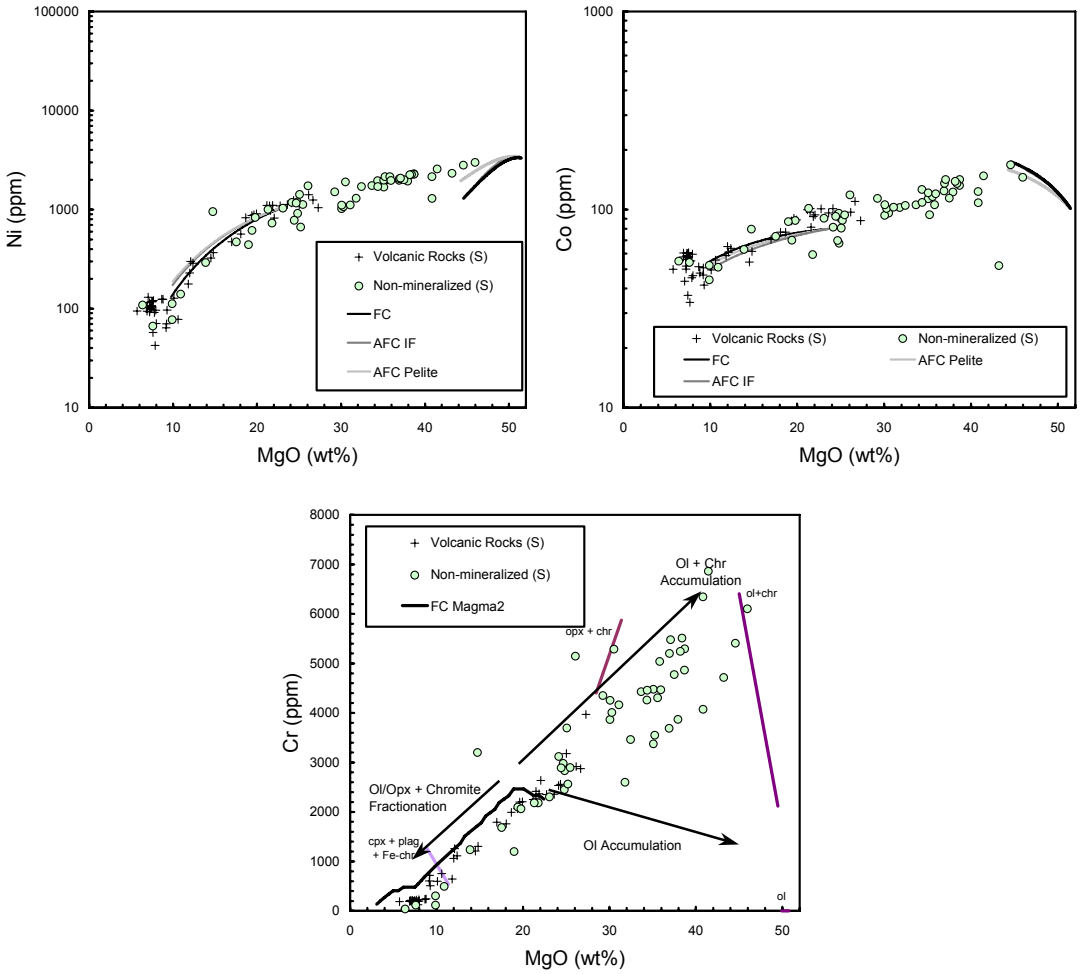

Figure 8.14 (cont.) Plots of compatible minor element contents versus MgO content for mafic and ultramafic rocks from the southern region of the TNB. Left, all data. Right, data for samples with < 0.1% sulfur (~ 0.25% sulfide). Data are broken down according to lithology and the mineralization status of ultramafic body (see **Appendix 2**). Fractionation trends calculated using the MELTS program of Ghiorso & Sack (1995) for MgO and iterative mass balance calculations using the bulk partition coefficients for Ni and Co after Beattie et al. (1991).

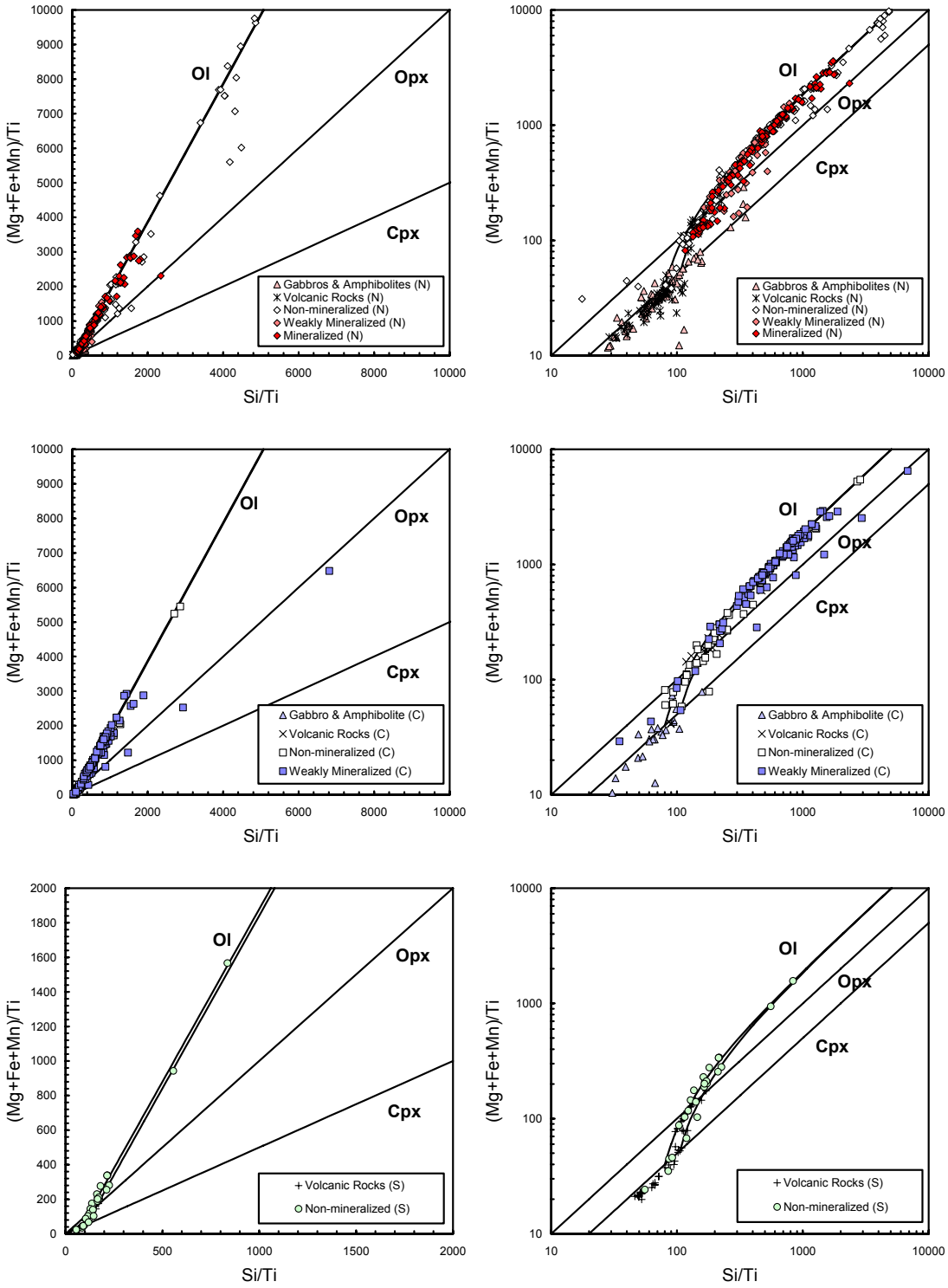

Figure 8.15 Pearce element ratio plots of molar (Mg + Fe + Mn)/Ti vs. Si/Ti for sulfide-poor (S < 0.3 wt%) samples from TNB ultramafic bodies. Top, Northern TNB; centre, Central TNB; bottom, Southern TNB. Right figures present the same data plotted on a log scale. Two alternative olivine fractionation lines are plotted for alternative initial magma compositions in the upper figures.

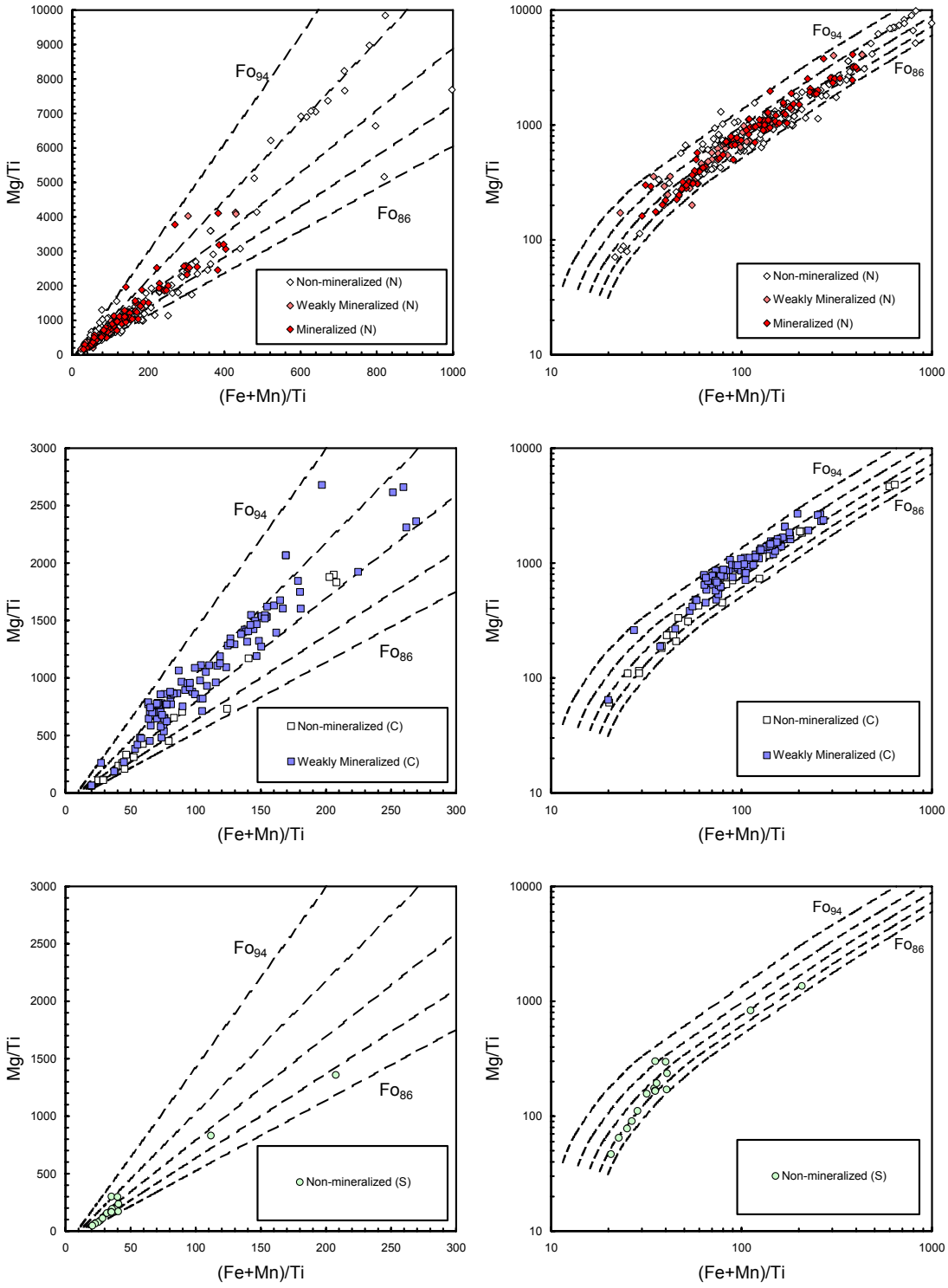

Figure 8.16 Pearce element ratio plots of molar Mg/Ti vs. (Fe+Mn)/Ti for S-poor (S<0.3%) mafic and ultramafic rocks from the central region of the TNB. Right figures present the same data plotted on a log scale. Trends expected for olivine composition from Fo_{86} to Fo_{94} plotted as dashed lines in each figure.

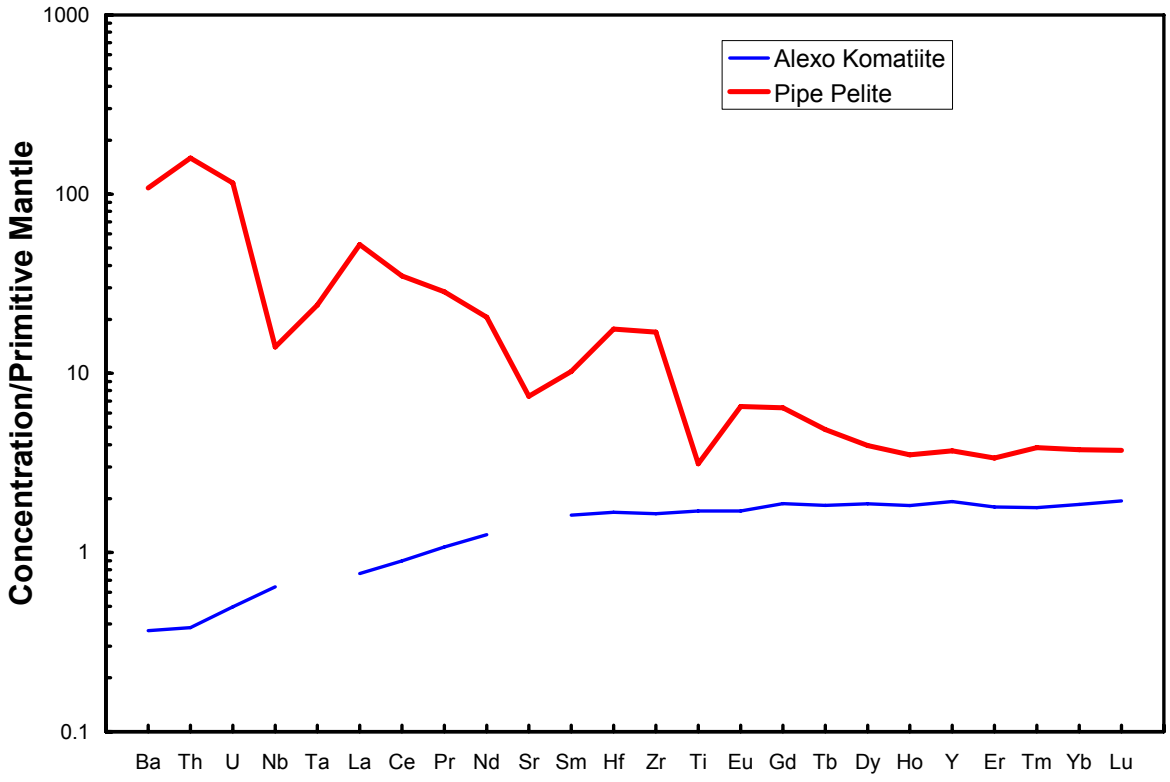

Figure 8.17 Comparison of typical trace element patterns for a komatiitic magma and upper crustal sediments. Data for Alexo komatiite from Lahaye & Arndt (1996). Data for Pipe pelite from sample CHA 33 (this study).

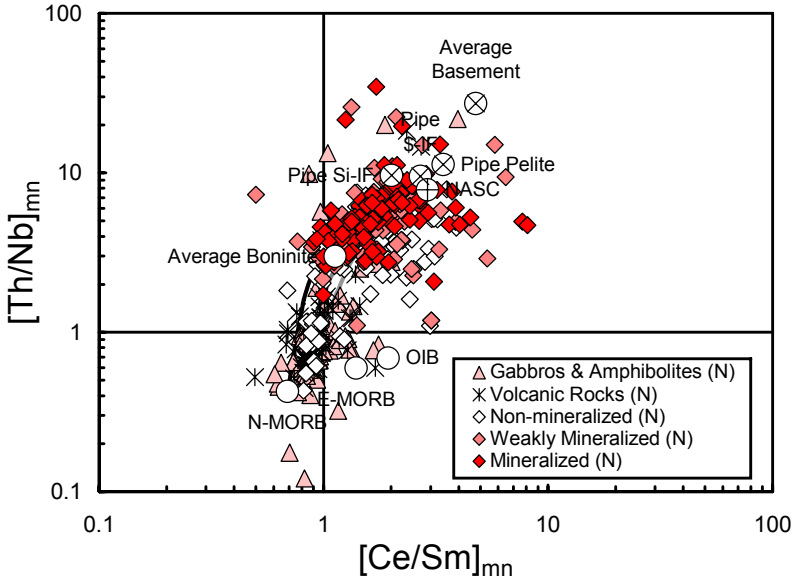

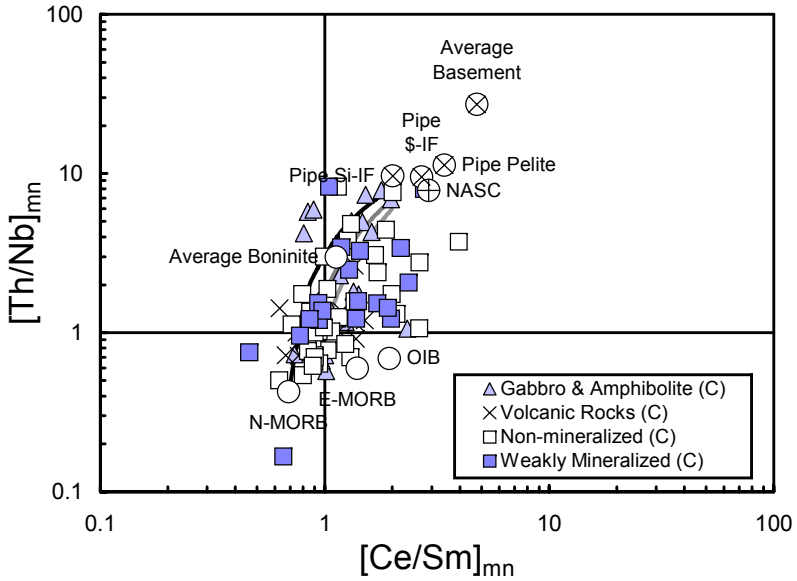

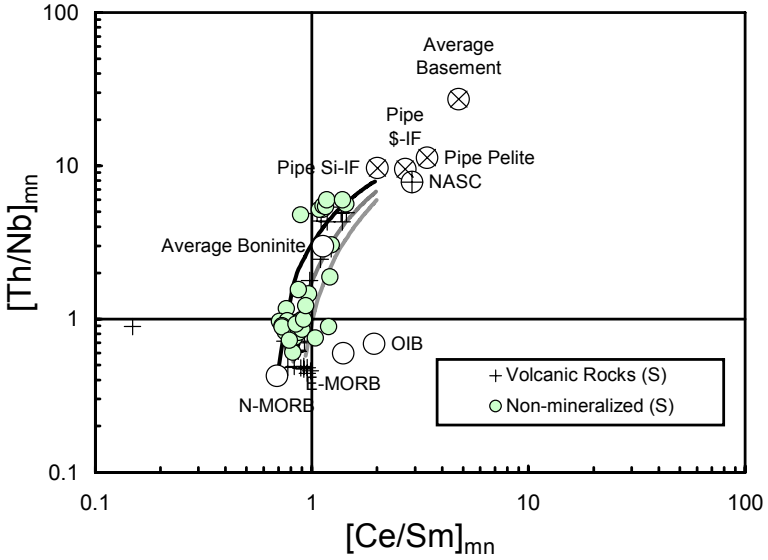

Figure 8.18 [La/Sm]mn vs.[Th/Nb]mn for ultramafic bodies of the TNB. Only samples with concentrations significantly above detection limit are plotted (Nb > 0.04ppm, Th > 0.04ppm, Ce > 0.17 ppm, Sm > 0.1 ppm). Mantle normalization values from McDonough and Sun (1995). Reference compositions: N-MORB, Normal MORB, Sun and McDonough (1989); E-MORB, enriched MORB, Sun and McDonough(1989); OIB, Ocean Island Basalt, trace elements from Taylor and McLennan (1985); Average Boninite, compiled from the Georoc database (http://georoc.mpch-mainz.gwdg.de/) by N.T. Arndt, pers. comm. (2002); NASC, North American Shale Composite, Gromet et al. (1984); Pipe $-IF, lowermost sulfide facies iron formation from Pipe Pit (CHA-35); Pipe Si-IF, P3 silicate facies iron formation from Pipe Pit (CHA125); Pipe Pelite (CHA33); Average Basement, average of 18 basement rocks collected during this project. AFC trajectories for the assimilation of pelitic sediment by olivine-saturated ultramafic magmas derived from depleted (N-MORB) or partially enriched (3% OIB component, dark grey; 6% OIB component, light grey) mantle sources are shown by thick lines.

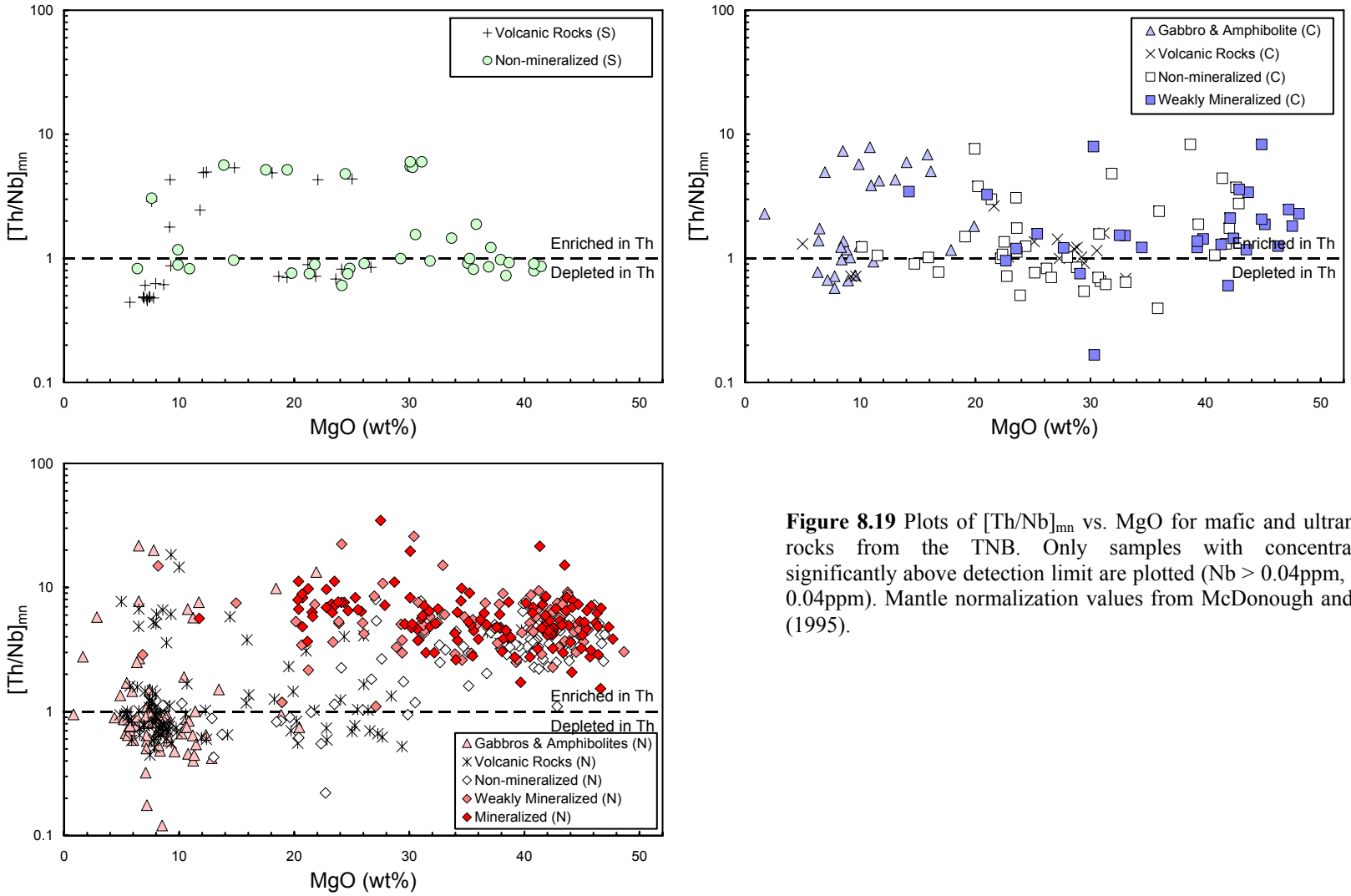

Figure 8.19 Plots of $[Th/Nb]_{mn}$ vs. MgO for mafic and ultramafic rocks from the TNB. Only samples with concentrations significantly above detection limit are plotted (Nb > 0.04ppm, Th > 0.04ppm). Mantle normalization values from McDonough and Sun (1995).

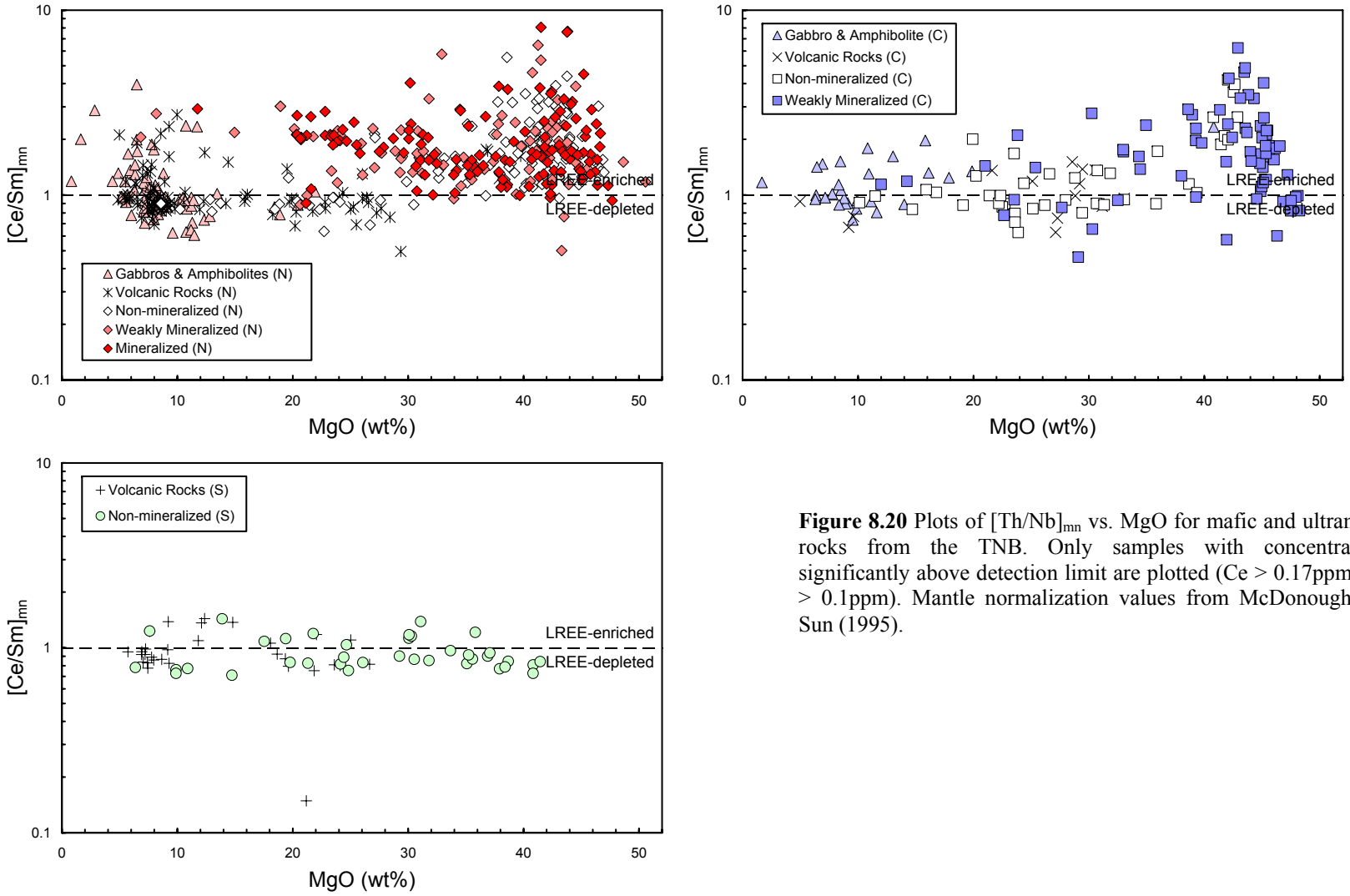

Figure 8.20 Plots of $[Th/Nb]_{mn}$ vs. MgO for mafic and ultramafic rocks from the TNB. Only samples with concentrations significantly above detection limit are plotted (Ce > 0.17ppm, Sm > 0.1ppm). Mantle normalization values from McDonough and Sun (1995).

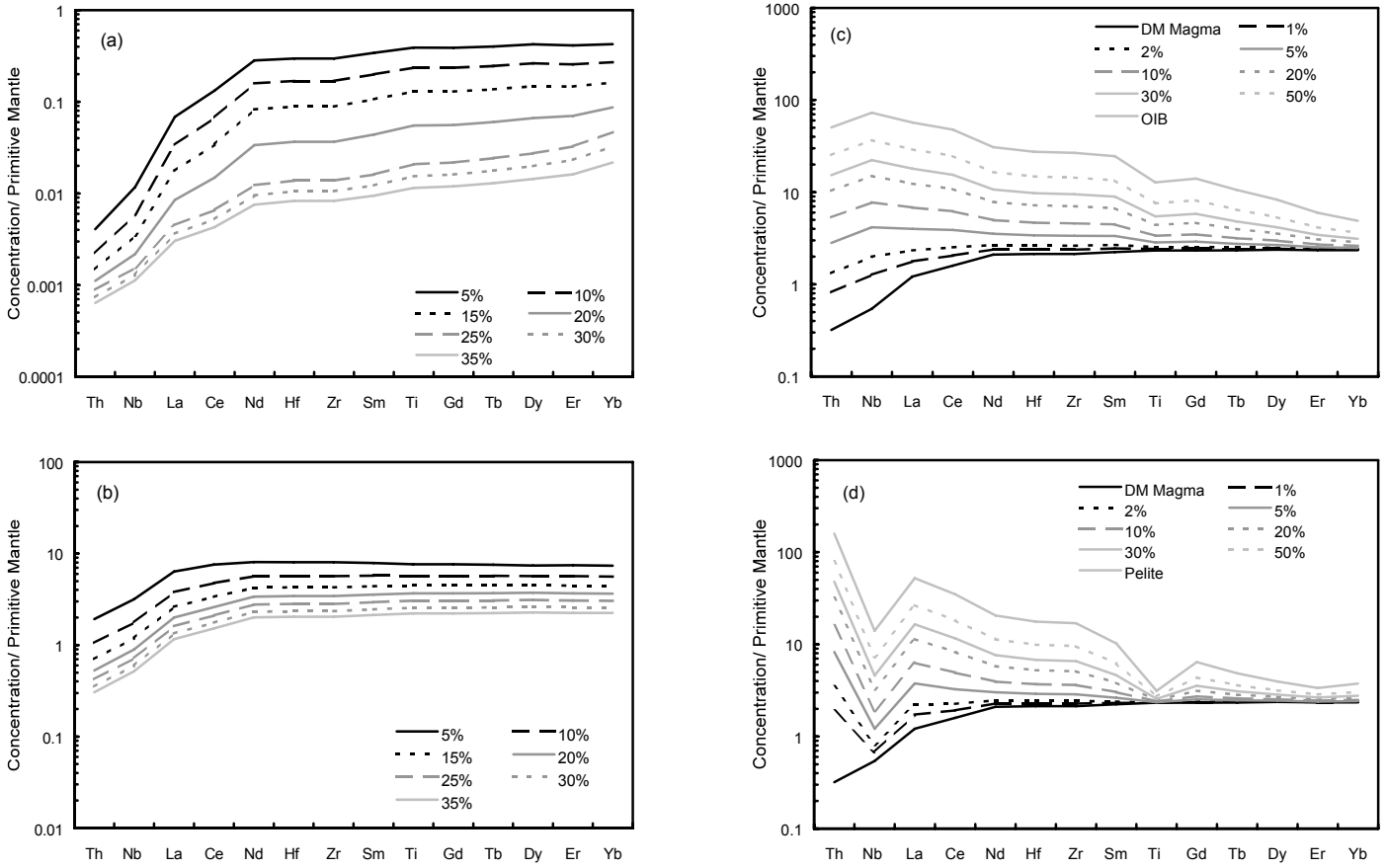

Figure 8.21 Condensed mantle normalized multi-element plot illustrating the expected trace element variations in a) residues after melt extraction from a primitive mantle source, b) melts derived from a mildly depleted mantle source (2% melt extraction), leading to pronounced depletion in Th and Nb relative to Ti, c) mixtures between magmas produced from depleted, N-MORB-like magmas (DM Magma) and a plume component similar to ocean island basalts (OIB), and d) assimilation of a sedimentary component by magmas derived by partial melting of a mildly depleted mantle source. Neither the addition of a plume component nor the assimilation of a sedimentary component leads to significant enrichment in Ti, but both strongly enrich the magma in LREE and Th, leading to high Th/Ti ratios. Mixing with enriched-mantle melts leads to pronounced enrichment in Nb and high Nb/Ti ratios, whereas assimilation produces only mild enrichment in Nb, leading to a significant increase in Nb/Ti only at high degrees of contamination. In (a) and (b), percentages denote amount of enriched component in each mixing model. In (c) and (d), percentages denote degree of melt extraction or partial melting in figures (a) and (b), respectively.

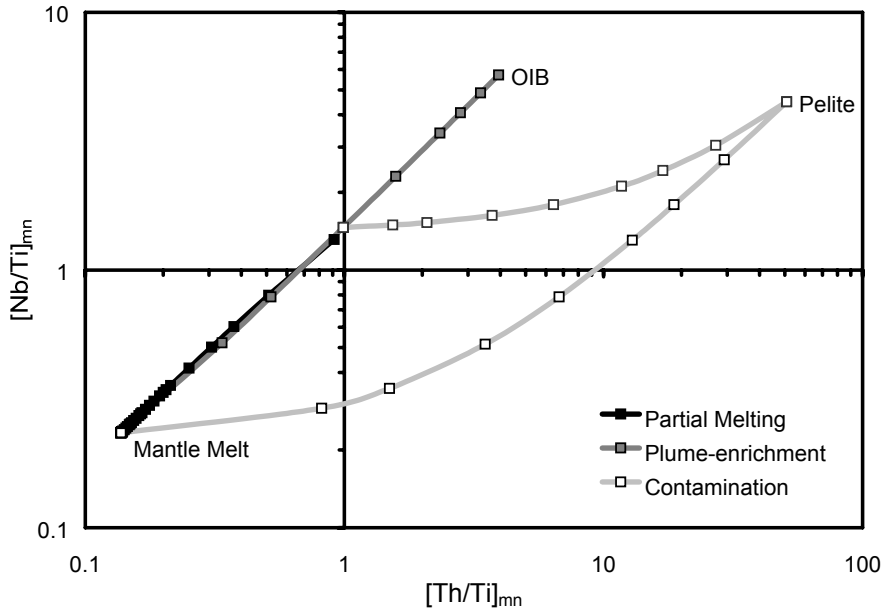

Figure 8.22 Plot of mantle-normalized Nb/Ti ratios as a function of Th/Ti for the different processes of mixing and/or contamination shown in **Figure 8.21**. Partial melting trend marked at ~1% melting intervals. Mixing trends with OIB and pelite marked at 1%, 2%, 5%, 10%, 20%, 30%, and 50% intervals. Data for OIB in from Sun & McDonough (1989). Pelite data from analyses of P_2 sediments from Pipe Pit. Mantle-normalization values from McDonough & Sun (1995). Although low degrees of partial melting can produce magmas of similar initial composition to those made by mixing magmas from enriched and depleted source regions, such low degree magmas will be magnesium-poor (< 10 wt% MgO).

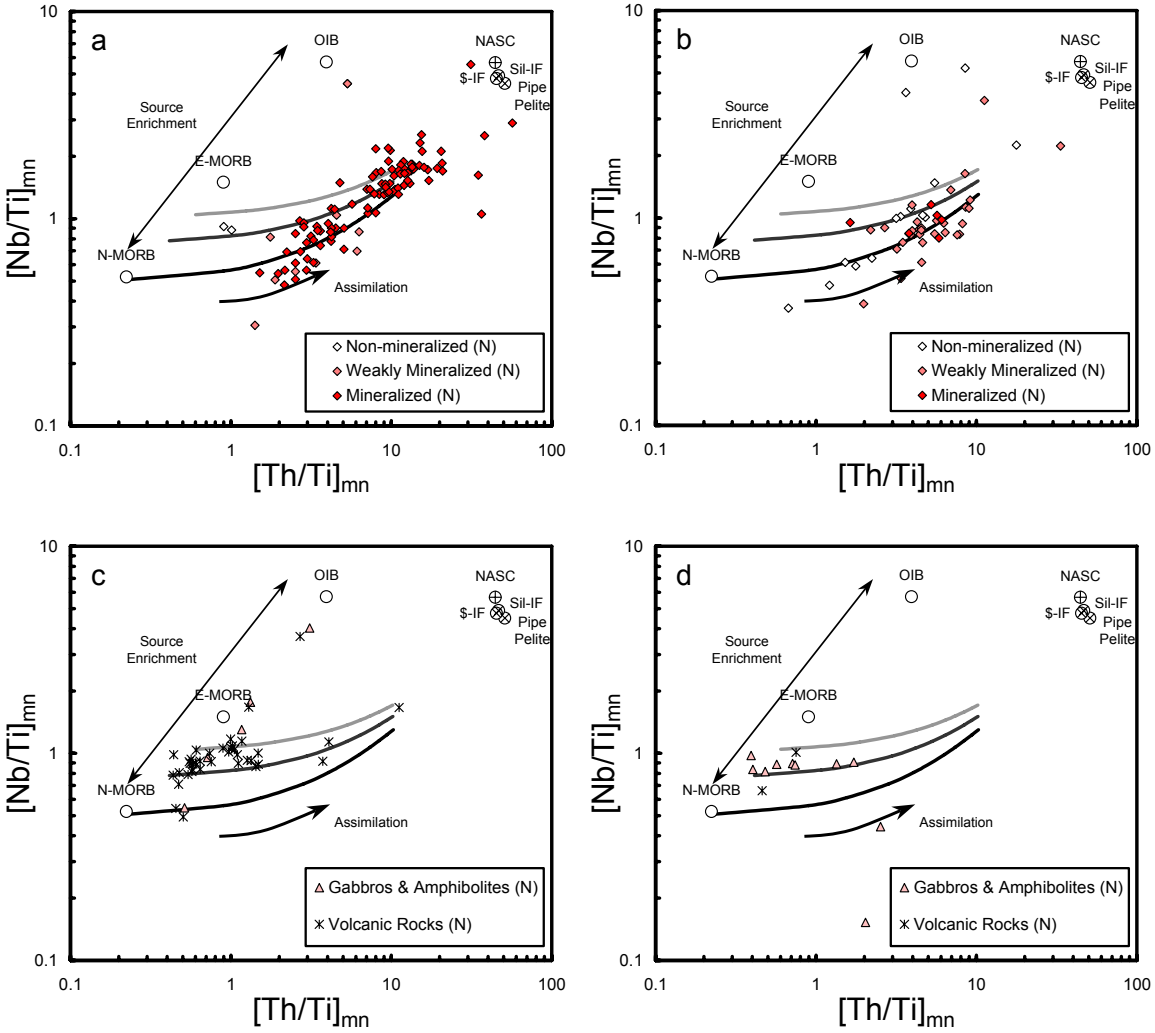

Figure 8.23 Plot of mantle-normalized Nb/Ti vs. Th/Ti for ultramafic rocks from a) Thompson, Birchtree, and Pipe, b) North Manasan, Halfway Lake and Spur South, c) volcanic rocks and dykes from the Pipe, Ospwagan Lake, Spur South, Taylor River and Halfway Lake areas, and d) Grass River and the Mystery-Moak area. Trend lines mark the AFC trajectories for the assimilation of Ospwagan Group pelitic rocks by magmas produced by high degrees of melting of N-MORB mantle containing 0%, 3% and 6% OIB component. Data for mantle components from Sun & McDonough (1989). Mantle-normalization values from McDonough & Sun (1995). Samples with low Th, Nb or Ti concentrations are excluded from the plots. Cut off values were 0.04 ppm Th, 0.04 ppm Nb and 0.05 wt% TiO_2, as determined by the reproducibility of internal standards.

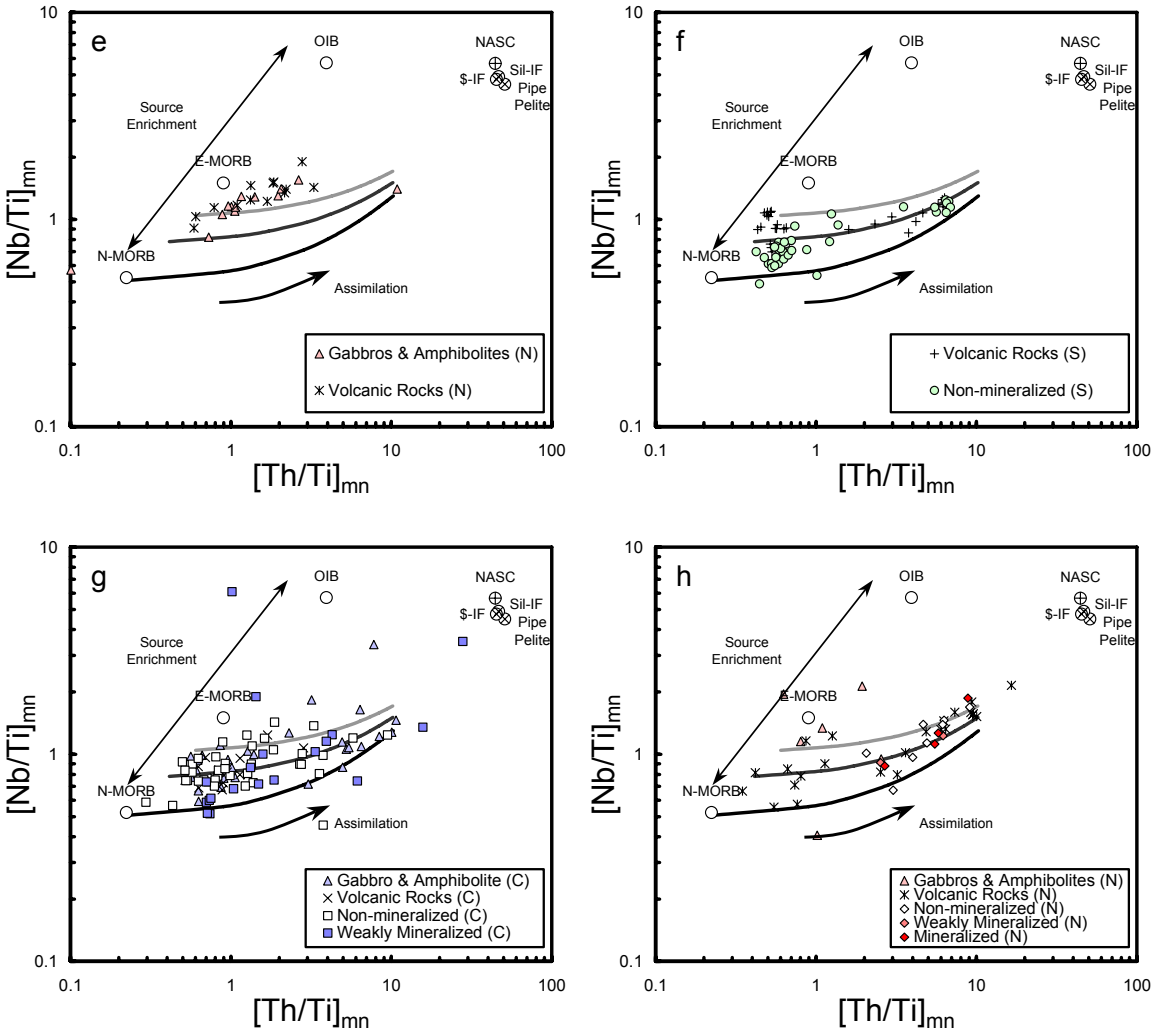

Figure 8.23 (contd.) Plot of mantle-normalized Nb/Ti vs. Th/Ti for mafic and ultramafic rocks from e) the southern part of the exposed TNB (Bah Lake, Setting Lake, Fish Lake, and Five Mile Lake), f) the southern region of the TNB (Winnipegosis komatiites), g) the central Region of the TNB (William Lake Dome, Sarak-Gormley Lake area**,** South Central TNB**,** Minago River area**,** area south of Norris Lake**,** William Lake area**,** Davidson Lake area**,** Minago River area**,** Northern Winnipegosis area), and h) the Mystery Lake area. Trend lines mark the AFC trajectories for the assimilation of Ospwagan Group pelitic rocks by magmas produced by high degrees of melting of N-MORB mantle containing 0%, 3% and 6% OIB component. Data for mantle components from Sun & McDonough (1989). Mantle-normalization values from McDonough & Sun (1995). Samples with low Th, Nb or Ti concentrations are excluded from the plots. Cut off values were 0.04 ppm Th, 0.04 ppm Nb and 0.05 wt% TiO_2, as determined by the reproducibility of internal standards.

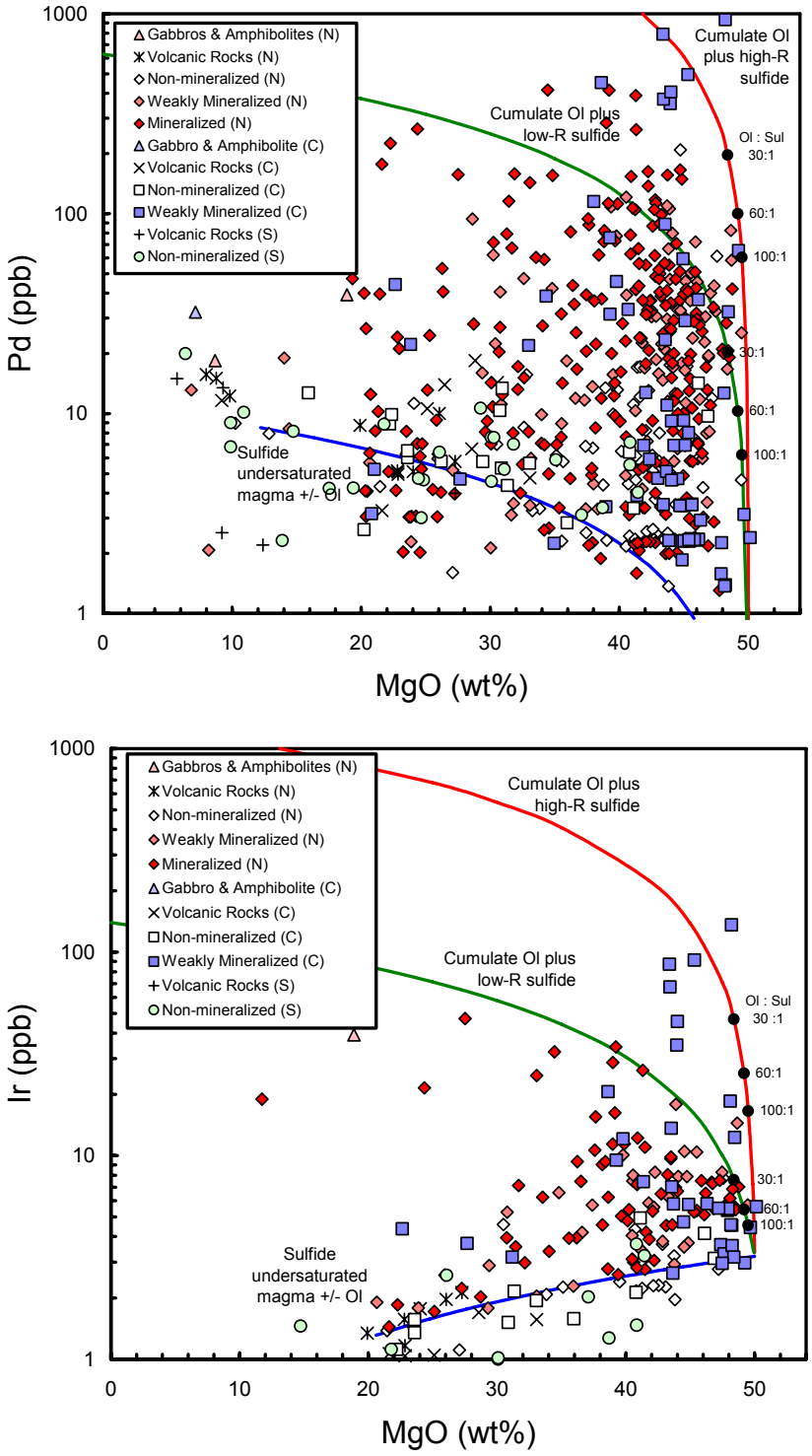

Figure 8.24 Variation in highly chalcophile element abundances as a function of MgO content for mafic and ultramafic rocks from all regions of the TNB. Red line, trend expected for an olivine adcumulate containing variable proportions of sulfide produced under high sulfide:silicate liquid ratios (R~1000). Green line, trend expected for an olivine adcumulate containing variable proportions of sulfide produced under low sulfide:silicate liquid ratios (R~100). Blue line, trend expected for a sulfide-undersaturated magma undergoing fractionation or accumulation of sulfide.

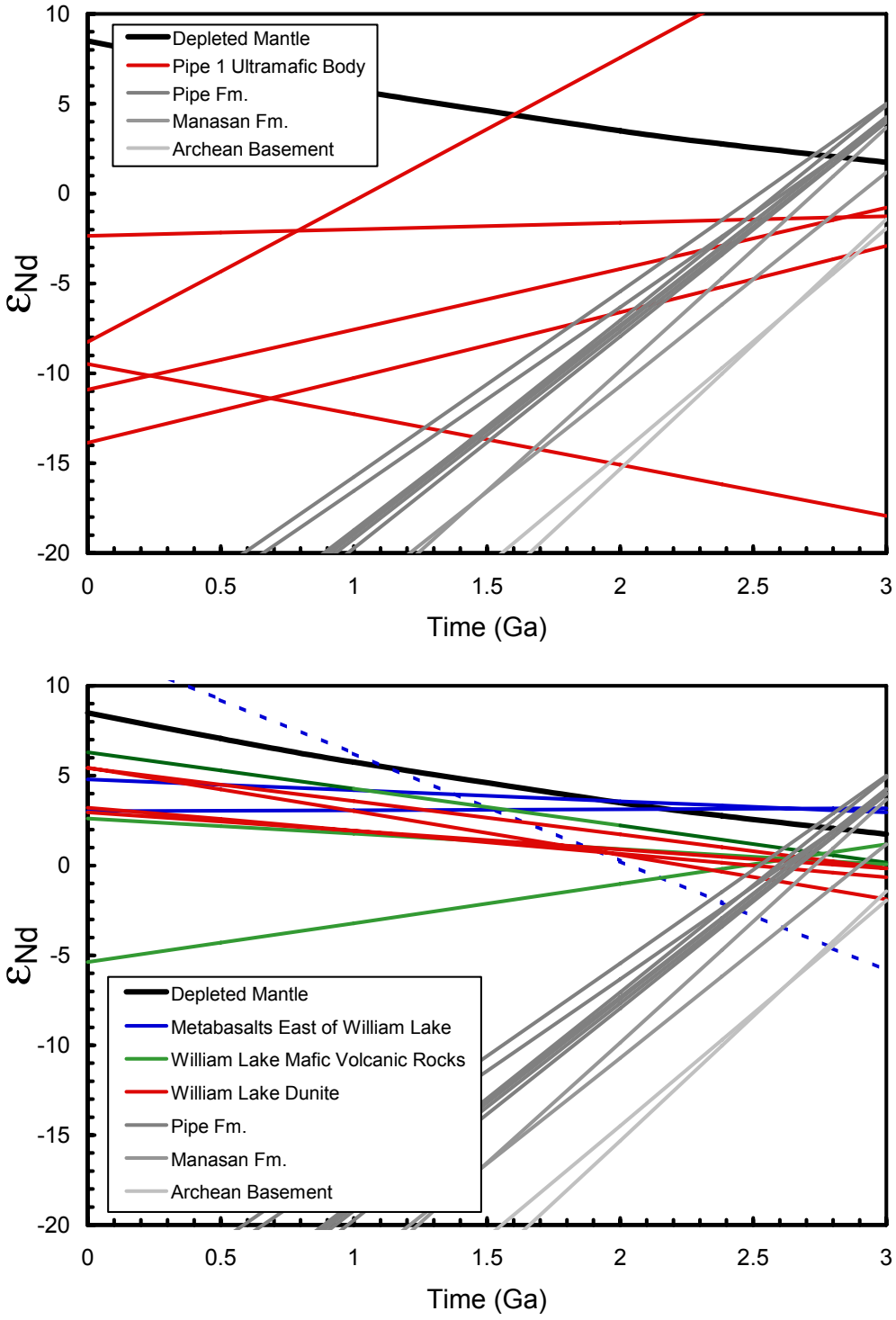

Figure 8.25 Plot of ε_{Nd} vs. time for mafic and ultramafic rocks from the Pipe 1 ultramafic body (top) and the central region of the TNB (bottom). Additional data for metasedimentary rocks of the Ospwagan Group from this study (**Section 8.4**) and Ansdell and Bleeker (1997). Depleted Mantle evolution curve from Ben Othman et al. (1984).

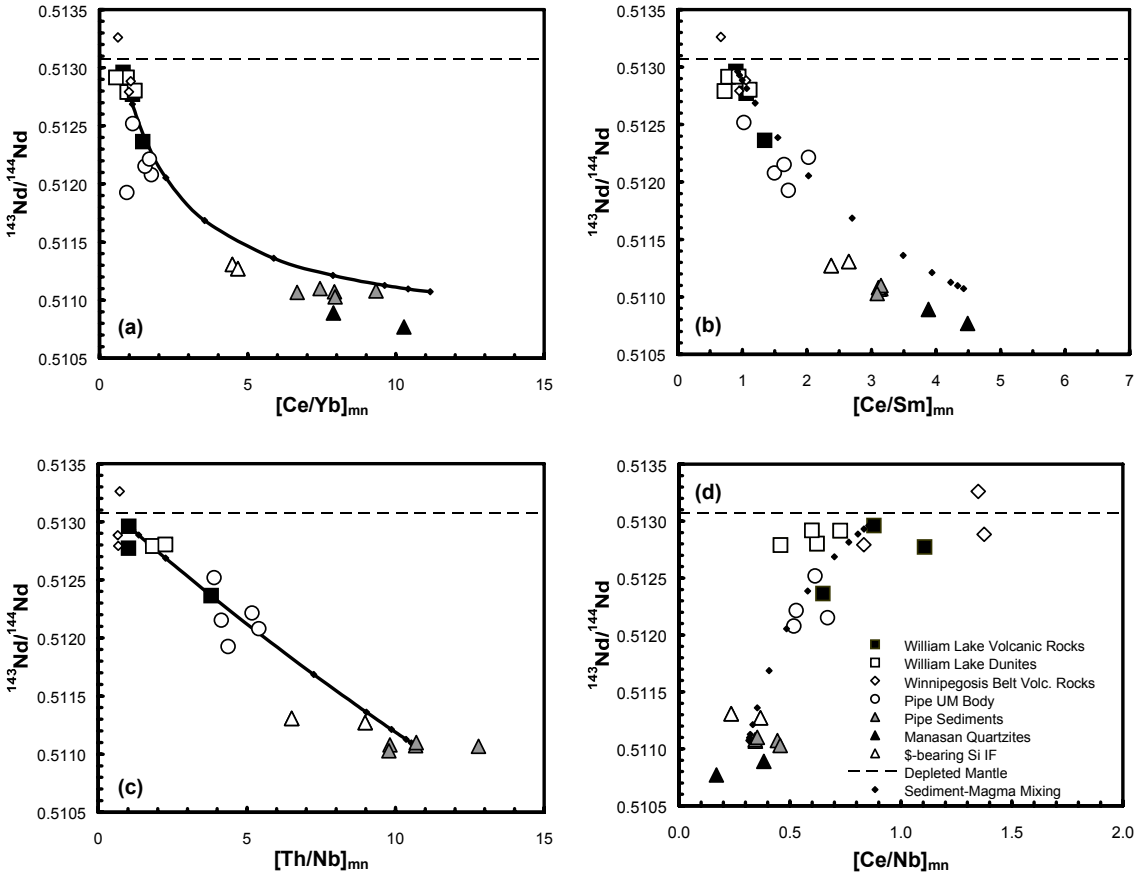

Figure 8.26 $^{143}Nd/^{144}Nd$ plotted as a function of incompatible element enrichment. a) mantle-normalized Ce/Yb, b) mantle-normalized Ce/Sm, c) mantle-normalized Th/Nb; and d) mantle-normalized Nb/Ce. Mantle-normalization values from McDonough & Sun (1995).

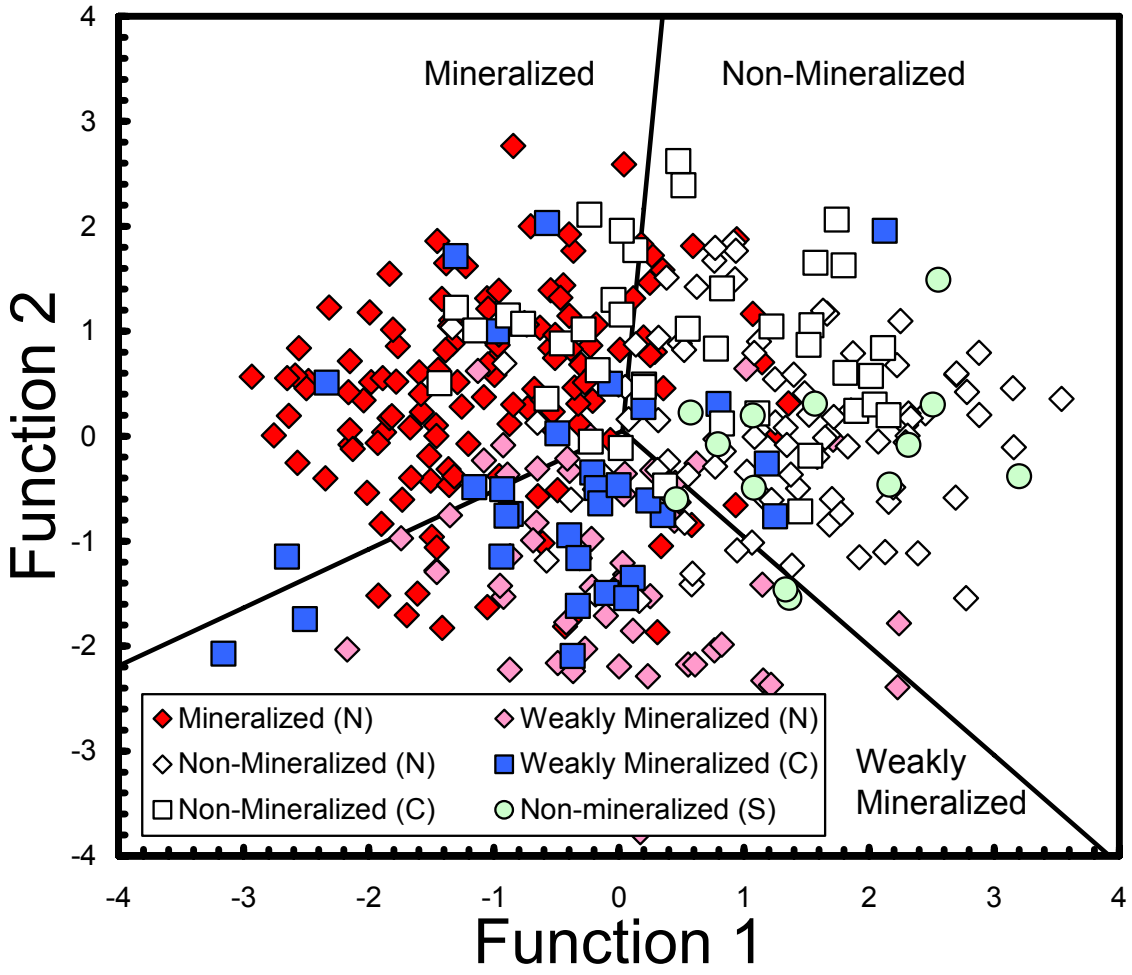

Figure 8.27 Discriminant function plot showing data for all TNB ultramafic bodies.

Function 1 = 0.091 SiO_2 + 2.193 log (TiO_2) - 3.273 log (Al_2O_3) + 0.222 FeO^t - 0.039 MgO - 0.468 log (CaO) + 1.158 log (Cr) - 1.146 log (Ni) - 0.872 log (Zn) - 0.396 log (Hf) + 0.821 log (Nb) - 1.725 log (Th) + 1.812 log (Yb) - 0.743 log (S) - 1.171

Function 2 = 0.188 SiO_2 - 0.267 log (TiO_2) - 1.903 log (Al_2O_3) + 0.319 FeO^t + 0.119 MgO + 0.402 log (CaO) + 1.41 log (Cr) - 1.476 log (Ni) + 0.426 log (Zn) + 2.234 log (Hf) + 1.05 log (Nb) - 0.702 log (Th) + 0.638 log (Yb) + 0.238 log (S) - 15.031

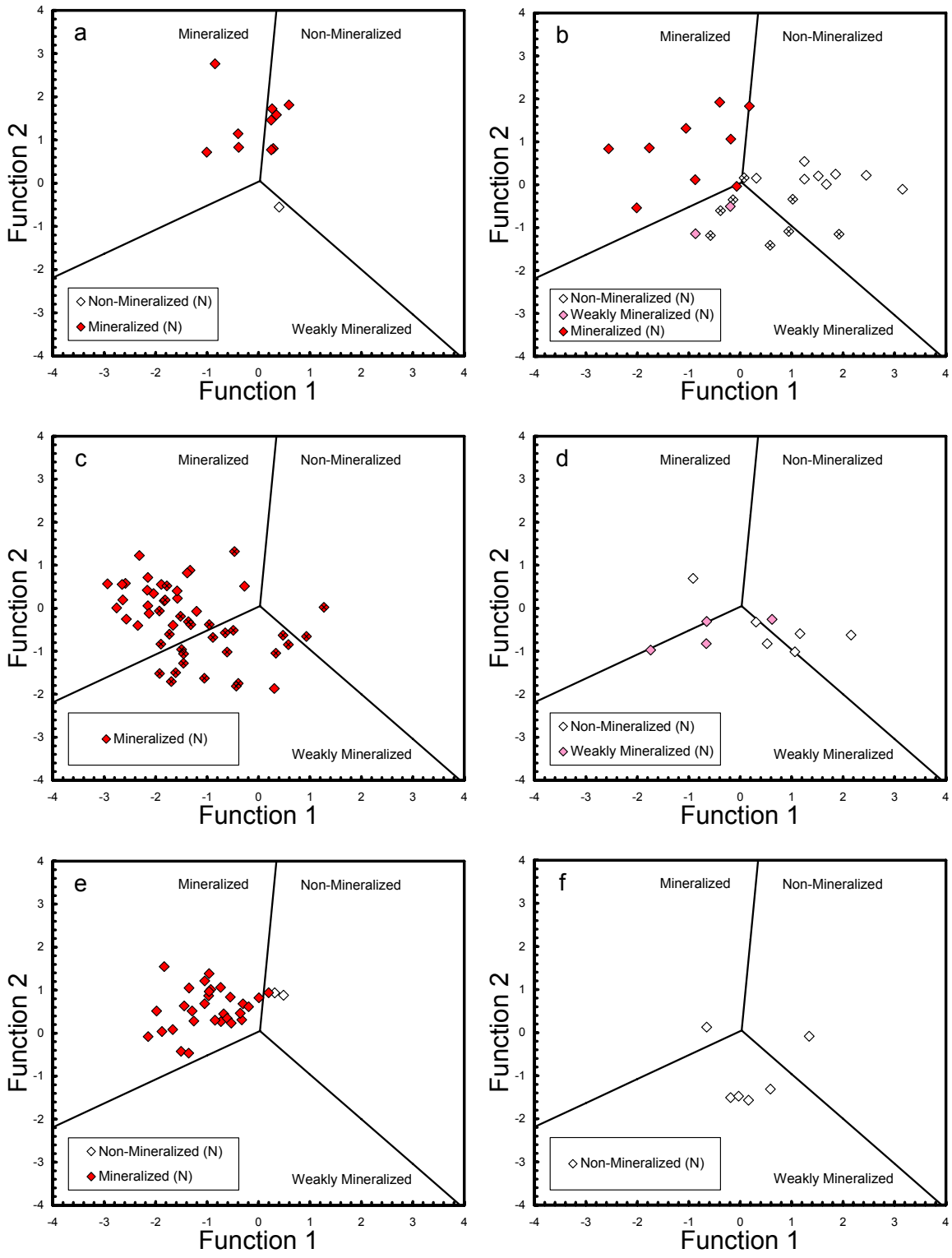

Figure 8.28 Discriminant function plots for individual TNB ultramafic bodies: a) Moak Lake, b) Mystery Lake (crosses, Mystery Lake East), c) Thompson (crosses, DDH 74381, 74378, 74379), d) Mid Lake, e) Pipe 1 and 2, and f) Spur South. Functions used:

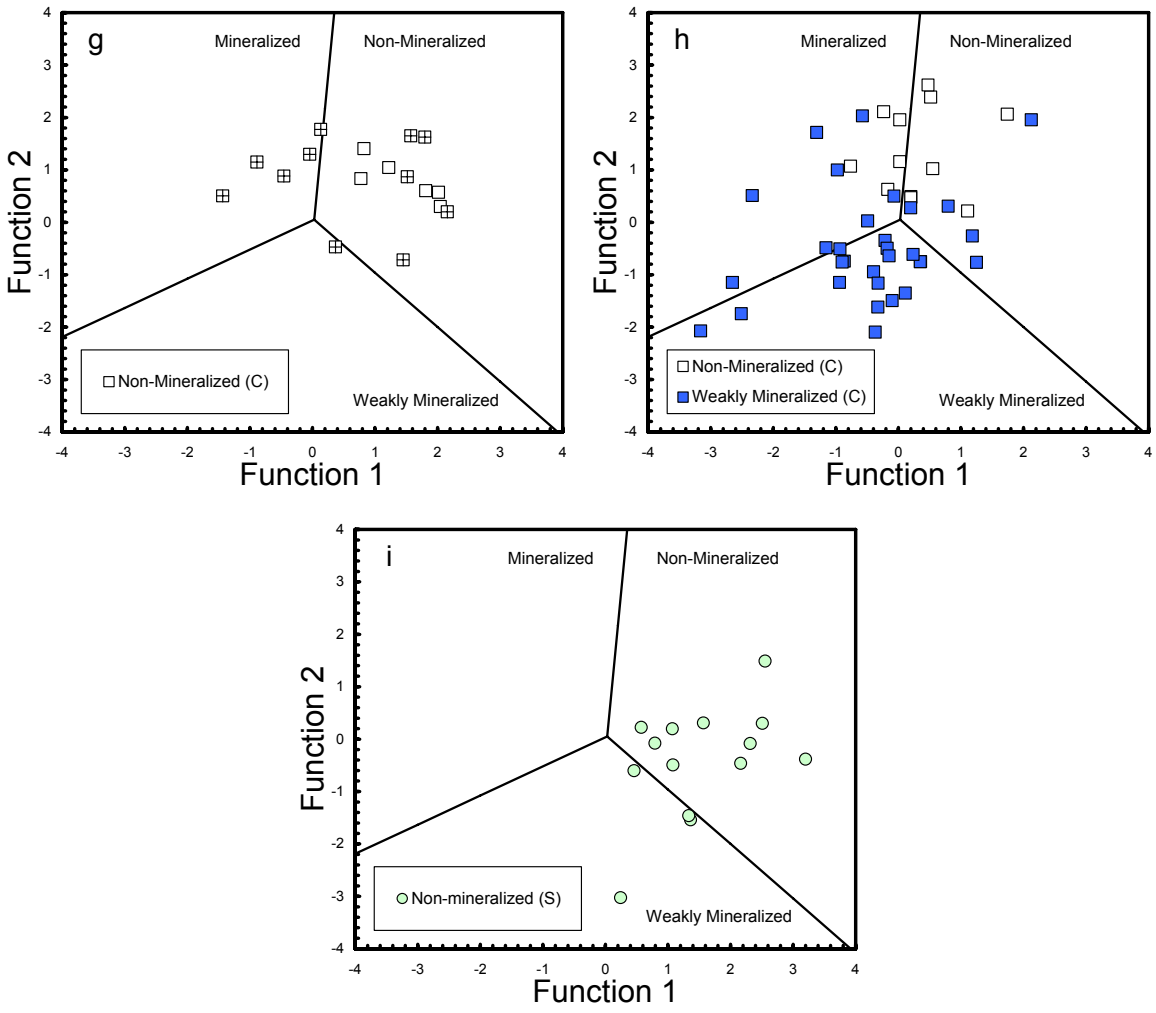

Figure 8.28 (contd.) Discriminant function plots for TNB ultramafic bodies: g) Northern Winnipegosis Belt (crosses, DDH BK93-64), h) William Lake, i) Winnipegosis Belt.

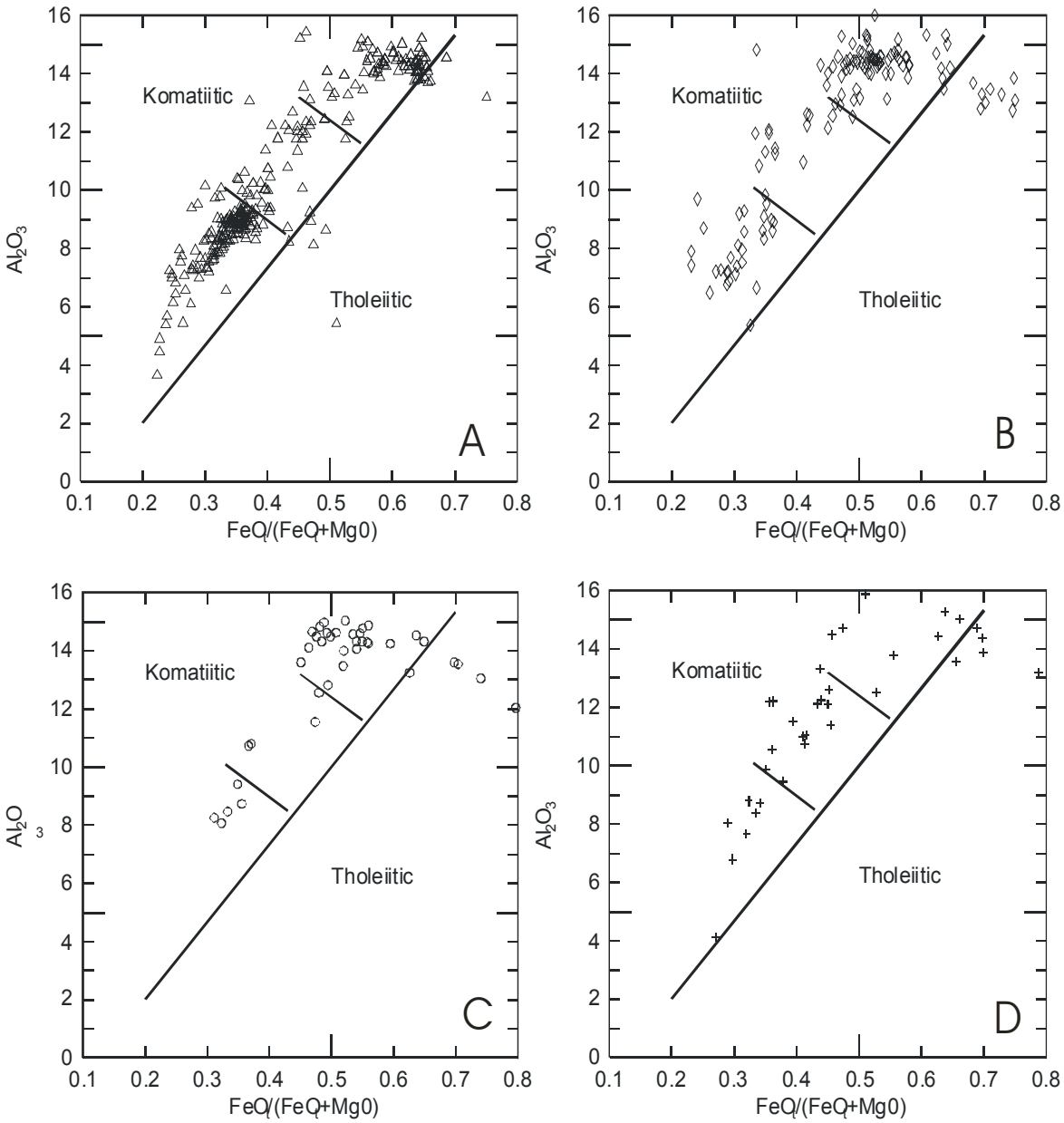

Figure 8.29 Komatiite-tholeiite discriminant plot for mafic and ultramafic volcanic rocks and associated sills and dykes in the TNB and WKB. A) Rabbit Point, Winnipegosis Belt, B) mafic and ultramafic flows, Thompson Belt, C) mafic dykes and sills, Thompson Belt, D) Molson dykes, Superior Province. Adapted from Arndt et al. (1977)

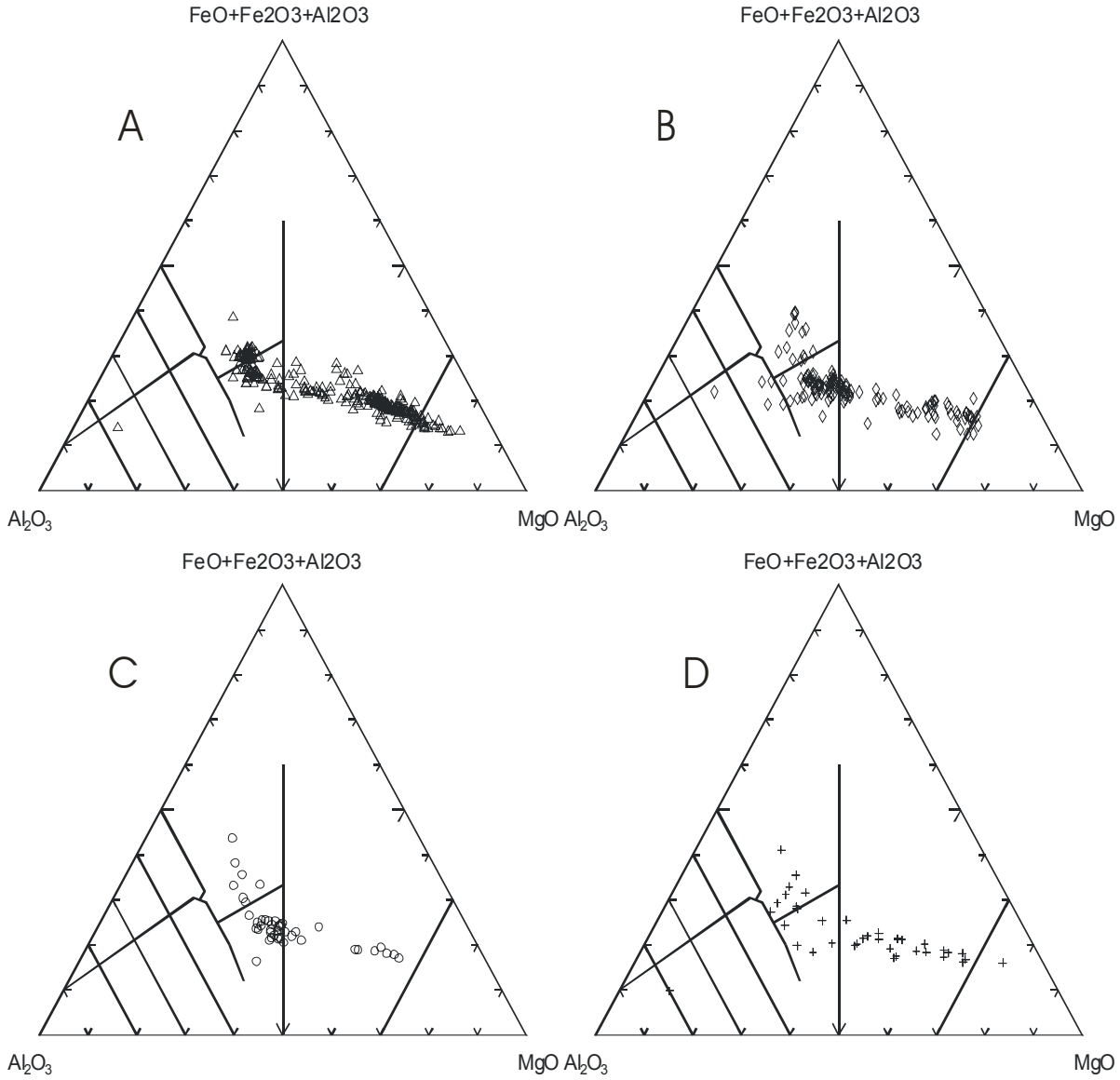

Figure 8.30 Jensen cation plot for mafic and ultramafic volcanic rocks and associated sills and dykes in the TNB and WKB. A) Rabbit Point, Winnipegosis Belt, B) mafic and ultramafic flows, Thompson Belt, C) mafic dykes and sills, Thompson Belt, D) Molson dykes, Superior Province. Adapted from Jensen (1976).

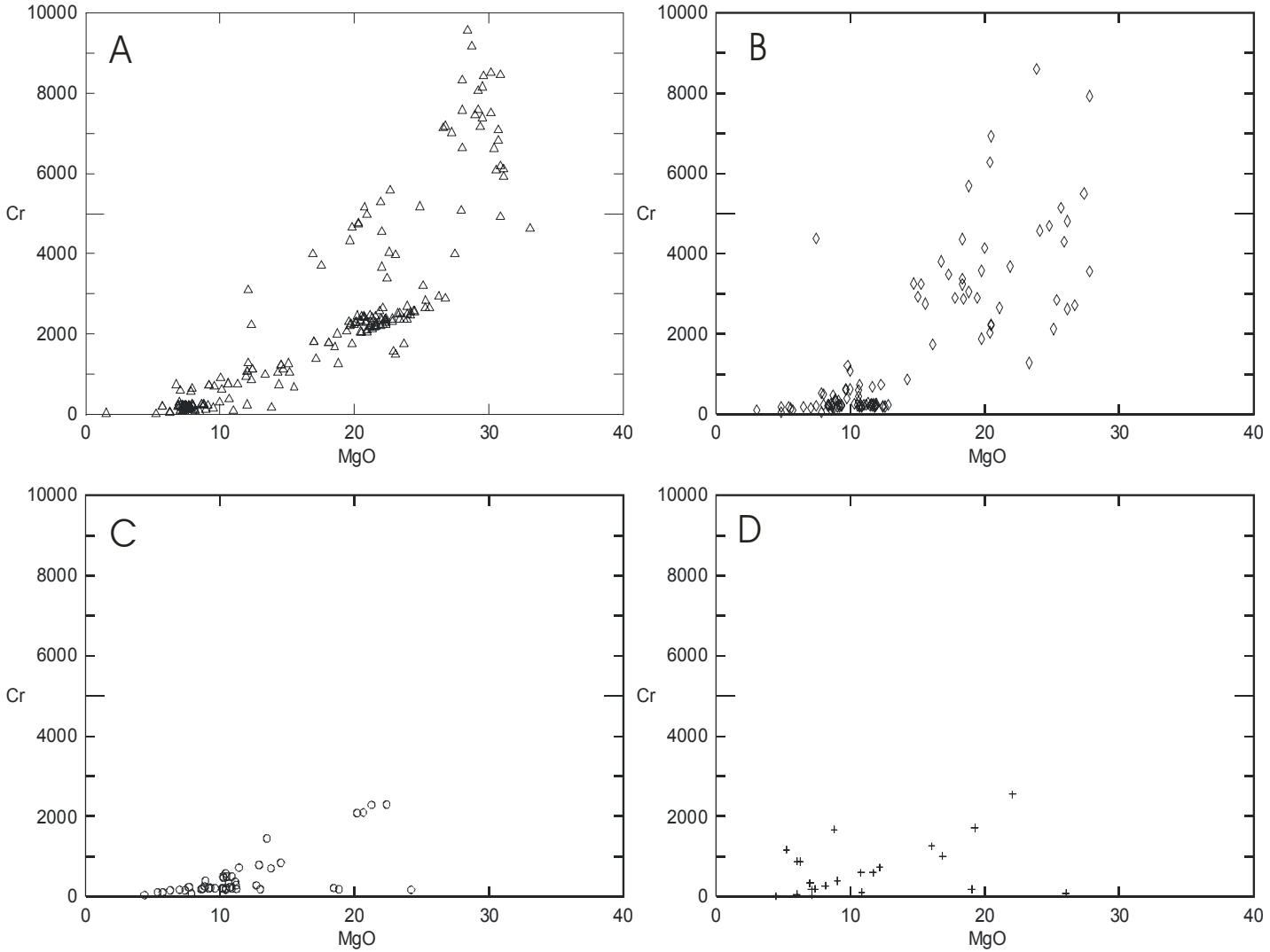

Figure 8.31 Plot of whole-rock Cr (ppm) and MgO (wt%) contents for mafic and ultramafic volcanic rocks and associated dykes and sills in the TNB and WKB. A) Rabbit Point, Winnipegosis Belt, B) mafic and ultramafic flows, Thompson Belt, C) mafic dykes and sills, Thompson Belt, D) Molson dykes, Superior Province.

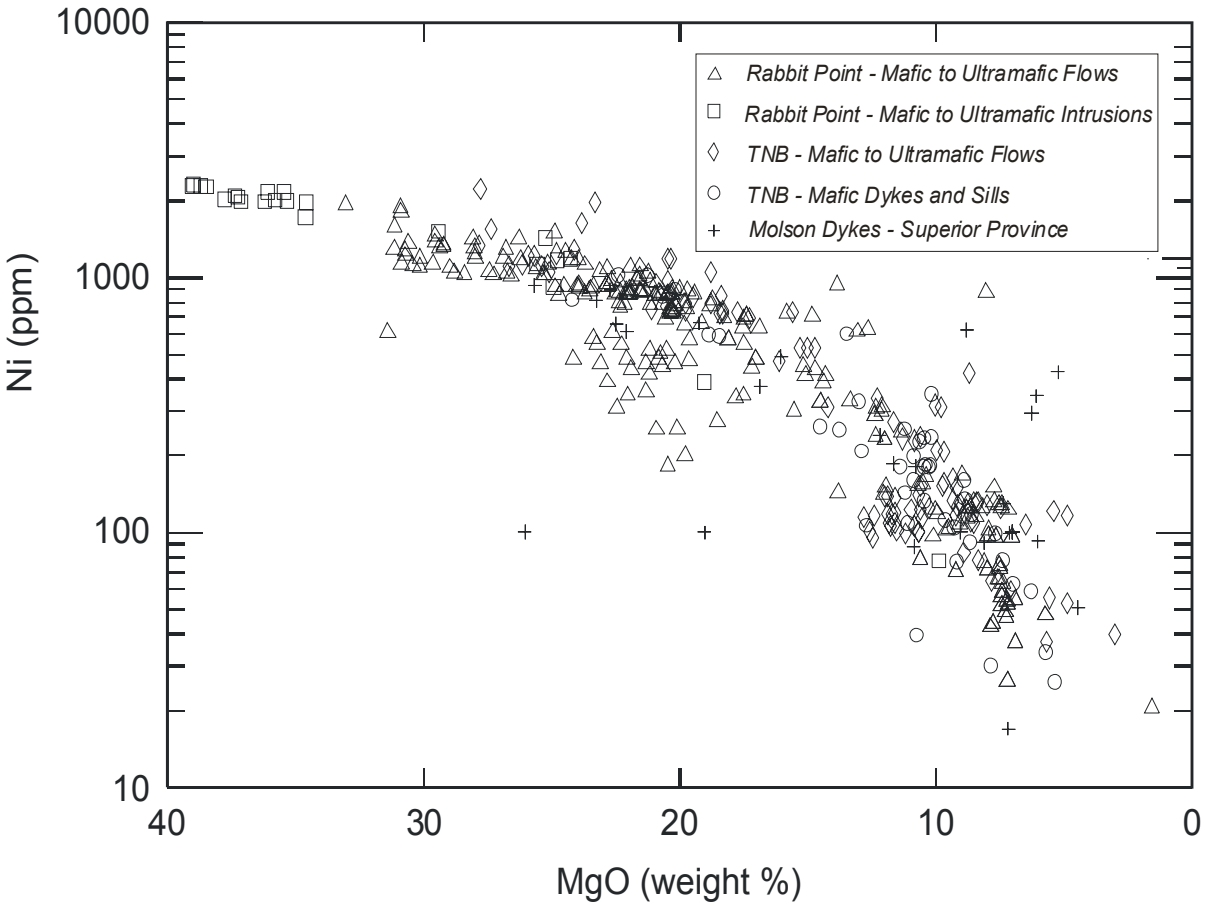

Figure 8.32 Plot of whole-rock MgO and Ni contents for mafic and ultramafic volcanic rocks and associated sills and dykes in the TNB and WKB.

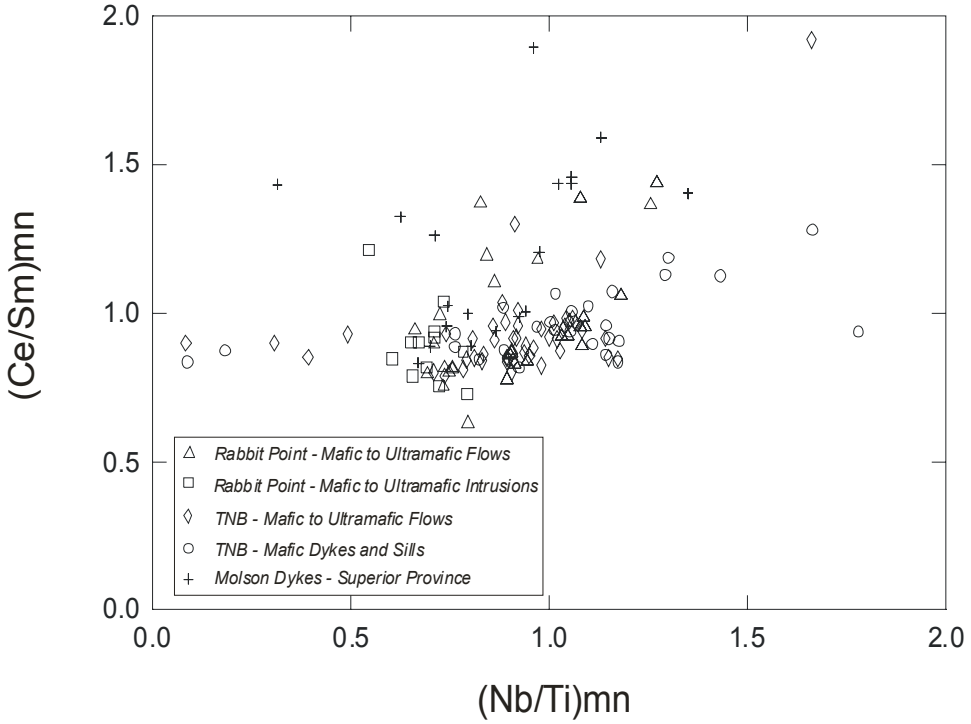

Figure 8.33 Plot of mantle normalized Ce/Sm and Nb/Ti ratios for mafic and ultramafic rocks in the TNB and WKB.

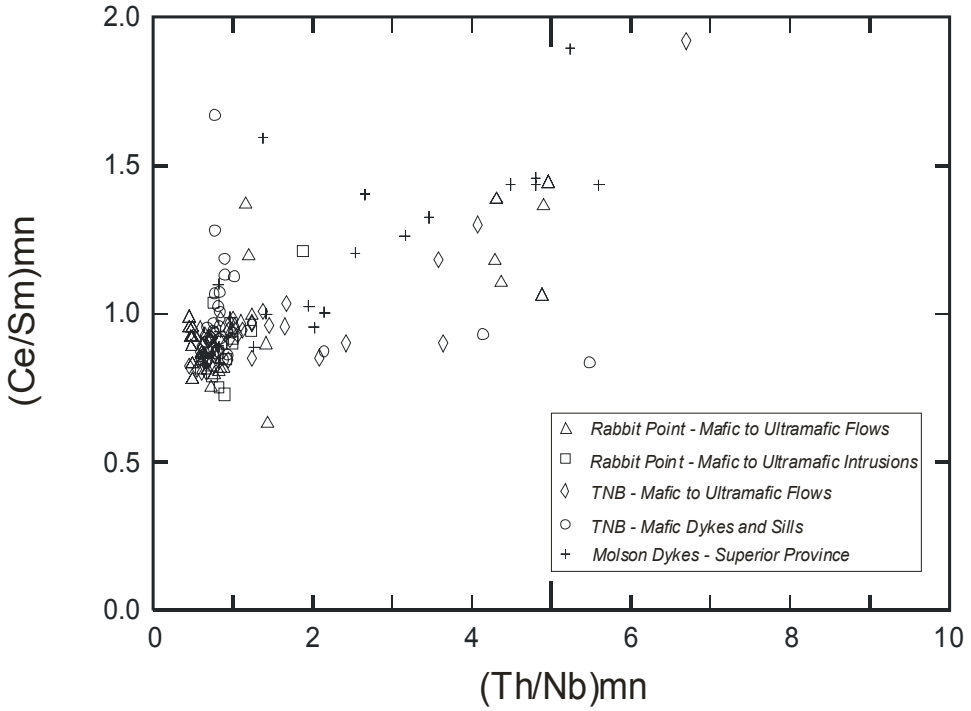

Figure 8.34 Plot of mantle normalized Ce/Sm and Th/Nb ratios for mafic and ultramafic rocks in the TNB and WKB.

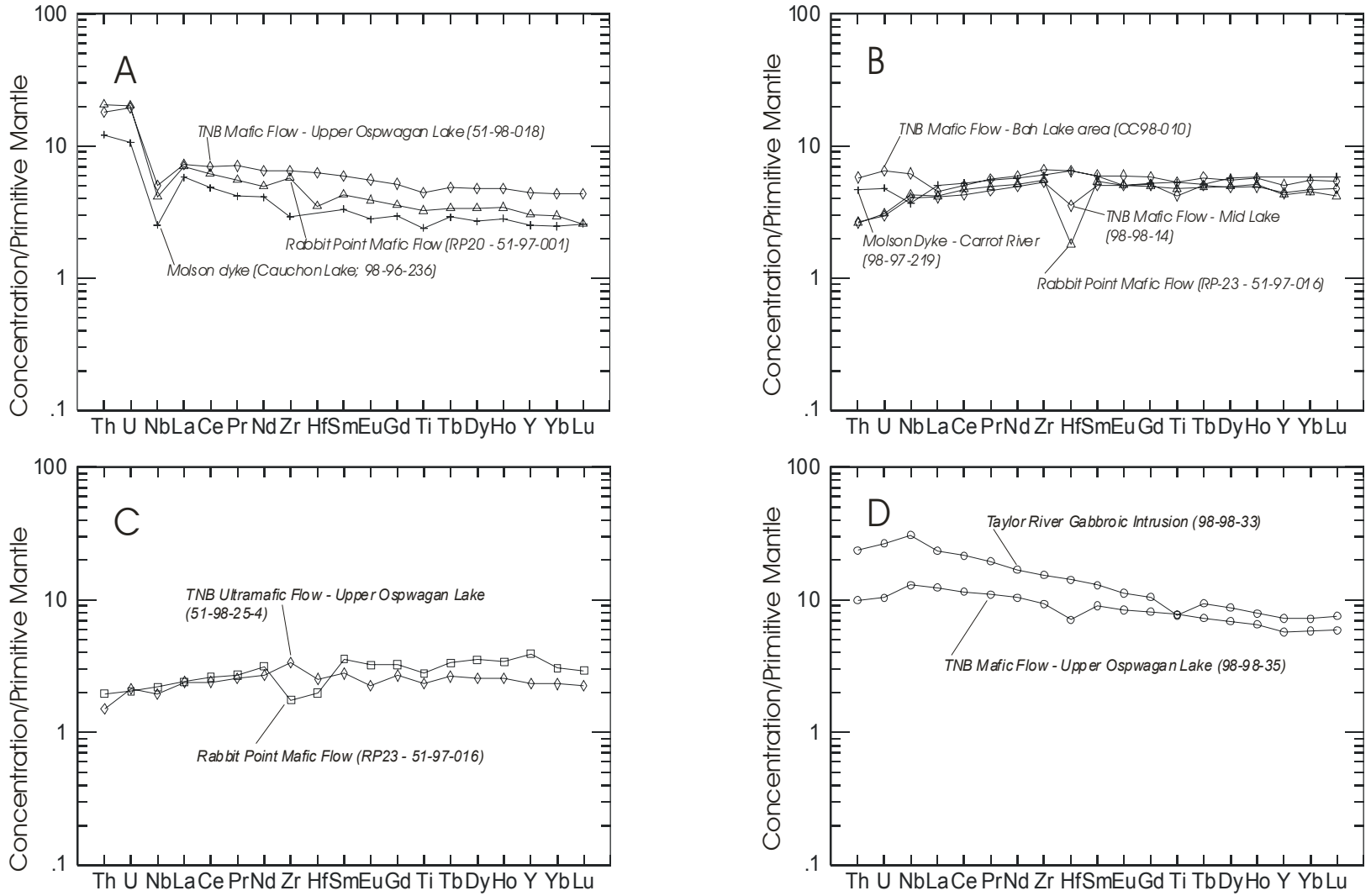

Figure 8.35 Mantle-normalized trace element abundances for selected, representative samples of mafic and ultramafic volcanic rocks and associated dykes and sills in the TNB and WKB. A) Rabbit Point, Winnipegosis Belt, B) mafic and ultramafic flows, Thompson Belt, C) mafic dykes and sills, Thompson Belt, D) Molson dykes, Superior Province. Mantle normalization values from Sun & McDonough (1995).

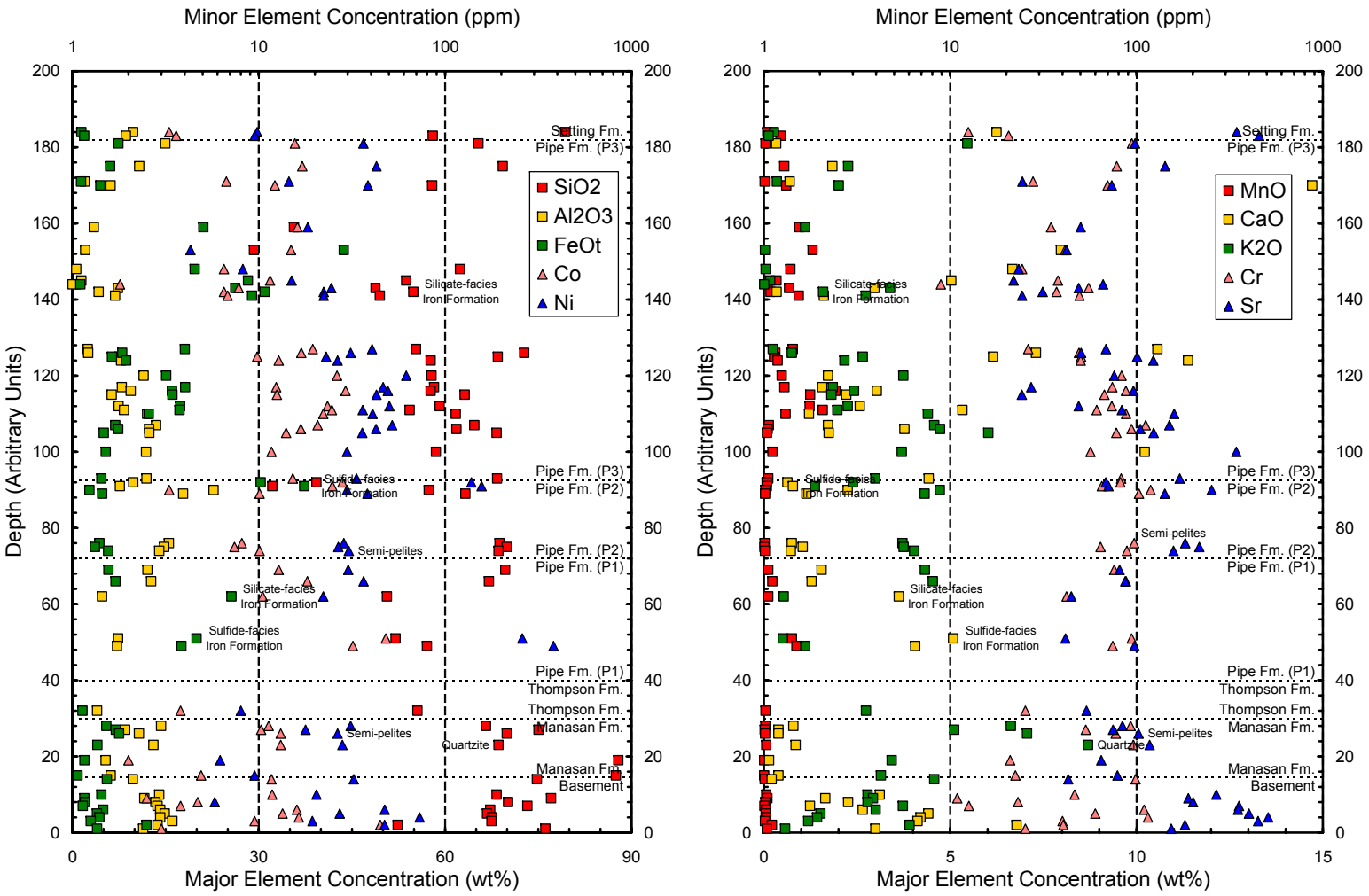

Figure 8.36 Chemostratigraphy of Ospwagan Group metasedimentary rocks from the type section at Pipe Pit. Note major elements plotted on linear scale, but minor elements plotted on logarithmic scale.

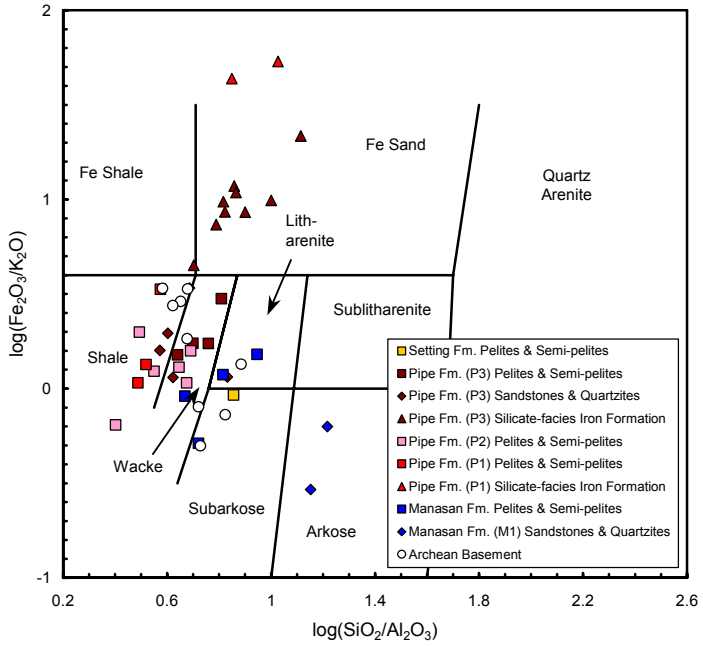

Figure 8.37 Chemical classification of TNB metasedimentary rocks and basement gneisses from the type sections at Pipe and Thompson Pits using $\log(Fe_2O_3/K_2O)$ vs. $\log(SiO_2/Al_2O_3)$. After Herron (1988).

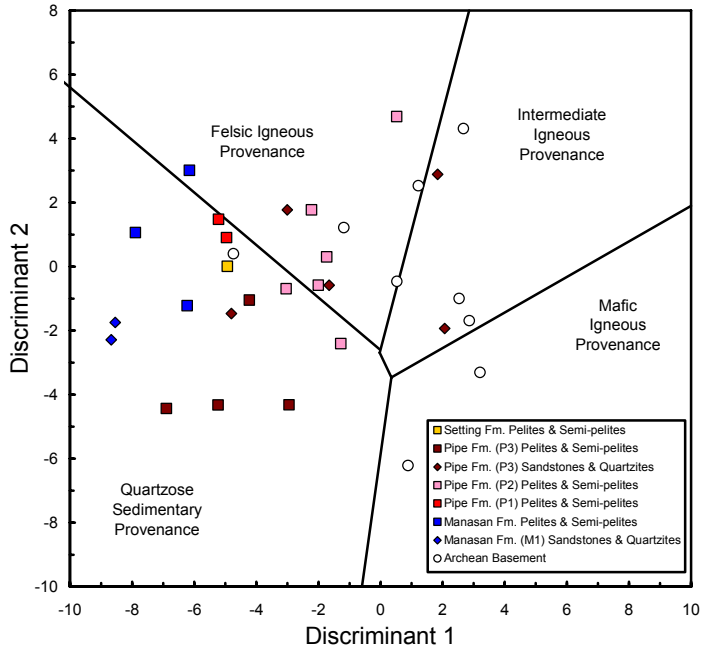

Figure 8.38 Discriminant function diagram for the provenance signatures of sandstone-mudstone suites from basement paragneisses and metasedimentary rocks from the type sections at Pipe and Thompson Pits based on major element compositions (after Roser & Korsch, 1988).

Discriminant 1 = $-1.773TiO_2 + 0.607Al_2O_3 + 0.76Fe_2O_3^t - 1.5MgO + 0.616CaO + 0.509Na_2O - 1.224K_2O - 9.09$
Discriminant 2 = $0.445TiO_2 + 0.07Al_2O_3 - 0.25Fe_2O_3^t - 1.142MgO + 0.438CaO + 1.475Na_2O - 1.426K_2O - 6.861$

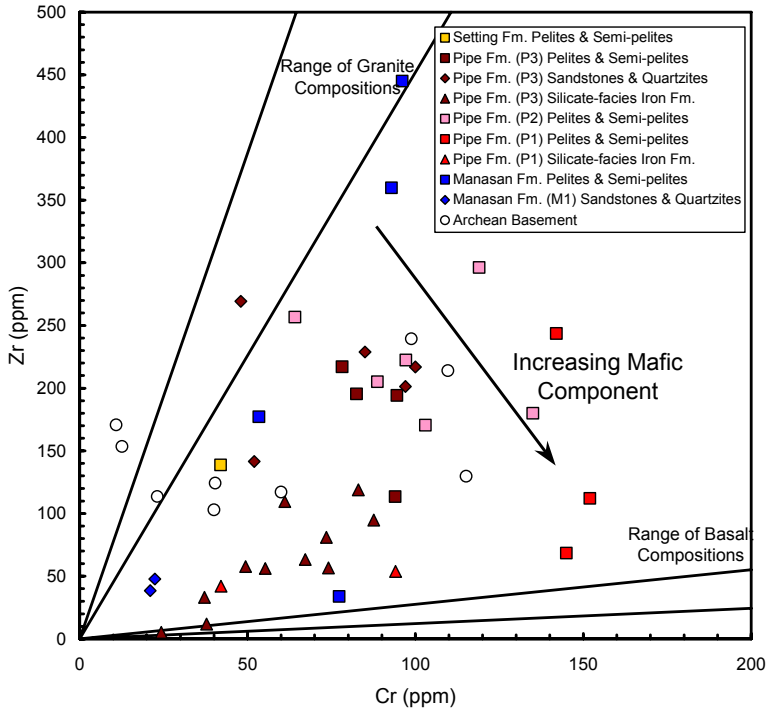

Figure 8.39 Cr vs. Zr in metasedimentary rocks and basement gneisses from the type sections at Pipe and Thompson Pits. Ranges for granites and basalts from samples collected as part of this study by project researchers.

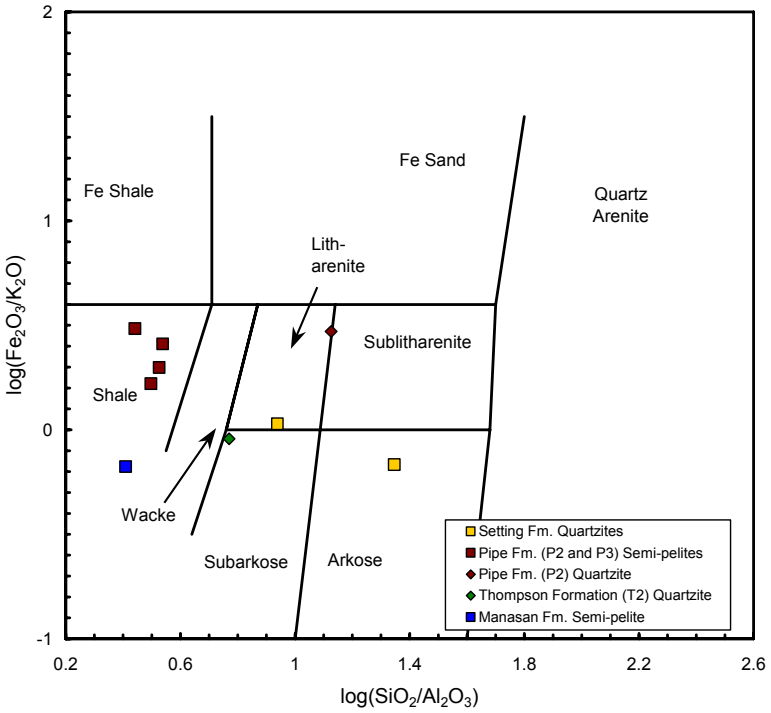

Figure 8.40 Chemical classification of metasedimentary rocks from the central TNB using $\log(Fe_2O_3/K_2O)$ vs. $\log(SiO_2/Al_2O_3)$. After Herron (1988).

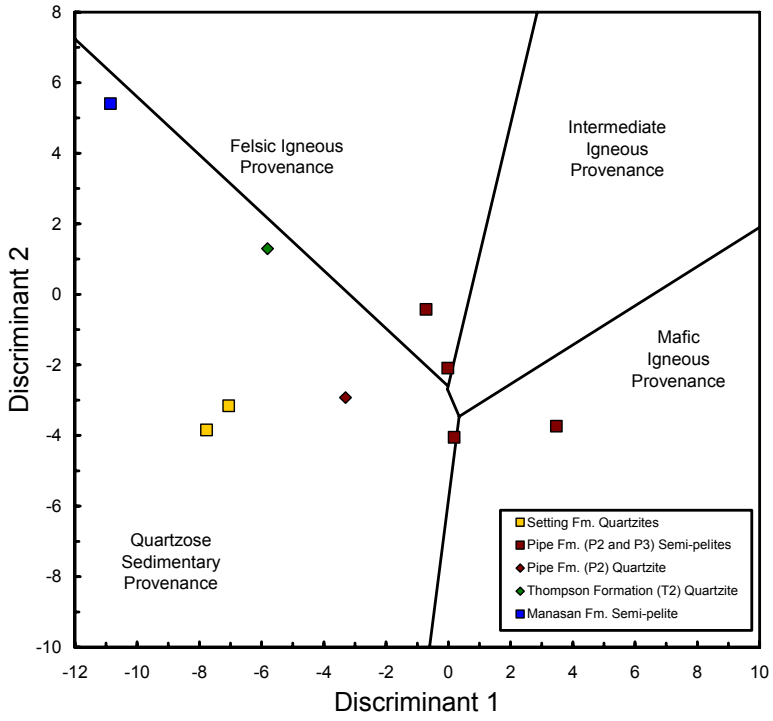

Figure 8.41 Discriminant function diagram for the provenance signatures of sandstone-mudstone suites from the central TNB based on major element compositions (after Roser & Korsch, 1988). Discriminant functions shown in caption for **Figure 8.36**.

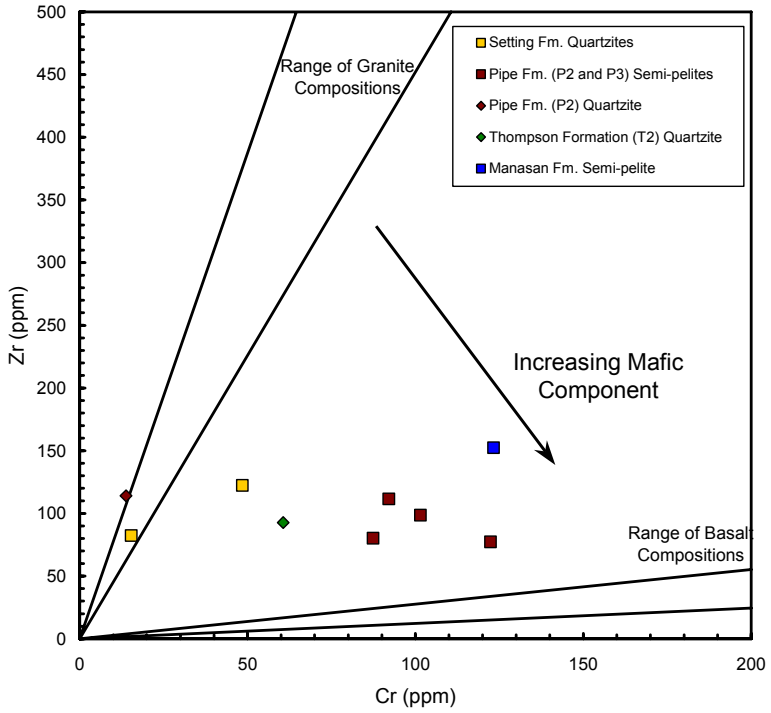

Figure 8.42 Cr vs. Zr in metasedimentary rocks from the central TNB. Ranges for granites and basalts from samples collected as part of this study by project researchers.

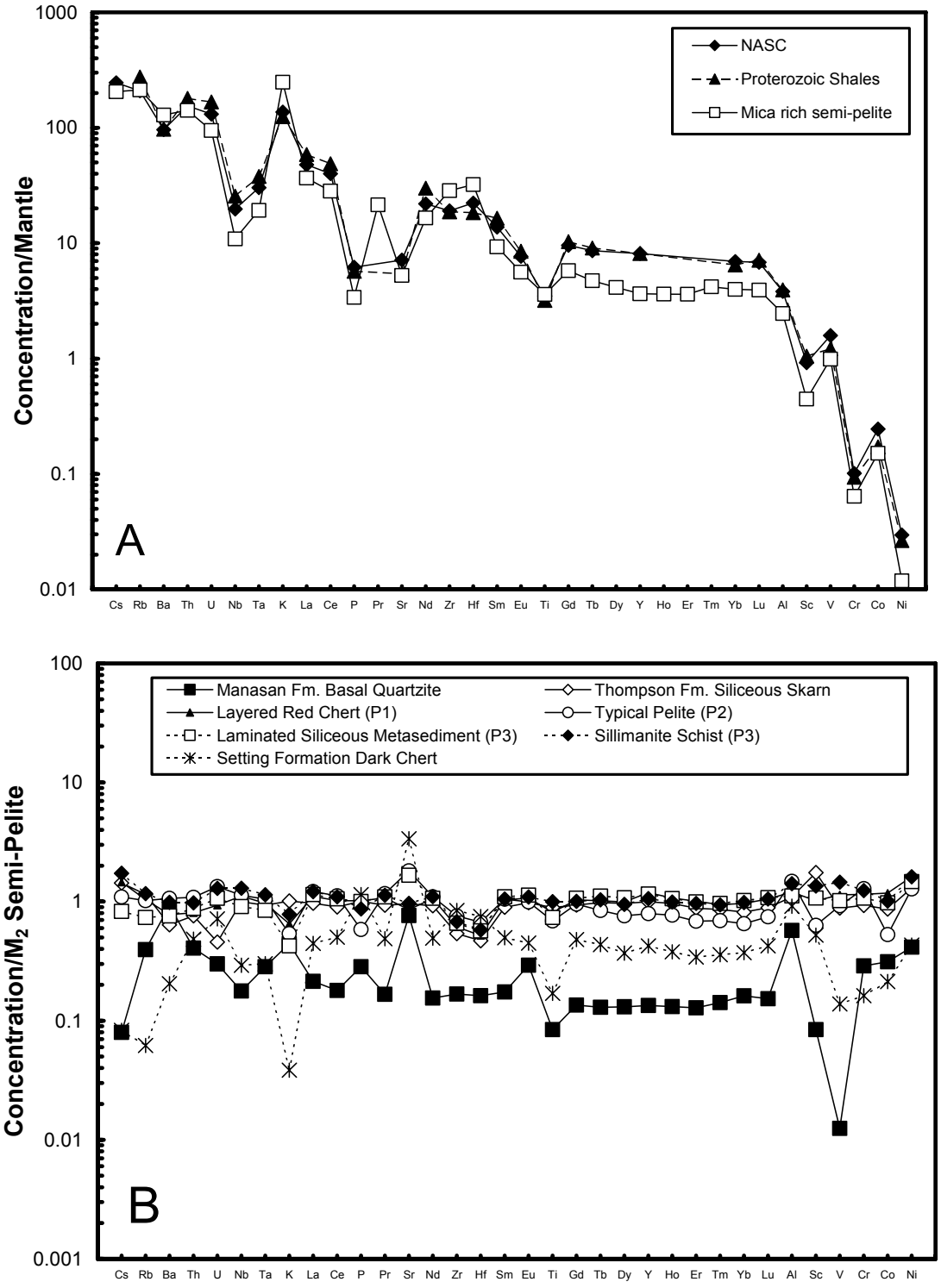

Figure 8.43 Multi-elemental plots for Ospwagan Group metasedimentary rocks from the type sections at the Pipe and Thompson Pits. A) Mantle-normalized values for a typical Manasan Formation semi-pelite relative t the North American Shale Composite (Gromet et al., 1984) and an average Proterozoic shale (Condie, 1993). B) Ospwagan Group clastic sedimentary rocks normalized to the typical semi-pelite shown in (A).

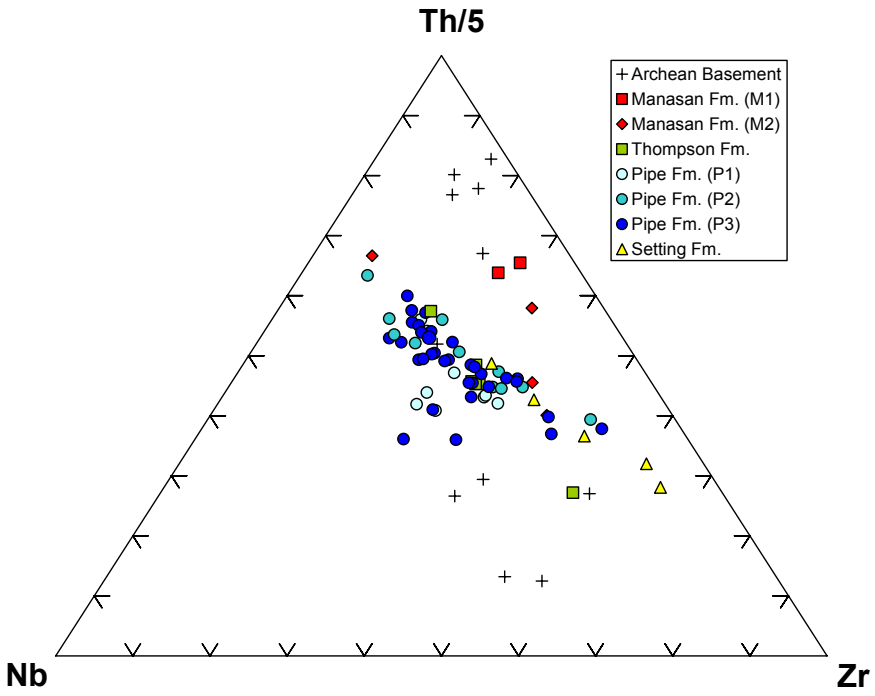

Figure 8.44 Mantle-normalized HFSE compositions of metapelites, quartzites, iron formations and basement rocks of the northern and central regions of the TNB.

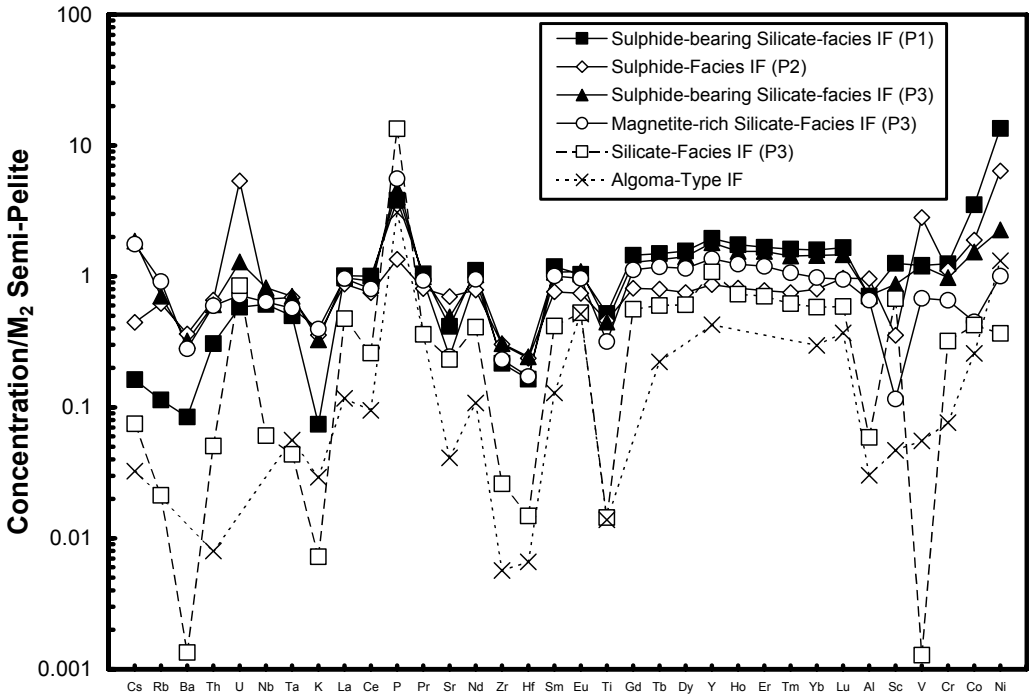

Figure 8.45 Multi-elemental plots for Ospwagan Group iron formations from the type sections at the Pipe and Thompson Pits. All data normalized to the typical semi-pelite shown in **Figure 8.43a**.

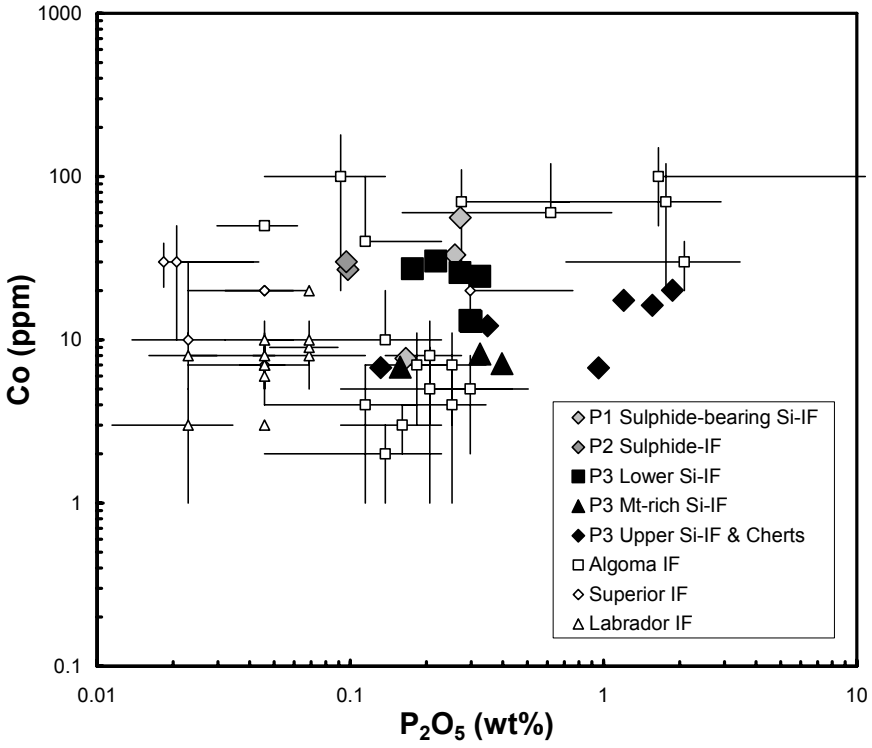

Figure 8.46 Co vs. P_2O_5 plot for the Pipe Formation iron formations relative to the average compositions of different iron formations within and around the Superior Province (additional data from Gross, 1990).

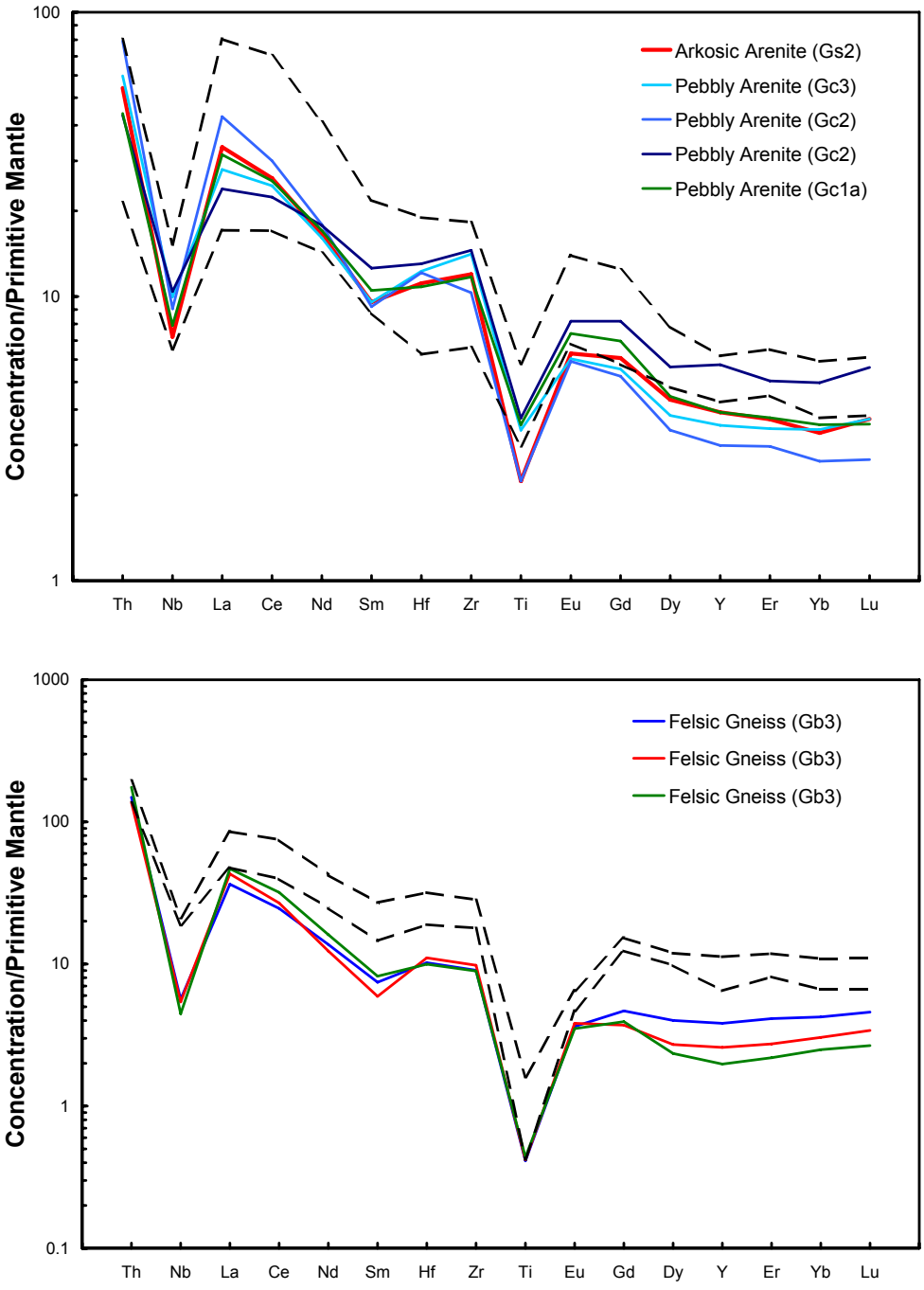

Figure 8.47 Mantle-normalized plots of metasediments and tuffs of the Grass River Group. A) Units Gc (lower pebbly arenite and conglomerate) and Gs (upper arkosic arenite). Shaded field, Missi Group volcanic rocks, south flank Kisseynew Domain (H. Zwanzig, unpublished data). B) Unit Gb3 (felsic gneisses). Shaded field, Missi Group rhyolite-derived gneiss, south flank Kisseynew Domain (H. Zwanzig, unpublished data). Mantle normalization values after McDonough & Sun (1995).

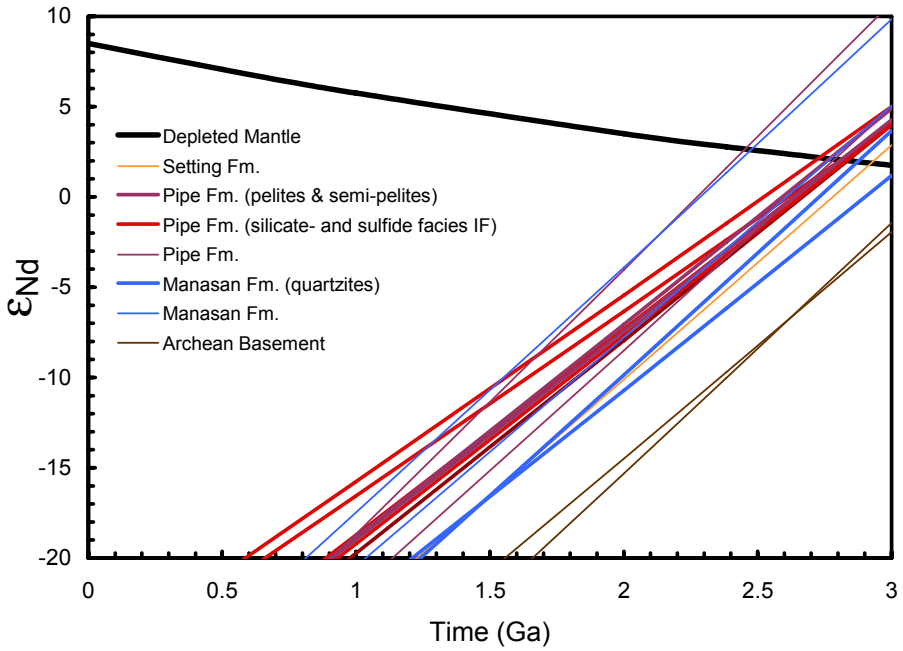

Figure 8.48 Plot of ε_{Nd} vs. time for sedimentary rocks from the TNB. Data sources: thick lines, this study; thin lines, Ansdell & Bleeker, 1997. Depleted Mantle evolution curve from Ben Othman et al. (1984).

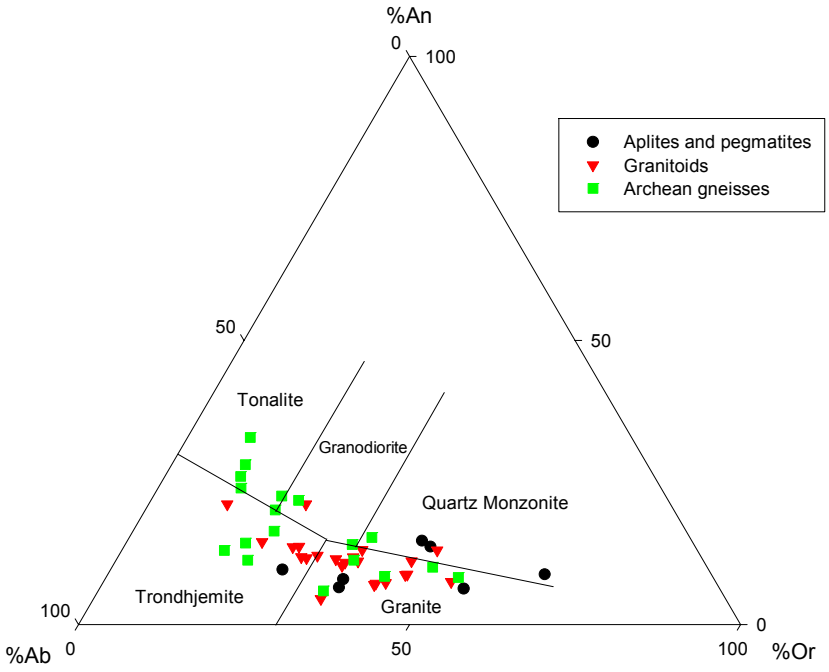

Figure 8.49 Classification of the felsic rocks of the TNB according to their molecular normative An-Ab-Or compositions (after Barker, 1979).

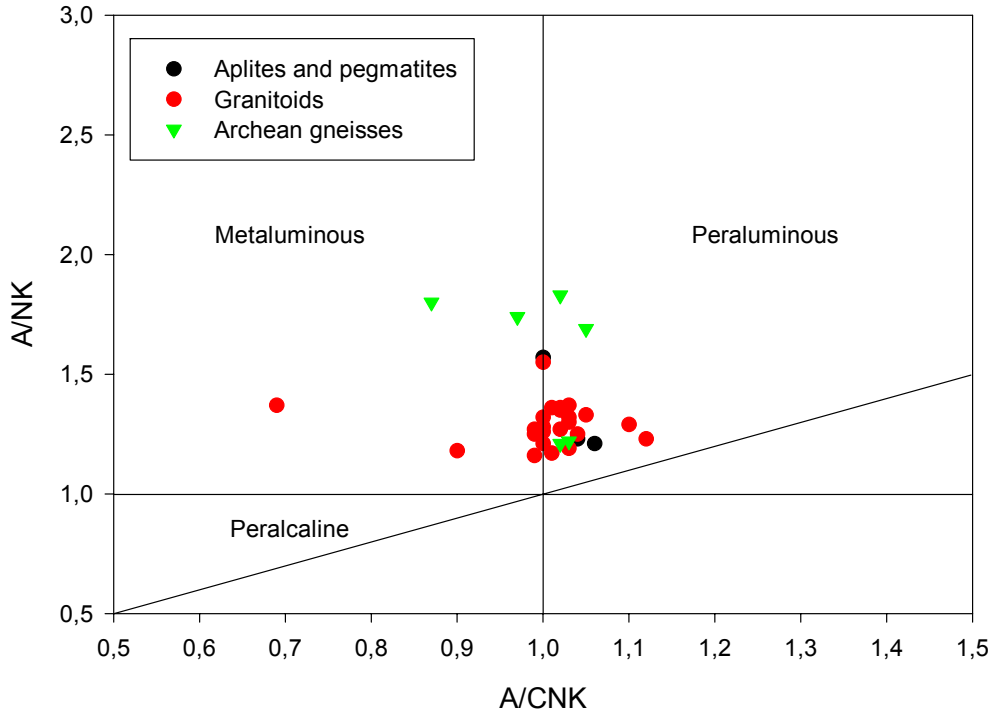

Figure 8.50 Plot of A/NK versus A/CNK illustrating the felsic magmatism of the TNB. (After Maniard and Picoli, 1989).

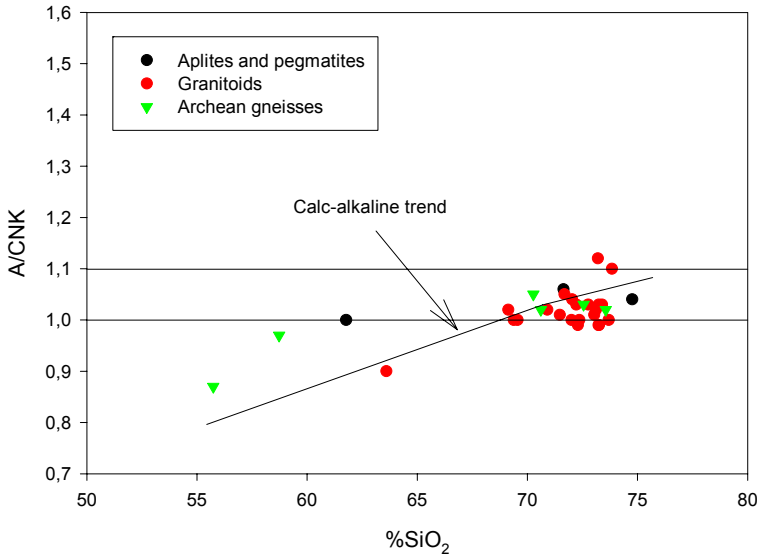

Figure 8.51 Plot of A/CNK versus SiO_2 illustrating the calc-alkaline affinity of the felsic magmatism of the TNB.

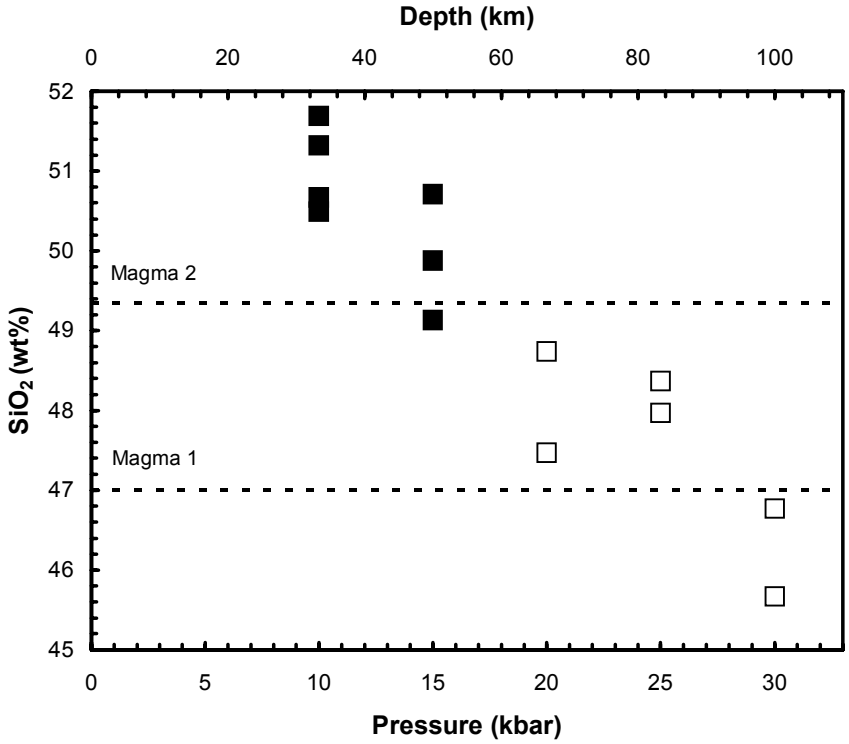

Figure 8.52 Comparison of SiO_2 contents in experimental melts obtained at a range of pressures with the inferred compositions of the parental magmas to the Bah Lake volcanic rocks (Magma 1) and the TNB ultramafic bodies (Magma 2). Experimental data from Hirose & Kushiro (1993). For full major element compositions of the inferred parental magmas, see **Table 8.2**.

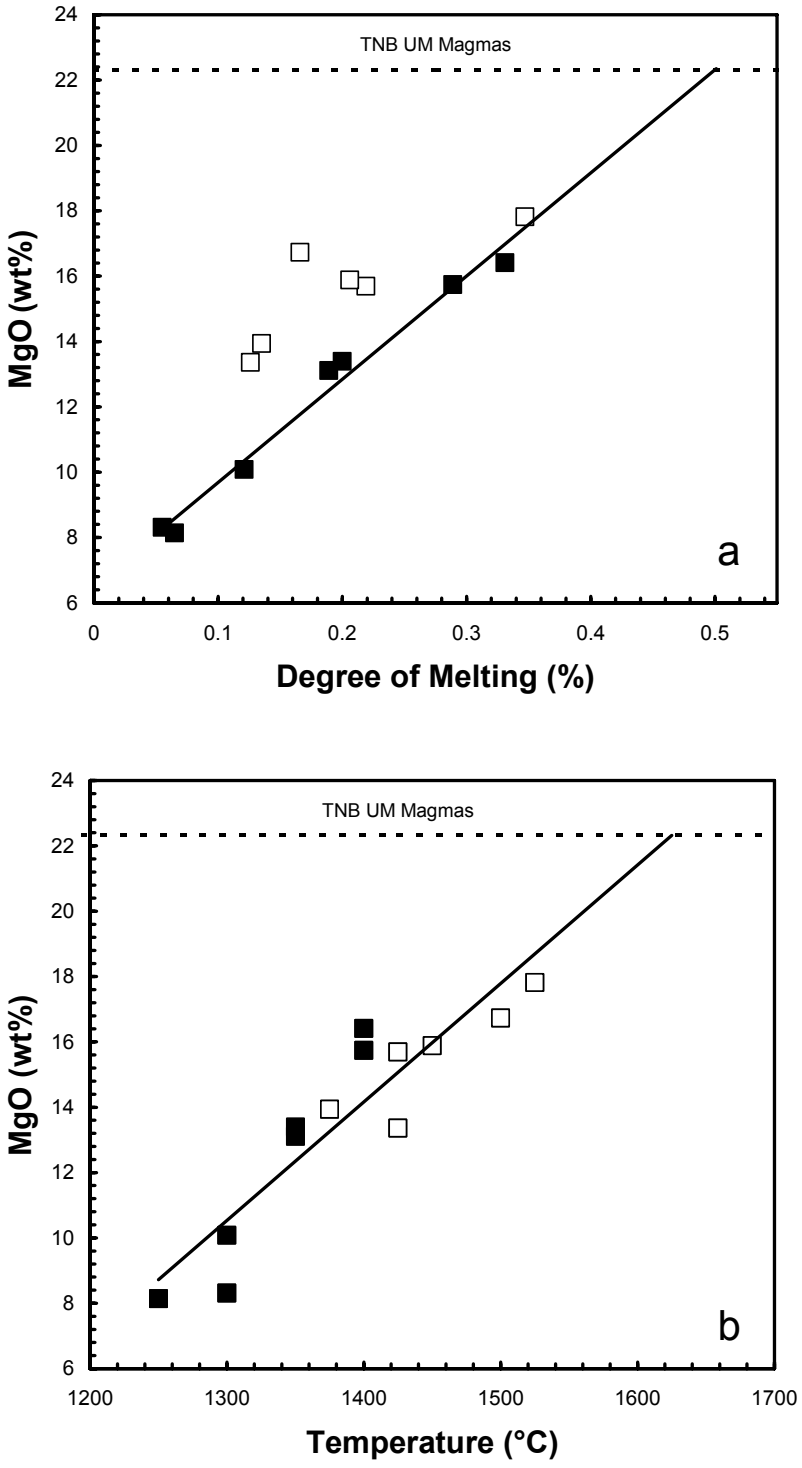

Figure 8.53 MgO contents of experimental melts as functions of a) degree of melting and b) temperature. Experimental data from Hirose & Kushiro (1993); open symbols at 10 and 15 kbar; closed symbols at 20, 25, and 30 kbar (see Fig. 8.52).

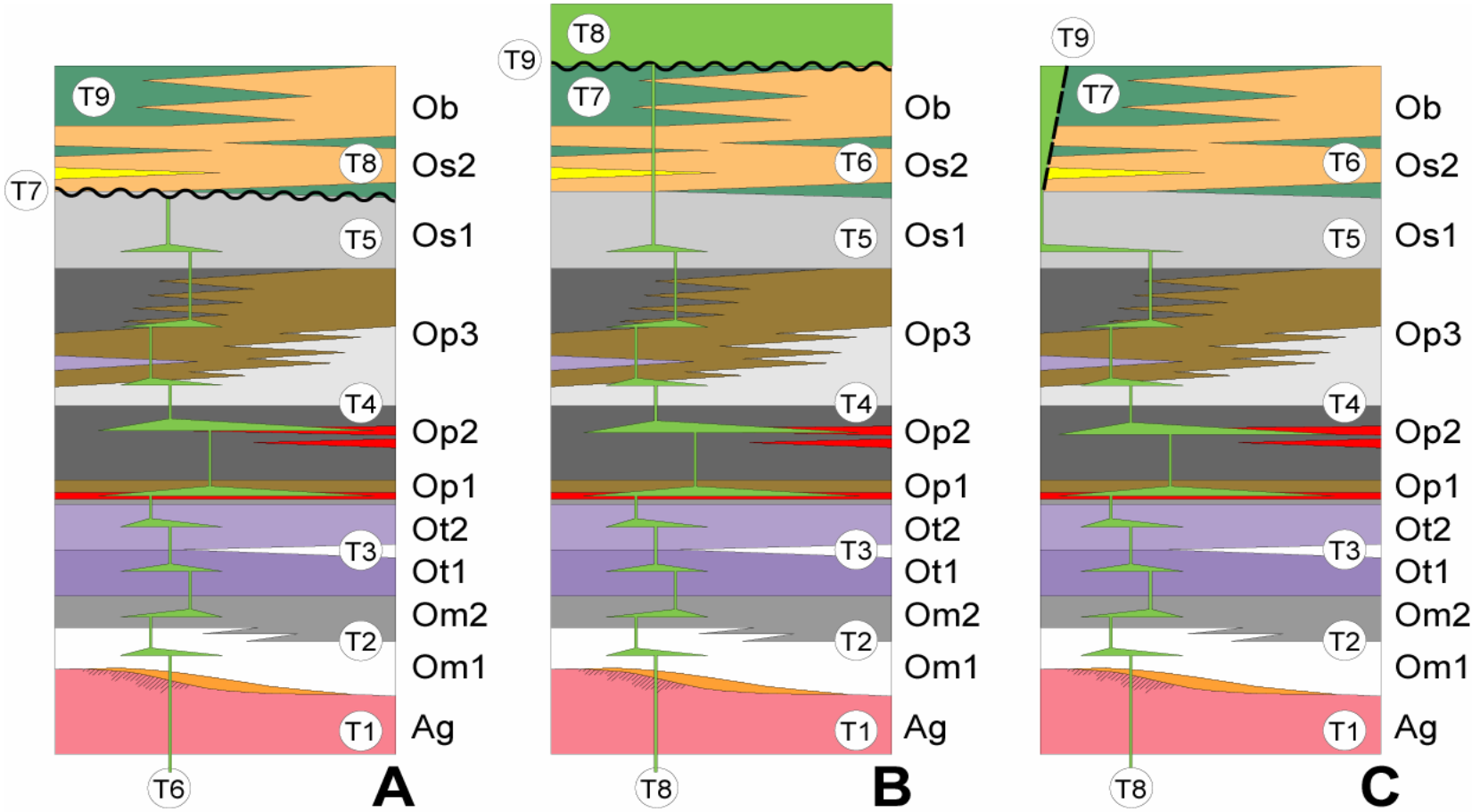

Figure 8.54 Three possible models for the timing of emplacement of the ultramafic sills in the Ospwagan Group of the Thompson Nickel Belt. A: Deposition of Manasan (Om), Thompson (Ot), Pipe (Op), and the Os1 member of the Setting Formation of the Ospwagan Group (T1-5), intrusion of ultramafic sills and eruption of derivative magmas (T6), erosion of derivative magmas (T7), deposition of Os2 member of Setting Formation (T8), and eruptions of Bah Lake Formation (Ob) (T9). B: Deposition of Manasan (Om), Thompson (Ot), Pipe (Op), and Setting Formation (Os) of the Ospwagan Group (T1-7), intrusion of ultramafic sills and eruption of derivative magmas (T8), erosion of derivative magmas (T9), C: Deposition of Manasan (Om), Thompson (Ot), Pipe (Op), and Setting Formation (Os) of the Ospwagan Group (T1-7), intrusion of ultramafic sills and eruption of derivative magmas in adjacent basin (T8), and fault separation of adjacent basin from TNB (T9).

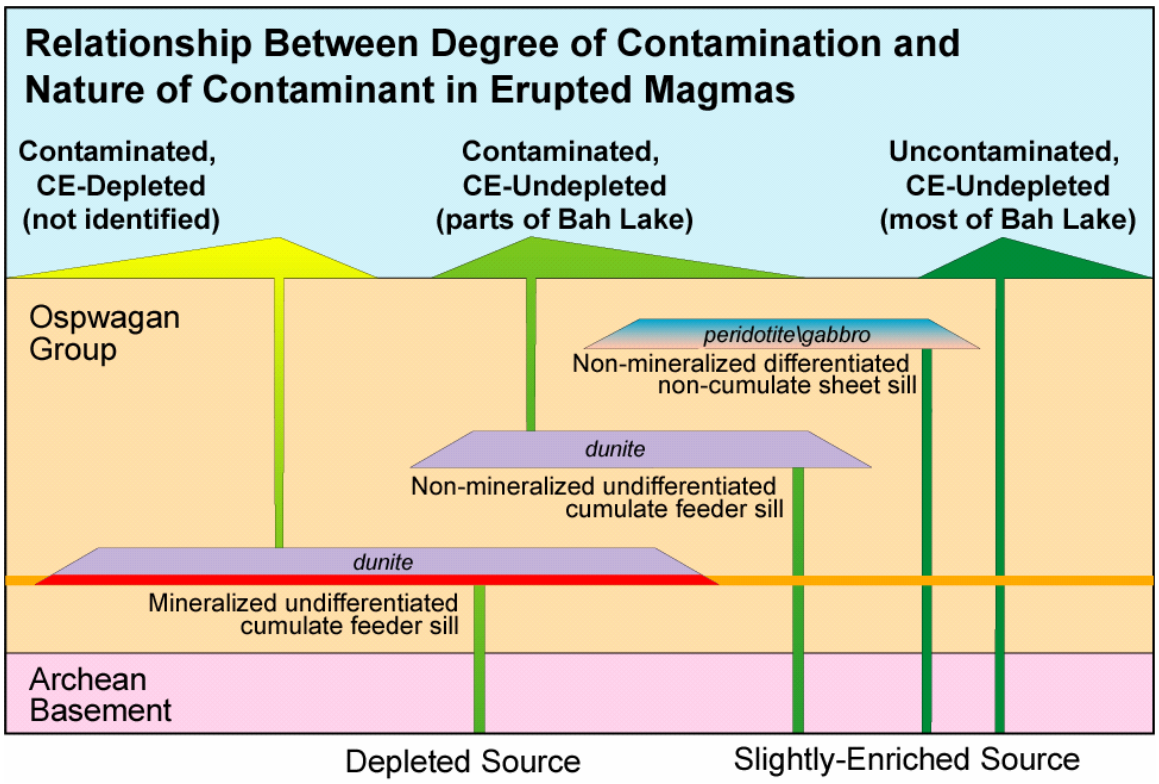

Figure 8.55 Schematic, interpretive model showing inferred petrogenetic relationships between mineralized undifferentiated cumulate feeder sills, non-mineralized undifferentiated cumulate feeder sills, non-mineralized differentiated cumulate sheet sills, contaminated chalcophile element-undepleted Bah Lake volcanic rocks; and uncontaminated chalcophile element-undepleted Bah Lake volcanic rocks in the TNB.

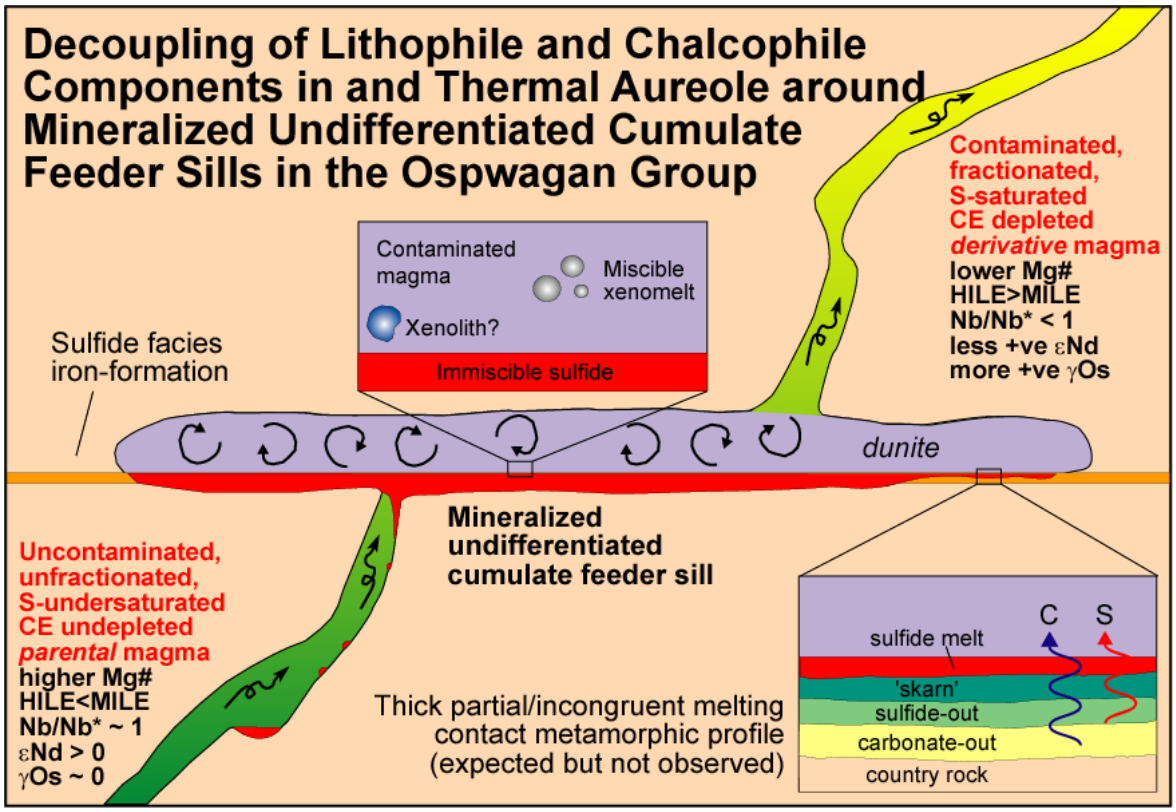

t-

Figure 8.56a Schematic, interpretive model showing decoupling of lithophile and chalcophile component in and the thermal aureole around *mineralized undifferentiated cumulate feeder sills* in the Ospwagan Group of the Thompson Nickel Belt (adapted from Lesher et al., 2001).

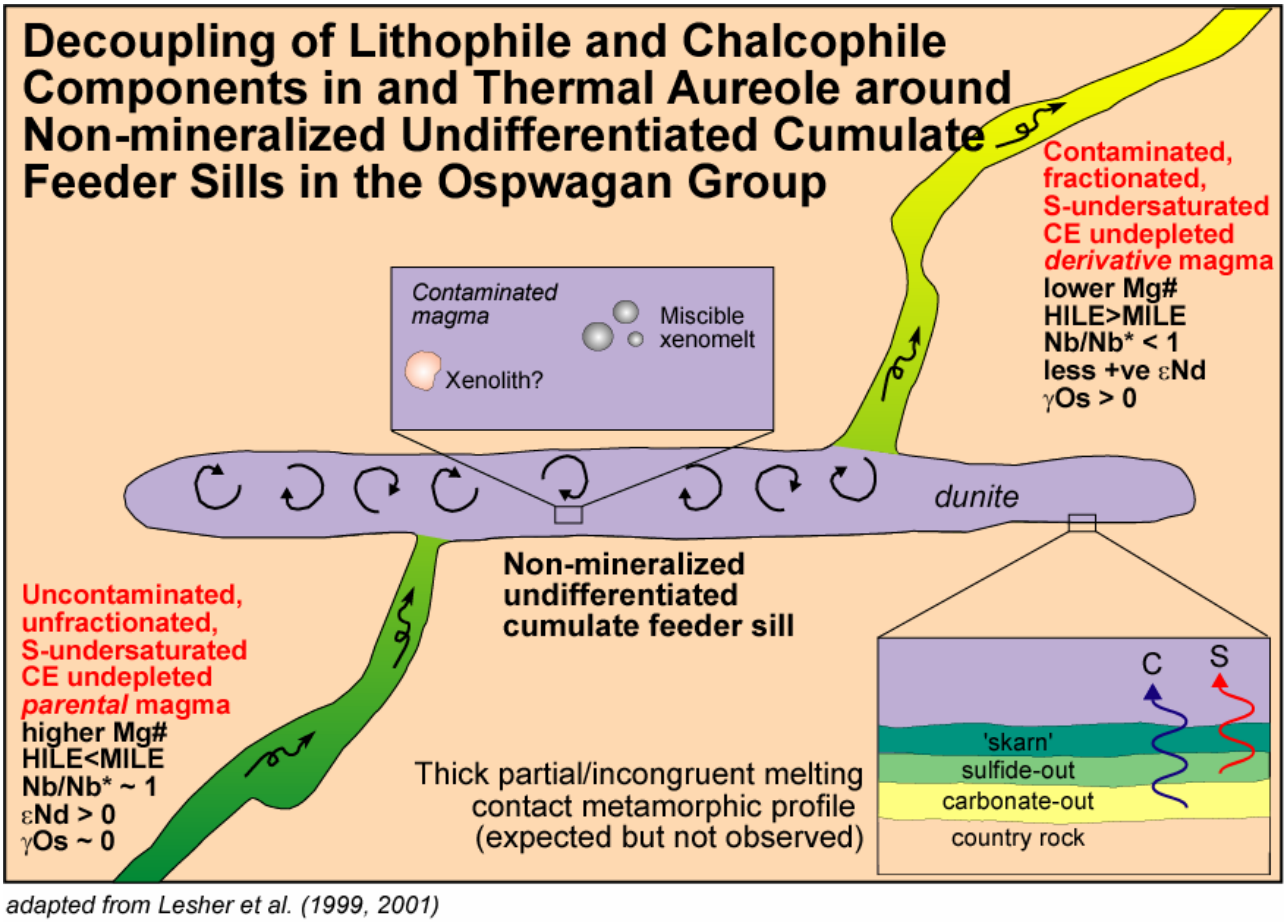

Figure 8.56b Schematic, interpretive model showing decoupling of lithophile and chalcophile component in and the thermal aureole around *non-mineralized undifferentiated cumulate feeder sills* in the Ospwagan Group of the Thompson Nickel Belt (adapted from Lesher et al., 2001).

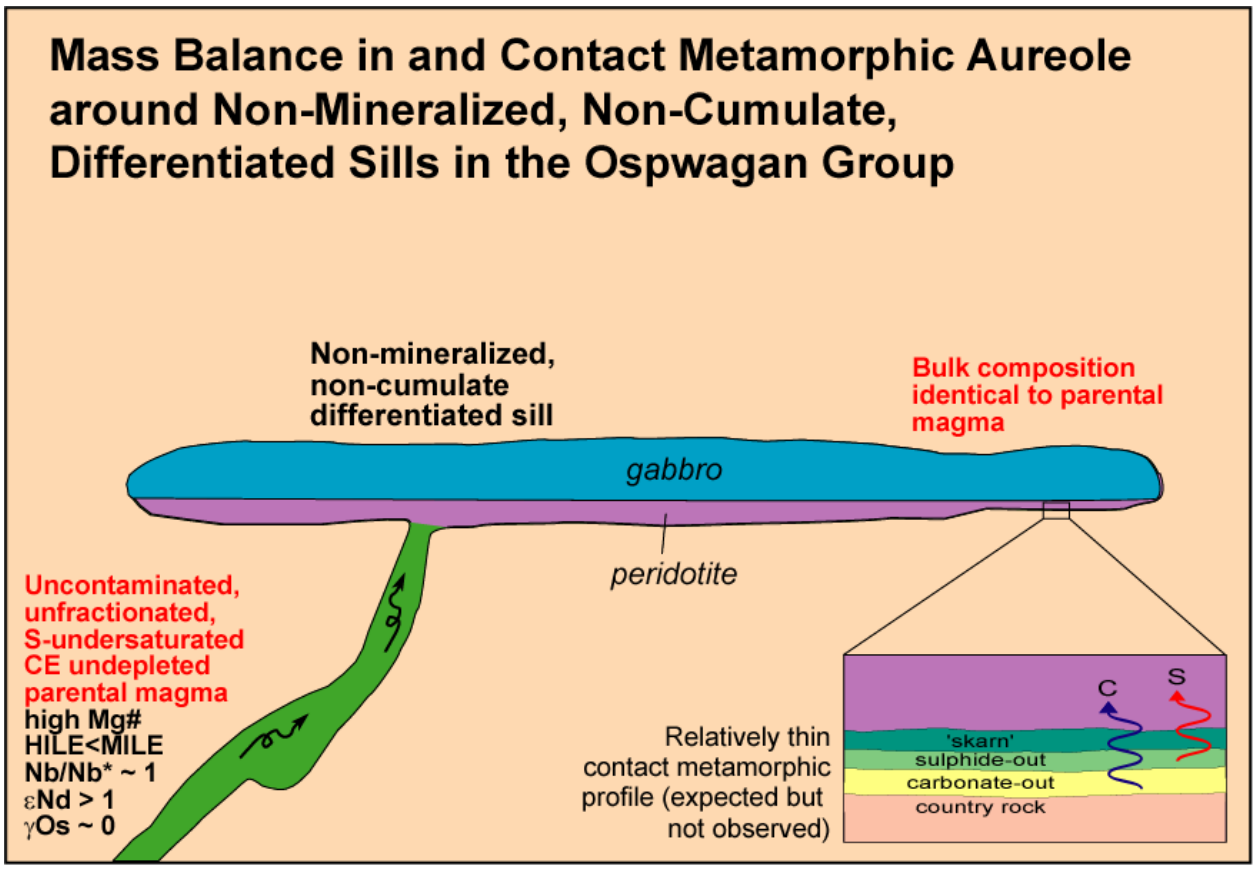

Figure 8.56c Schematic, interpretive model showing decoupling of lithophile and chalcophile component in and the thermal aureole around *non-mineralized differentiated non-cumulate sills* in the Ospwagan Group of the Thompson Nickel Belt (adapted from Lesher et al., 2001).